72-8065

McMANUS, Paul Francis, 1946-
LATERAL BUCKLING OF CURVED PLATE GIRDERS.

Carnegie-Mellon University, Ph.D., 1972
Engineering, civil

University Microfilms, A XEROX Company, Ann Arbor, Michigan

THIS DISSERTATION HAS BEEN MICROFILMED EXACTLY AS RECEIVED

Reproduced with permission of the copyright owner. Further reproduction prohibited without permission.

LATERAL BUCKLING OF

CURVED PLATE GIRDERS

by

Paul F. McManus

BE(CE), Manhattan College, 1967
MSCE, Carnegie-Mellon University, 1968

Submitted in Partial Fulfillment of the
Requirements for the Degree of
Doctor of Philosophy
Department of Civil Engineering
Carnegie-Mellon University
Pittsburgh, Pennsylvania

September, 1971

Reproduced with permission of the copyright owner. Further reproduction prohibited without permission.

Carnegie-Mellon University

CARNEGIE INSTITUTE OF TECHNOLOGY

THESIS

SUBMITTED IN PARTIAL FULFILLMENT OF THE REQUIREMENTS

FOR THE DEGREE OF Doctor of Philosophy

TITLE LATERAL BUCKLING OF CURVED PLATE GIRDERS

PRESENTED BY Paul F. McManus

ACCEPTED BY THE DEPARTMENT OF Civil Engineering

Charles Culver — MAJOR PROFESSOR — Sept 23, 1971 — DATE

Irving Oh — DEPARTMENT HEAD — Sept. 23, 1971 — DATE

APPROVED BY THE COMMITTEE ON GRADUATE DEGREES

[signature] — CHAIRMAN — 9/29/71 — DATE

Reproduced with permission of the copyright owner. Further reproduction prohibited without permission.

PLEASE NOTE:

Some Pages have indistinct print. Filmed as received.

UNIVERSITY MICROFILMS

Reproduced with permission of the copyright owner. Further reproduction prohibited without permission.

TABLE OF CONTENTS

		Page
LIST OF FIGURES		ii
LIST OF TABLES		v
ABSTRACT		vii
ACKNOWLEDGMENTS		viii
1. INTRODUCTION		1
2. DEVELOPMENT OF MATHEMATICAL MODEL		2
	2.1 General	2
	2.2 Derivation of Departure Equations	3
	2.3 Girder Subjected to End Loads	14
	2.4 Deflection Amplification Problem	23
3. NUMERICAL RESULTS		27
	3.1 Method of Solution	27
	3.2 Determination of Critical Loads	31
	3.3 Deflection Amplification Problem	34
4. SIMPLIFIED ANALYSIS AND COMPARISON WITH TESTS		38
	4.1 Development of Simple Model	38
	4.2 Comparison with Experiments	41
5. DESIGN APPLICATIONS		49
	5.1 General	49
	5.2 Elastic Behavior	54
	5.3 Inelastic Behavior	62
	5.4 Bracing Forces	74
6. DESIGN RECOMMENDATIONS		78
	6.1 General	78
	6.2 Initial Yield	82
	6.3 Ultimate Strength	90
	6.4 Bracing Requirements	94
	6.5 Comparison with State of Pennsylvania Interim Criteria	99
7. SUMMARY AND CONCLUSIONS		104
8. NOMENCLATURE		105
9. APPENDIX		108
10. TABLES AND FIGURES		113
11. REFERENCES		187

Reproduced with permission of the copyright owner. Further reproduction prohibited without permission.

LIST OF FIGURES

		Page
Fig. 1	- Element of Curved Plate Girder	136
Fig. 2	- Displacement Components	137
Fig. 3	- Curved Plate Girder Subjected to End Loads	138
Fig. 4	- Internal Stress Resultants - No Gradient	139
Fig. 5	- Internal Stress Resultants - Gradient on Moment	140
Fig. 6	- Internal Stress Resultants - Gradient on Bimoment	141
Fig. 7	- Comparison of Deflections	142
Fig. 8	- Deflection Ratios	143
Fig. 9	- Lateral Deflection Amplification	144
Fig. 10	- Vertical Deflection Amplification	145
Fig. 11	- Amplification of Angle of Twist	146
Fig. 12	- Growth of Internal Stress Resultants with Load - 5°	147
Fig. 13	- Growth of Internal Stress Resultants with Load - 30°	148
Fig. 14	- Ratio of Internal Stress Resultants	149
Fig. 15	- Projection of Internal Stress Resultants	150
Fig. 16	- Growth of Stresses with Load - Straight Case	151
Fig. 17	- Growth of Stresses with Load - 30°	152
Fig. 18	- Experimental Test Setup	153
Fig. 19	- Cross-Sectional Deformation Loading	154
Fig. 20	- Idealized Single Span Model	155
Fig. 21	- Idealized Flange Loading	156
Fig. 22	- Stress Variations in Compression Flange	157
Fig. 23	- Initial Yield Curves - $\alpha = 2°$	158
Fig. 24	- Initial Yield Curves - $\alpha = 20°$	159

Reproduced with permission of the copyright owner. Further reproduction prohibited without permission.

LIST OF FIGURES (Cont.)

Page

Fig. 25 - Influence of Direction of Flange Moment (Initial Yield) 160

Fig. 26 - Influence of Curvature on Initial Yield 161

Fig. 27 - Contribution of Various Effects - $\alpha \approx 0°$ (Initial Yield) 162

Fig. 28 - Contribution of Various Effects - $\alpha = 20°$ (Initial Yield) 163

Fig. 29 - Interaction with AASHO Curve 164

Fig. 30 - Ultimate Strength Curves - $\alpha = 2°$ 165

Fig. 31 - Ultimate Strength Curves - $\alpha = 6°$ 166

Fig. 32 - Influence of Direction of Flange Moment - Ultimate Strength 167

Fig. 33 - Influence of Curvature on Ultimate Strength 168

Fig. 34 - Contributions of Various Effects - $\alpha \approx 0°$ (Ultimate Strength) 169

Fig. 35 - Contributions of Various Effects - $\alpha = 6°$ (Ultimate Strength) 170

Fig. 36 - Initial Yield Design Curves L/R = 0.01 171

Fig. 37 - Initial Yield Design Curves L/R = 0.05 172

Fig. 38 - Initial Yield Design Curves L/R = 0.1 173

Fig. 39 - Curvature Correction Factor ρ_B for Allowable Stress - Initial Yield 174

Fig. 40 - Curvature Correction Factor ρ_w for Allowable Stress - Initial Yield 175

Fig. 41 - Ultimate Strength Design Curves - L/R = 0.01 176

Fig. 42 - Ultimate Strength Design Curves - L/R = 0.05 177

Fig. 43 - Ultimate Strength Design Curves - L/R = 0.10 178

Fig. 44 - Curvature Correction Factor ρ_B For Allowable Stress - Ultimate Strength 179

Reproduced with permission of the copyright owner. Further reproduction prohibited without permission.

Page

Fig. 45 - Curvature Correction Factor ρ_w for Allowable Stress-Ultimate Strength 180

Fig. 46 - Brace Forces - Initial Yield 181

Fig. 47 - Brace Forces - Ultimate Strength 182

Fig. 48 - Comparison With Pennsylvania Interim Criteria - L/R = 0.01 183

Fig. 49 - Comparison With Pennsylvania Interim Criteria - L/R = 0.05 184

Fig. 50 - Comparison With Pennsylvania Interim Criteria - L/R = 0.08 185

Fig. 51 - Comparison With Test Results 186

Reproduced with permission of the copyright owner. Further reproduction prohibited without permission.

LIST OF TABLES

		Page
Table 1 -	Finite Difference Convergence	114
Table 2 -	Effect of Curvature on Critical Moment	114
Table 3 -	Effect of Bimoment on Critical Moment	114
Table 4 -	Effect of Moment Gradient on Critical Moment	115
Table 5 -	Influence of Boundary Conditions on Critical Moment	116
Table 6 -	Influence of Bimoment on Deflection (Mid Span)	117
Table 7 -	Comparison of Simple Model and Deflection Amplification Results	118
Table 8 -	Test Comparison - Braces Rigid	119
Table 9 -	Test Comparison - Measured Brace Torque	119
Table 10 -	Test Comparison - Third Approach	120
Table 11 -	Influence of Direction of Flange Moment - Initial Yield	121
Table 12 -	Influence of Residual Stress on Initial Yielding of Compression Flange	122
Table 13 -	Lateral Bracing Forces - Initial Yield	123
Table 14 -	Lateral Bracing Forces - Ultimate Strength	124
Table 15 -	Comparison of Yield and Local Buckling Moments	125
Table 16 -	Summary of Compression Flange Width - Thickness Ratio	126
Table 17 -	Approximation Involved in Design Formula - Initial Yield	127
Table 18 -	Curvature Correction Factor ρ_B For Allowable Stress - Initial Yield	128
Table 19 -	Curvature Correction Factor ρ_w For Allowable Stress - Initial Yield	129
Table 20 -	Influence of Yield Stress on Design Equations	130

Reproduced with permission of the copyright owner. Further reproduction prohibited without permission.

Page

Table 21 - Approximation Involved in Design Formula - Ultimate Strength 131

Table 22 - Curvature Correction Factor ρ_B For Allowable Stress - Ultimate Strength 132

Table 23 - Curvature Correction Factor ρ_w For Allowable Stress - Ultimate Strength 133

Table 24 - Compression Flange Brace Force Design Values - Initial Yield 134

Table 25 - Compression Flange Brace Force Design Values - Ultimate Strength 135

Reproduced with permission of the copyright owner. Further reproduction prohibited without permission.

ABSTRACT

A study was made of the lateral bending of horizontally curved girders loaded normal to the plane of curvature. An elastic stability approach was taken with results showing only a slight reduction in the buckling loads due to curvature. A deflection amplification approach indicated that even though this is true, the growth of lateral deflection is gradual starting from the beginning of loading and has a significant effect on the initial yield load of the girder. A simple model was devised for exhibiting this gradual build up of deflections and stresses and includes an approximation to the cross sectional deformation which has been observed in tests. This simple model was used to determine the initial yield and ultimate strength loads of curved girders and to determine the forces developed in the lateral braces due to lateral bending and cross sectional deformation at these loads. Design formulas and recommendations were developed for compact and non compact girders and for composite members. Requirements for bracing forces are included for these cases.

Reproduced with permission of the copyright owner. Further reproduction prohibited without permission.

ACKNOWLEDGMENTS

The author wishes to thank his advisor, Dr. C. G. Culver, for his many ideas and constant interest throughout this study. The support of the Department of Civil Engineering is appreciated. Special thanks are extended to Professor John D. Mozer for his cooperation and for the use of some of his results and to James Cook for his help with the tables and figures.

Reproduced with permission of the copyright owner. Further reproduction prohibited without permission.

1. INTRODUCTION

Lateral buckling of straight beams and plate girders has been studied extensively. Analytical solutions in both the elastic range (1,2,3)* and inelastic range (4,5) and experimental studies (6,7) have been conducted. An extensive bibliography of the research in this area was presented by Lee (8). The results of this work have been used to formulate design provisions related to lateral buckling for both buildings and bridges (9,10).

The behavior of horizontally curved beams loaded normal to the plane of curvature has also been studied extensively (19). However, existing studies deal primarily with the linear load-deformation behavior and very little work has been done on the stability of curved girders. Information on lateral buckling, similar to that established for straight girders, is currently (1971) lacking.

The purpose of this report is to develop a mathematical model for determining the lateral buckling behavior of horizontally curved girders of I-shaped cross-section loaded normal to the plane of curvature. This model will then be used to determine critical combinations of end loads. In addition, lateral bracing requirements will be evaluated, for use in both elastic and inelastic ranges.

*Numbers in parentheses refer to references listed in Section 10.

Reproduced with permission of the copyright owner. Further reproduction prohibited without permission.

2. DEVELOPMENT OF MATHEMATICAL MODEL

2.1 General

Horizontally curved beams loaded normal to the plane of curvature bend in the plane of loading and also twist. A first-order theory for determining the stresses and deformations in such structures was developed by Vlasov (3) and Dabrowski (11). For thin-walled open sections, normal stresses due to bending and torsion, nonuniform torsion or warping torsion, are developed. The importance of these normal stresses due to torsion from the design standpoint has been discussed previously (12).

In the first-order theory developed by Vlasov, the equilibrium equations were formulated on the original undeformed structure. No consideration was given to the possibility of buckling. In the development of the mathematical model in this report, the equilibrium equations will be formulated on the deformed structure and the resulting equations may be considered as second order equations. The object of the derviation is to determine linear departure equations from a reference state equilibrium configuration using a method described by I. Ojalvo and M. Newman (13). The method consists of writing each of the internal stress resultants, displacements and curvatures as the sum of two terms. The first term is the value of the variable at some reference configuration which is in equilibrium; the second is a departure from the reference configuration value. When these variables are substituted into the general equilibrium equations presented by Love (14) for a naturally bent and twisted rod and the products of departure terms neglected, a set of differential equations

Reproduced with permission of the copyright owner. Further reproduction prohibited without permission.

is obtained. Subtracting from these equations the terms which correspond to the reference state equilibrium equations leaves a set of equilibrium departure equations for the second configuration which differs slightly from the reference state.

The departure variables may be considered the changes in the displacements and curvatures, and consequently in the internal stress resultants, as the girder moves from a prebuckled to a buckled configuration. Whether or not the external loads change, in either magnitude or direction of application, during buckling depends on the physical problem considered and must be taken into account in writing the equilibrium departure equations and in specifying the boundary conditions. If the departure variables are considered small, nonlinear terms in the equilibrium departure equations may be dropped. Once a similar set of operations is performed on the moment curvature equations, a set of linear homogeneous differential equations is obtained in the departure variables which may be solved for the critical reference state loading parameters.

2.2 Derivation of Departure Equations

Consider an element of a horizontally curved plate girder with an initial radius of curvature R, as shown in its reference state configuration in Fig. 1. The girder is loaded by distributed forces q_x and q_y and distributed torque m_z. The loads are resisted by internal shears V_{x_1}, V_{y_1} and V_{z_1} and internal moments M_{x_1}, M_{y_1} and M_{z_1}. The general equilibrium equations for the reference state are (14)

Reproduced with permission of the copyright owner. Further reproduction prohibited without permission.

$$V'_{x_1} - \tau_1 V_{y_1} + \kappa_{y_1} V_{z_1} + q_x = 0 \qquad (1a)$$

$$V'_{y_1} + \tau_1 V_{x_1} - \kappa_{x_1} V_{z_1} + q_y = 0 \qquad (1b)$$

$$V'_{z_1} - \kappa_{y_1} V_{x_1} + \kappa_{x_1} V_{y_1} = 0 \qquad (1c)$$

$$M'_{x_1} - \tau_1 M_{y_1} + \kappa_{y_1} M_{z_1} - V_{y_1} = 0 \qquad (1d)$$

$$M'_{y_1} + \tau_1 M_{x_1} - \kappa_{x_1} M_{z_1} + V_{x_1} = 0 \qquad (1e)$$

$$M'_{z_1} + \kappa_{x_1} M_{y_1} - \kappa_{y_1} M_{x_1} + m_z = 0 \qquad (1f)$$

where κ_{x_1}, κ_{y_1} are the components of curvature in the x_1 and y_1 directions, τ_1 is the twist, and the primes refer to derivatives with respect to the arc length z_1. The cross-section of the girder is assumed to retain its shape and the centroid moves through displacements u_1, v_1, and w_1, measured in the direction of the original x_o, y_o, and z_o axes, and rotates by an amount Φ_1, measured in the original x_o, y_o plane, in going from the unloaded configuration, denoted as state 0, to the reference configuration, denoted as state 1, as shown in Fig. 2. The x and y axes at each state coincide with the principal centroidal axes of the cross-section, and the z axis at each state coincides with the direction of the tangent to the center line of the girder. The center line, being both the line of shear centers and the line of centroids for the doubly symmetric cross-section,

Reproduced with permission of the copyright owner. Further reproduction prohibited without permission.

is assumed inextensible. The direction cosines between the x_o, y_o, z_o axes at state 0 and the x_1, y_1, z_1 axes at state 1 are given by Love (14) as

	x_o	y_o	z_o
x_1	1	Φ_1	$-u_1' + \tau_o v_1 - \kappa_{y_o} w_1$
y_1	$-\Phi_1$	1	$-v_1' + \kappa_{x_o} w_1 - \tau_o u_1$
z_1	$u_1' - \tau_o v_1 + \kappa_{y_o} w_1$	$v_1' - \kappa_{x_o} w_1 + \tau_o u_1$	1

(2)

where the inextensibility condition

$$w_1' - u_1 \kappa_{y_o} + v_1 \kappa_{x_o} = 0 \tag{3}$$

has been used. The formulas for the curvatures and twist at state 1 given by Love are

$$\kappa_{x_1} = \kappa_{x_o} + \Phi_1 \kappa_{y_o} - (v_1' - \kappa_{x_o} w_1 + \tau_o u_1)' - \tau_o (u_1' - \tau_o v_1 + \kappa_{y_o} w_1) \tag{4a}$$

$$\kappa_{y_1} = \kappa_{y_o} - \Phi_1 \kappa_{x_o} + (u_1' - \tau_o v_1 + \kappa_{y_o} w_1)' - \tau_o (v_1' - \kappa_{x_o} w_1 + \tau_o u_1) \tag{4b}$$

$$\tau_1 = \tau_o + \Phi_1' + \kappa_{x_o} (u_1' - \tau_o v_1 + \kappa_{y_o} w_1) + \kappa_{y_o} (v_1' - \kappa_{x_o} w_1 + \tau_o u_1) \tag{4c}$$

Since the girder at state 0 lies in a plane and is circularly curved to a radius R, the values of the state 0 curvatures are $\kappa_{x_o} = \tau_o = 0$ and $\kappa_{y_o} = \frac{1}{R}$. Thus, the general inextensibility relation becomes

Reproduced with permission of the copyright owner. Further reproduction prohibited without permission.

$$w_1' - \frac{u_1}{R} = 0 \tag{5}$$

and the curvatures at state 1 become, to the first order

$$\kappa_{x_1} = -v_1'' + \frac{\phi_1}{R} \tag{6a}$$

$$\kappa_{y_1} = \frac{1}{R} + u_1'' + \frac{u_1}{R^2} \tag{6b}$$

$$\tau_1 = \phi_1' + \frac{v_1'}{R} \tag{6c}$$

The moment curvature expressions for bending and twisting of the curved beam from state O to state 1 will be taken as

$$M_{x_1} = EI_x(\kappa_{x_1} - \kappa_{x_o}) \tag{7a}$$

$$M_{y_1} = EI_y(\kappa_{y_1} - \kappa_{y_o}) \tag{7b}$$

$$M_{z_1} = GK_T(\tau_1 - \tau_o) - EI_w(\tau_1'' - \tau_o'') \tag{7c}$$

which reduce to

$$M_{x_1} = EI_x(-v_1'' + \frac{\phi_1}{R}) \tag{8a}$$

$$M_{y_1} = EI_y(u_1'' + \frac{u_1}{R^2}) \tag{8b}$$

$$M_{z_1} = GK_T(\phi_1' + \frac{v_1'}{R}) - EI_w(\phi_1''' + \frac{v_1'''}{R}) \tag{8c}$$

Reproduced with permission of the copyright owner. Further reproduction prohibited without permission.

Eqs. 8 have been used previously by Vlasov (3) and Dabrowski (11). They are a simple extension to curved beams of the accepted constitutive equations for straight beams. Eqs. 8a and 8b are extensions of the Bernoulli-Euler hypothesis. The first term of 8c expresses the proportionality of the change of twist to the torque due to the action of Saint-Venant shearing stresses, and the second term relates the second derivative of the twist to the torque due to the action of warping normal stresses. The fact that equation 8c follows from the assumption of linear elastic behavior and the usual assumptions of ordinary beam theory has been demonstrated by Dabrowski (11) and Cheney (15).

Eqs. 1, 6, and 8 completely determine the reference state equilibrium configuration for a given loading. It is now possible to determine the departure equations.

It is assumed that the applied distributed loads q_x, q_y, and m_z change neither in direction or magnitude in moving to the departure configuration, denoted as state 2, as shown in Fig. 2. Since the equilibrium departure equations are written on the state 2 axes, however, there will appear in these equations loadings which are the projections of q_x, q_y, and m_z on the state 2 axes. The girder moves through displacements u_2, v_2, and w_2, measured in the direction of the x_1, y_1, z_1 axes, in moving to state 2. The direction cosines between state 2 and state 1 are

Reproduced with permission of the copyright owner. Further reproduction prohibited without permission.

	x_1	y_1	z_1
x_2	1	Φ_2	$-u_2' + \tau_1 v_2 - \kappa_{y_1} w_2$
y_2	$-\Phi_2$	1	$-v_2' + \kappa_{x_1} w_2 - \tau_1 u_2$
z_2	$u_2' - \tau_1 v_2 + \kappa_{y_2} w_2$	$v_2' - \kappa_{x_1} w_2 + \tau_1 u_2$	1

(9)

where the inextensibility condition

$$w_2' - u_2 \kappa_{y_1} + v_2 \kappa_{x_1} = 0 \tag{10}$$

has again been used. Using Eqs. 6 and neglecting nonlinear product terms gives the following first-order expressions for these direction cosines

	x_1	y_1	z_1
x_2	1	Φ_2	$-u_2' - \frac{w_2}{R}$
y_2	$-\Phi_2$	1	$-v_2'$
z_2	$u_2' + \frac{w_2}{R}$	v_2'	1

(11)

and the inextensibility condition is

$$w_2' - \frac{u_2}{R} = 0 \tag{12}$$

Assuming that $\frac{w_2}{R}$ is small compared to u_2' (3), the projections of q_x, q_y, and m_z on the state 2 axes can be written as

Reproduced with permission of the copyright owner. Further reproduction prohibited without permission.

$$q_{x_2} = q_x + \Phi_2 q_y \tag{13a}$$

$$q_{y_2} = -\Phi_2 q_x + q_y \tag{13b}$$

$$q_{z_2} = u_2' q_x + v_2' q_y \tag{13c}$$

$$m_{x_2} = -u_2' m_z \tag{13d}$$

$$m_{y_2} = -v_2' m_z \tag{13e}$$

$$m_{z_2} = m_z \tag{13f}$$

In moving from state 1 to state 2, the curvatures and internal stress resultants change slightly. Denoting the state 2 values of the curvatures and the twist as

$$\kappa_{x_2} = \kappa_{x_1} + \Delta\kappa_x \tag{14a}$$

$$\kappa_{y_2} = \kappa_{y_1} + \Delta\kappa_y \tag{14b}$$

$$\tau_2 = \tau_1 + \Delta\tau \tag{14c}$$

and of the internal stress resultants as

$$V_{x_2} = V_{x_1} + \Delta V_x \tag{15a}$$

$$V_{y_2} = V_{y_1} + \Delta V_y \tag{15b}$$

$$V_{z_2} = V_{z_1} + \Delta V_z \tag{15c}$$

$$M_{x_2} = M_{x_1} + \Delta M_x \tag{15d}$$

$$M_{y_2} = M_{y_1} + \Delta M_y \tag{15e}$$

$$M_{z_2} = M_{z_1} + \Delta M_z \tag{15f}$$

Reproduced with permission of the copyright owner. Further reproduction prohibited without permission.

the state 2 equilibrium equations become

$$(V_{x_1}+\Delta V_x)' - (\tau_1+\Delta\tau)(V_{y_1}+\Delta V_y) + (\kappa_{y_1}+\Delta\kappa_y)(V_{z_1}+\Delta V_z) + q_x + \Phi_2 q_y = 0 \tag{16a}$$

$$(V_{y_1}+\Delta V_y)' + (\tau_1+\Delta\tau)(V_{x_1}+\Delta V_x) - (\kappa_{x_1}+\Delta\kappa_x)(V_{z_1}+\Delta V_z) - \Phi_2 q_x + q_y = 0 \tag{16b}$$

$$(V_{z_1}+\Delta V_z)' - (\kappa_{y_1}+\Delta\kappa_y)(V_{x_1}+\Delta V_x) + (\kappa_{x_1}+\Delta\kappa_x)(V_{y_1}+\Delta V_y) + u_2' q_x + v_2' q_y = 0 \tag{16c}$$

$$(M_{x_1}+\Delta M_x)' - (\tau_1+\Delta\tau)(M_{y_1}+\Delta M_y) + (\kappa_{y_1}+\Delta\kappa_y)(M_{z_1}+\Delta M_z) - (V_{y_1}+\Delta V_y) - u_2' m_2 = 0 \tag{16d}$$

$$(M_{y_1}+\Delta M_y)' + (\tau_1+\Delta\tau)(M_{x_1}+\Delta M_x) - (\kappa_{x_1}+\Delta\kappa_x)(M_{z_1}+\Delta M_z) + (V_{x_1}+\Delta V_x) - v_2' m_z = 0 \tag{16e}$$

$$(M_{z_1}+\Delta M_z)' + (\kappa_{x_1}+\Delta\kappa_x)(M_{y_1}+\Delta M_y) - (\kappa_{y_1}+\Delta\kappa_y)(M_{x_1}+\Delta M_x) + m_z = 0 \tag{16f}$$

In these equations, the primes denote differentiation with respect to z_2, the arc length at state 2. Since inextensibility of the center line has been assumed, derivatives with respect to z_1 or z_2 are identical.

Expanding Eqs. 16, dropping quadratic terms in the departure variables, and subtracting off the reference state equilibrium equations, Eqs. 1, the following equilibrium departure equations are obtained

$$\Delta V_x' - \tau_1 \Delta V_y - \Delta\tau V_{y_1} + \kappa_{y_1}\Delta V_z + \Delta\kappa_y V_{z_1} + \Phi_2 q_y = 0 \tag{17a}$$

$$\Delta V_y' + \tau_1 \Delta V_x + \Delta\tau V_{x_1} - \kappa_{x_1}\Delta V_z - \Delta\kappa_x V_{z_1} - \Phi_2 q_x = 0 \tag{17b}$$

$$\Delta V_z' - \kappa_{y_1}\Delta V_x - \Delta\kappa_y V_{x_1} + \kappa_{x_1}\Delta V_y + \Delta\kappa_x V_{y_1} + u_2' q_x + v_2' q_y = 0 \tag{17c}$$

$$\Delta M_x' - \tau_1 \Delta M_y - \Delta\tau M_{y_1} + \kappa_{y_1}\Delta M_z + \Delta\kappa_y M_{z_1} - \Delta V_y - u_2' m_z = 0 \tag{17d}$$

$$\Delta M_y' + \tau_1 \Delta M_x + \Delta\tau M_{x_1} - \kappa_{x_1}\Delta M_z - \Delta\kappa_x M_{z_1} + \Delta V_x - v_2' m_z = 0 \tag{17e}$$

$$\Delta M_z' + \kappa_{x_1}\Delta M_y + \Delta\kappa_x M_{y_1} - \kappa_{y_1}\Delta M_x - \Delta\kappa_y M_{x_1} = 0 \tag{17f}$$

Reproduced with permission of the copyright owner. Further reproduction prohibited without permission.

Again making use of Love's formulas, the curvatures at state 2 become

$$\kappa_{x_2} = \kappa_{x_1} + \Phi_2\kappa_{y_1} - (v_2' - \kappa_{x_1}w_2 + \tau_1 u_2)' - \tau_1(u_2' - \tau_1 v_2 + \kappa_{y_1}w_2) \quad (18a)$$

$$\kappa_{y_2} = \kappa_{y_1} - \Phi_2\kappa_{x_1} + (u_2' - \tau_1 v_2 + \kappa_{y_1}w_2)' - \tau_1(v_2' - \kappa_{x_1}w_2 + \tau_1 u_2) \quad (18b)$$

$$\tau_2 = \tau_1 + \Phi_2' + \kappa_{x_1}(u_2' - \tau_1 v_2 + \kappa_{y_1}w_2) + \kappa_{y_1}(v_2' - \kappa_{x_1}w_2 + \tau_1 u_2) \quad (18c)$$

Using Eqs. 6 and the inextensibility condition, Eq. 12, Eqs. 18 to the first order reduce to

$$\kappa_{x_2} = -v_1'' + \frac{\Phi_1}{R} - v_2'' + \frac{\Phi_2}{R} \quad (19a)$$

$$\kappa_{y_2} = \frac{1}{R} + u_1'' + \frac{u_1}{R^2} + u_2'' + \frac{u_2}{R^2} \quad (19b)$$

$$\tau_2 = \Phi_1' + \frac{v_1'}{R} + \Phi_2' + \frac{v_2'}{R} \quad (19c)$$

Noting the form of Eqs. 14, it is possible to write for the curvature departures

$$\Delta\kappa_x = -v_2'' + \frac{\Phi_2}{R} \quad (20a)$$

$$\Delta\kappa_y = u_2'' + \frac{u_2}{R^2} \quad (20b)$$

$$\Delta\tau = \Phi_2' + \frac{v_2'}{R} \quad (20c)$$

The moment curvature expressions for bending and twisting of the curved beam from state 0 to state 2 will be taken as

Reproduced with permission of the copyright owner. Further reproduction prohibited without permission.

$$M_{x_2} = EI_x(\kappa_{x_2} - \kappa_{x_o}) \tag{21a}$$

$$M_{y_2} = EI_y(\kappa_{y_2} - \kappa_{y_o}) \tag{21b}$$

$$M_{z_2} = GK_T(\tau_2 - \tau_o) - EI_w(\tau_2'' - \tau_o'') \tag{21c}$$

Substituting Eqs. 14, Eqs. 15d-15f, and subtracting Eqs. 7, the moment curvature departure equations become

$$\Delta M_x = EI_x \Delta\kappa_x \tag{22a}$$

$$\Delta M_y = EI_y \Delta\kappa_y \tag{22b}$$

$$\Delta M_z = GK_T \Delta\tau - EI_w \Delta\tau'' \tag{22c}$$

Eqs. 17, 20, and 22 completely determine the departure from the reference state configuration, if values of the reference state internal stress resultants are obtained from solution of Eqs. 1, 6, and 8. Appropriate boundary conditions must be imposed, of course, for the solution of either set of equations.

If the further assumption is made that products of internal stress resultants and displacement variables for the reference state can be neglected, Eqs. 1 become

$$V_{x_1}' + \frac{V_z}{R} + q_x = 0 \tag{23a}$$

$$V_{y_1}' + q_y = 0 \tag{23b}$$

$$V_{z_1}' - \frac{V_{x_1}}{R} = 0 \tag{23c}$$

$$M_{x_1}' + \frac{M_{z_1}}{R} - V_{y_1} = 0 \tag{23d}$$

Reproduced with permission of the copyright owner. Further reproduction prohibited without permission.

$$M'_{y_1} + V_{x_1} = 0 \tag{23e}$$

$$M'_{z_1} - \frac{M_{x_1}}{R} + m_z = 0 \tag{23f}$$

Eqs. 23, 6, and 8 are the equations used by Vlasov (3) and Dabrowski (11) for determining the linear load-deformation response of curved girders. These equations are assumed to be adequate for determining expressions for the internal stress resultants at state 1 in terms of the external loading parameters. Making the further approximation that reference state curvature and twist expressions can be taken as equal to the unloaded values in the equilibrium departure equations, Eqs. 17 reduce to

$$\Delta V'_x - \Delta\tau V_{y_1} + \frac{\Delta V_z}{R} + \Delta\kappa_y V_{z_1} + \Phi_2 q_y = 0 \tag{24a}$$

$$\Delta V'_y + \Delta\tau V_{x_1} - \Delta\kappa_x V_{z_1} - \Phi_2 q_x = 0 \tag{24b}$$

$$\Delta V'_z - \frac{\Delta V_x}{R} - \Delta\kappa_y V_{x_1} + \Delta\kappa_x V_{y_1} + u'_2 q_x + v'_2 q_y = 0 \tag{24c}$$

$$\Delta M'_x - \Delta\tau M_{y_1} + \frac{\Delta M_z}{R} + \Delta\kappa_y M_{z_1} - \Delta V_y - u'_2 m_z = 0 \tag{24d}$$

$$\Delta M'_y + \Delta\tau M_{x_1} - \Delta\kappa_x M_{z_1} + \Delta V_x - v'_2 m_z = 0 \tag{24e}$$

$$\Delta M'_z + \Delta\kappa_x M_{y_1} - \frac{\Delta M_x}{R} - \Delta\kappa_y M_{x_1} = 0 \tag{24f}$$

Eliminating the internal shear departures ΔV_x, ΔV_y, and ΔV_z from Eqs. 24 gives

Reproduced with permission of the copyright owner. Further reproduction prohibited without permission.

$$\Delta M_y''' + (\Delta\tau M_{x_1})'' - (\Delta\kappa_x M_{z_1})'' + (\Delta\tau V_{y_1})' - (\Delta\kappa_y V_{z_1})' + \frac{\Delta M_y'}{R} + \frac{\Delta\tau M_{x_1}}{R^2}$$

$$- \frac{\Delta\kappa_x M_{z_1}}{R^2} - \frac{\Delta\kappa_y V_{x_1}}{R} + \frac{\Delta\kappa_x V_{y_1}}{R} + \frac{u_2' q_x}{R} + \frac{v_2' q_y}{R} - (\Phi_2 q_y)'$$

$$- \frac{v_2' m_z}{R^2} - (v_2' m_z)'' = 0 \qquad (25a)$$

$$\Delta M_x'' - (\Delta\tau M_{y_1})' + (\Delta\kappa_y M_{z_1})' + \frac{\Delta M_z'}{R} + \Delta\tau V_{x_1} - \Delta\kappa_x V_{z_1} - \Phi_2 q_x$$

$$- (u_2' m_z)' = 0 \qquad (25b)$$

$$\Delta M_z' + \Delta\kappa_x M_{y_1} - \Delta\kappa_y M_{x_1} - \frac{\Delta M_x}{R} = 0 \qquad (25c)$$

Eqs. 25, Eqs. 20 and Eqs. 22 determine a set of linear homogeneous, differential equations which can be used to determine critical values of the loading parameters.

2.3 Girder Subjected to End Loads

Consider a segment of a curved plate girder of arc length L and central angle α subjected to applied end moments and bimoments, as shown in Fig. 3. The bimoment which results from non-uniform torsion is represented vectorially by equal and opposite flange moments. This loading, as shown, represents a positive bimoment. The internal stress resultants at state 1 can be found from the solution of the reference state equations, Eqs. 8 and 23. This was done by Dabrowski (11) and the following expressions were determined (note that the sign convention for bimoment adopted herein is opposite to that used by Dabrowski and in this respect Eqs. 26 differ from the expressions given in Reference 11).

Reproduced with permission of the copyright owner. Further reproduction prohibited without permission.

$$V_{x_1} = 0 \tag{26a}$$

$$V_{y_1} = \frac{M}{L}(\eta - 1) - \frac{B}{LR}(\beta - 1) \tag{26b}$$

$$V_{z_1} = 0 \tag{26c}$$

$$M_{x_1} = M\left[(\sin\frac{L-z}{R} + \eta \sin\frac{z}{R})/\sin\frac{L}{R}\right] \tag{26d}$$

$$M_{y_1} = 0 \tag{26e}$$

$$M_{z_1} = M\left[(\cos\frac{L-z}{R} - \eta \cos\frac{z}{R})/\sin\frac{L}{R}\right] + \frac{MR}{L}(\eta - 1) - \frac{B}{L}(\beta - 1) \tag{26f}$$

The segment was considered simply supported at the ends, consequently the boundary conditions used to obtain Eqs. 26 were $u_1 = u_1'' = v_1 = v_1'' = \phi_1 = 0$ at $z_1 = 0, L$; $-v_1'' = \frac{M}{EI_x}$ and $\phi_1'' + \frac{v_1''}{R} = \frac{B}{EI_w}$ at $z_1 = 0$; and $-v_1'' = \frac{\eta M}{EI_x}$ and $\phi_1'' + \frac{v_1''}{R} = \frac{\beta B}{EI_w}$ at $z_1 = L$.

Taking into account Eqs. 26a, 26c, and 26e, Eqs. 25 become

$$\Delta M_y''' + \frac{\Delta M_y'}{R^2} + (\Delta\tau M_{x_1})'' - (\Delta\kappa_x M_{z_1})'' + (\Delta\tau V_{y_1})' + \frac{\Delta\tau M_{x_1}}{R^2} - \frac{\Delta\kappa_x M_{z_1}}{R^2} + \frac{\Delta\kappa_x V_{y_1}}{R} = 0 \tag{27a}$$

$$\Delta M_x'' + \frac{\Delta M_z'}{R} + (\Delta\kappa_y M_{z_1})' = 0 \tag{27b}$$

$$\Delta M_z' - \frac{\Delta M_x}{R} - \Delta\kappa_y M_{x_1} = 0 \tag{27c}$$

Reproduced with permission of the copyright owner. Further reproduction prohibited without permission.

There are two possible types of applied end loads to be considered: (1) end moments and bimoments which follow the deformation of the girder during buckling (analogous to hydrostatic loading), (2) end loads which remain constant in direction. In either case, they will be considered constant in magnitude. Bolotin (16) discusses both types of loading and points out that buckling equations derived by the Euler method of elastic stability, which is the method employed above, give correct solutions to problems where the external loads are conservative, as in Case 2. If external loads are non-conservative, as in Case 1, the Euler method may not describe the buckling problem completely, and the oscillatory forms of instability discussed by Bolotin must be investigated. In some situations for Case 1 loading, the Euler method will yield linear, homogeneous differential equations for which no eigenvalues exist, notably the fixed-free column subjected to an axial load which rotates with the free end of the column during buckling. This investigation considers only Case 2 loading.

Noting that the terms $(\Delta\tau V_{y_1})' + \frac{\Delta\kappa_x V_{y_1}}{R}$ can be expanded and reduced to $(\Phi_2'' + \frac{\Phi_2}{R^2})V_{y_1}$, it becomes evident that Eq. 27a can be written in the form $f''(z) + \frac{f(z)}{R^2} = 0$, where

$$f(z) = \Delta M_y' + \Delta\tau M_{x_1} - \Delta\kappa_x M_{z_1} + \Phi_2 V_{y_1} \tag{28}$$

By substituting from Eqs. 20 and making use of Eqs. 23b, 23d, and 23f, Eq. 28 can be written as

$$f(z) = \Delta M_y' + (\Phi_2 M_{x_1})' + (v_2' M_{z_1})' \tag{29}$$

Reproduced with permission of the copyright owner. Further reproduction prohibited without permission.

Keeping in mind that the end moments and bimoments are constant in magnitude and direction, it is evident that they must be balanced by the internal stress resultants at any arbitrary section of the girder, for the girder to be in equilibrium. Thus, if the departure configuration, state 2, is to be in equilibrium, the internal stress resultants at an arbitrary section must be statically equivalent to the internal stress resultants at the same section for the reference state equilibrium configuration, state 1. Indeed, each set of internal stress resultants must balance the external load which remains constant in magnitude and direction during buckling. Using the direction cosines presented above, and noting Fig. 2, the moment to the first order about the state 2 y_2-axis becomes

$$M_{y_2} = -\Phi_2 M_{x_1} - v_2' M_{z_1} \tag{30}$$

If the assumption is made, as above, that the state 1 curvatures may be taken as identical to the unloaded values, the moment-curvature expression, Eq. 21b may be written

$$M_{y_2} = EI_y(\kappa_{y_2} - \kappa_{y_o}) = EI_y(\kappa_{y_1} + \Delta\kappa_y - \kappa_{y_o}) \cong EI_y \Delta\kappa_y \tag{31}$$

Combining Eqs. 30 and 31, making use of Eq. 22b, the buckling condition is obtained that

$$\Delta M_y + \Phi_2 M_{x_1} + v_2' M_{z_1} = 0 \tag{32}$$

Differentiating Eq. 32, it becomes evident from Eq. 28, that Eq. 27a can be broken down into the simple form $f(z) = 0$, or

Reproduced with permission of the copyright owner. Further reproduction prohibited without permission.

$$\Delta M_y' + \Delta\tau M_{x_1} - \Delta\kappa_x M_{z_1} + \phi_2 V_{y_1} = 0 \tag{33}$$

For convenience in handling the boundary conditions, Eq. 33 is differentiated once to give

$$\Delta M_y'' + (\Delta\tau M_{x_1})' - (\Delta\kappa_x M_{z_1})' + (\phi_2 V_{y_1})' = 0 \tag{34}$$

Eqs. 34, 27b, and 27c together with Eqs. 20, 22, and 26 determine a set of linear, homogeneous differential equations for buckling of a simply supported curved girder loaded by end moments and bimoments. Substituting Eqs. 20 and 22, into Eqs. 34, 27b, and 27c, the buckling equations, expressed in terms of the departure state displacements, become

$$EI_y\left[u_2^{IV} + \frac{u_2''}{R^2}\right] + \left[M_{x_1}\phi_2'\right]' + \left[\frac{M_{x_1}v_2'}{R}\right]' + \left[M_{z_1}v_2''\right]' - \left[\frac{M_{z_1}\phi_2}{R}\right]' + V_{y_1}\phi_2' = 0 \tag{35a}$$

$$\left[EI_x + \frac{EI_w}{R^2}\right]v_2^{IV} + \frac{EI_w\phi_2^{IV}}{R} - \frac{GK_T v_2''}{R^2} - \left[\frac{EI_x + GK_T}{R}\right]\phi_2'' - \left[M_{z_1}u_2''\right]' - \left[\frac{M_{z_1}u_2}{R^2}\right]' = 0 \tag{35b}$$

$$EI_w\phi_2^{IV} + \frac{EI_w v_2^{IV}}{R} - GK_T\phi_2'' - \left[\frac{EI_x + GK_T}{R}\right]v_2'' + \frac{EI_x\phi_2}{R^2} + M_{x_1}u_2'' + \frac{M_{x_1}u_2}{R^2} = 0 \tag{35c}$$

Letting R approach infinity, setting $M_{z_1} = 0$, and setting $V_{y_1} = M_{x_1}'$ reduces Eqs. 35 to the equations for the lateral-torsional buckling of a straight girder subject to unequal end moments given by Galambos (6).

Reproduced with permission of the copyright owner. Further reproduction prohibited without permission.

Before a solution to Eqs. 35 can be found, it is necessary to establish the boundary conditions appropriate for a simply supported girder. A simple support is considered to be a support where displacements u_2, v_2, and rotation ϕ_2 are zero. Thus, the geometric boundary conditions $u_2 = v_2 = \phi_2 = 0$ at $z_2 = 0,L$ are immediately established. In addition, using the direction cosines, Eqs. 11, and writing equilibrium at the boundaries in the direction of the state 2 axes, the following statical boundary conditions are established.

$$(M_{x_1} + \Delta M_x)\Big|_{z_2=0,L} = \bar{M}_x\Big|_{z_2=0,L} - (u_2'\bar{M}_z)\Big|_{z_2=0,L} \tag{36a}$$

$$(M_{y_1} + \Delta M_y)\Big|_{z_2=0,L} = \bar{M}_y\Big|_{z_2=0,L} - (v_2'\bar{M}_z)\Big|_{z_2=0,L} \tag{36b}$$

$$(M_{z_1} + \Delta M_z)\Big|_{z_2=0,L} = (u_2'\bar{M}_x)\Big|_{z_2=0,L} - (v_2'\bar{M}_y)\Big|_{z_2=0,L} + \bar{M}_z\Big|_{z_2=0,L} \tag{36c}$$

where $\bar{M}_x$, $\bar{M}_y$, and $\bar{M}_z$ are the reactions at the ends of the girder. Moreover, writing the boundary conditions for bending of the girder to state 1, utilizing the assumption that the external loading remains constant as the girder moves from state 1 to state 2 yields

$$M_{x_1}\Big|_{z_2=0,L} = \bar{M}_x\Big|_{z_2=0,L} \tag{37a}$$

$$M_{y_1}\Big|_{z_2=0,L} = \bar{M}_y\Big|_{z_2=0,L} \tag{37b}$$

Reproduced with permission of the copyright owner. Further reproduction prohibited without permission.

$$M_{z_1}\Big|_{z_2=0,L} = \bar{M}_z\Big|_{z_2=0,L} \tag{37c}$$

If the conditions, Eqs. 37, are substituted into Eqs. 36, for the case of loading by end moments and bimoments (where $M_{y_1} = 0$), the following statical boundary conditions are obtained

$$\Delta M_x\Big|_{z_2=0,L} = (-u_2' M_{z_1})\Big|_{z_2=0,L} \tag{38a}$$

$$\Delta M_y\Big|_{z_2=0,L} = (-v_2' M_{z_1})\Big|_{z_2=0,L} \tag{38b}$$

$$\Delta M_z\Big|_{z_2=0,L} = (u_2' M_{x_1})\Big|_{z_2=0,L} \tag{38c}$$

These conditions have been established as statical conditions without regard to the geometrical conditions discussed above. It is evident that Eqs. 38a,b are consistent with these geometrical conditions in that there is no restraint implied to bending about the x_2 and y_2 axes. However it is impossible to prescribe the geometrical condition $\phi_2 = 0\Big|_{z_2=0,L}$ as well as the statical condition, Eq. 38c, at the same time since the former implies a restraint to twisting about the z_2 axis. This is analogous to the situation that occurs when natural boundary conditions are derived using the Calculus of Variations. A product of a statical boundary condition and a geometrical boundary condition is found to be equal to zero. Either one or the other condition should be set to zero, but not both (1). Thus Eq. 38c is not an appropriate statical boundary condition for simple supports.

Reproduced with permission of the copyright owner. Further reproduction prohibited without permission.

Eq. 38c can be replaced by the condition that the ends of the girder be free to warp during buckling. This condition is commonly used to describe simple supports in the analysis of lateral buckling of straight girders. It is equivalent to the condition that the bimoment doesn't change during buckling, and may be written

$$\Delta B\Big|_{z_2=0,L} = 0 \tag{39}$$

Introducing into Eqs. 38a,b and Eq. 39 the moment curvature expressions, Eqs. 20 and the well known relationship (11)

$$\Delta B = EI_w \Delta\tau' = EI_w\left(\phi_2'' + \frac{v_2''}{R}\right) \tag{40}$$

the statical boundary conditions may be written as

$$EI_x v_2''\Big|_{z_2=0,L} - \left(u_2' M_{z_1}\right)\Big|_{z_2=0,L} = 0 \tag{41a}$$

$$EI_y u_2''\Big|_{z_2=0,L} + \left(v_2' M_{z_1}\right)\Big|_{z_2=0,L} = 0 \tag{41b}$$

$$\left(\phi_2'' + \frac{v_2''}{R}\right)\Big|_{z_2=0,L} = 0 \tag{41c}$$

The girder of length L shown in Fig. 3 could be considered to be a segment between supports of a continuous girder, and the end loads could be considered to be the values of the moment and bimoment obtained from an analysis of the continuous girder system. In such a system, the portions of the girders not shown in Fig. 3 would provide some restraint

Reproduced with permission of the copyright owner. Further reproduction prohibited without permission.

to the rotations $u_2'\big|_{z=0,L}$ and $v_2'\big|_{z_2=0,L}$ as well as the warping displacements over the interior supports during buckling and a limiting case could be obtained by taking $u_2'\big|_{z_2=0,L} = v_2'\big|_{z_2=0,L} = \phi_2'\big|_{z_2=0,L} = 0$. Even though a complete solution would require formulating the buckling problem for the continuous girder as a system, the limiting case may yield some useful results. The boundary conditions in this case are entirely geometrical and can be written simply as $u_2 = v_2 = \phi_2 = u_2' = v_2' = \phi_2' = 0$ at $z_2 = 0,L$.

Eqs. 35 together with Eqs. 26b, 26d, and 26f and either set of boundary conditions discussed above constitute a linear eigenvalue problem which can be solved for critical combinations of M, M_F, η, and β.

The assumptions made above that the internal stress resultants at state 1 can be obtained from the linearized equations, Eqs. 23, and that the geometry of state 1 configuration can be taken as identical to that of the unloaded girder in the determination of the departure equations, Eqs. 35, were also made by M. Ojalvo, et al. (17), and by I. Ojalvo and M. Newman (13). The first assumption was made in order to avoid the necessity of solving the nonlinear equations for state 1, Eqs. 1. It is still possible to include the effect of state 1 displacements, with some approximation, by including the values of the state 1 curvatures obtained from the linear state 1 equations in the determination of the departure equations. Based on the results discussed by O. Pettersson (18) from a similar type analysis of the lateral-torsional buckling of straight girders,

Reproduced with permission of the copyright owner. Further reproduction prohibited without permission.

including the effects of reference state deflections, however, the authors believe that, at least for practical girders, such a step will have little effect on the critical loads obtained. For this reason and because of the considerable simplification obtained in the final departure equations, the second assumption is employed in this analysis.

The above derivation is identical to that presented in Reference 20, with the exception that while Eqs. 38c and 41c were discussed, they were considered to be roughly equivalent. It can now be seen, however, that this is not true since Eq. 38c is not appropriate.

2.4 Deflection Amplification Problem

It is possible to obtain a linearized description of the bending of the girder from state 0 to state 2 using the relationships developed in Section 2.3. This is done by adding the linearized equations describing the girder's behavior in bending to state 1 to the departure equations describing the girder's behavior in further bending to state 2.

Eliminating the internal shears Eq. 23 becomes

$$M''_{x_1} + \frac{M'_{z_1}}{R} + q_y = 0 \tag{42a}$$

$$M'''_{y_1} + \frac{M'_{y_1}}{R^2} - q'_x = 0 \tag{42b}$$

$$M''_{z_1} - \frac{M'_{x_1}}{R} + m'_z = 0 \tag{42c}$$

Adding these equations to Eqs. 27, where Eq. 27c has been differentiated

Reproduced with permission of the copyright owner. Further reproduction prohibited without permission.

once, for the case of a girder loaded by end moments and bimoments ($q_y = q_x' = m_z' = 0$), gives

$$M_{x_1}'' + \Delta M_x'' + \frac{M_{z_1}'}{R} + \frac{\Delta M_z'}{R} + \left(\Delta\kappa_y M_{z_1}\right)' = 0 \tag{43a}$$

$$M_{y_1}''' + \Delta M_y''' + \frac{M_{y_1}'}{R^2} + \frac{\Delta M_y'}{R^2} + \left(\Delta\tau M_{x_1}\right)'' - \left(\Delta\kappa_x M_{z_1}\right)'' + \left(\Delta\tau V_{y_1}\right)'$$

$$+ \frac{\Delta\tau M_{x_1}}{R^2} - \frac{\Delta\kappa_x M_{z_1}}{R^2} + \frac{\Delta\kappa_x V_{y_1}}{R} = 0 \tag{43b}$$

$$M_{z_1}'' + \Delta M_z'' - \frac{M_{x_1}'}{R} - \frac{\Delta M_x'}{R} - \left(\Delta\kappa_y M_{x_1}\right)' = 0 \tag{43c}$$

These equations represent the bending of the girder from state 0 to state 2. The appropriate boundary conditions are obtained by adding the boundary conditions appropriate for the girder's behavior in bending from state 0 to state 1 given by

$$M_{y_1} = 0 \qquad M_{x_1} = M \qquad B_1 = B \qquad \text{at } z = 0 \tag{44a}$$

$$M_{y_1} = 0 \qquad M_{x_1} = \eta M \qquad B_1 = \beta B \qquad \text{at } z = L \tag{44b}$$

to the boundary conditions appropriate for the girder's behavior in bending from state 1 to state 2, Eqs. 41, to obtain

$$M_{x_1} + \Delta M_x + u_2' M_{z_1} = M \qquad M_{y_1} + \Delta M_y + v_2' M_{z_1} = 0$$

$$B_1 + \Delta B = B \qquad \text{at } z = 0 \tag{45a}$$

Reproduced with permission of the copyright owner. Further reproduction prohibited without permission.

and

$$M_{x_1} + \Delta M_x + u_2' M_{z_1} = \eta M \qquad M_{y_1} + \Delta M_y + v_2' M_{z_1} = 0$$

$$B_1 + \Delta B = \beta B \qquad \text{at } z = L \tag{45b}$$

Rewriting Eqs. 43 and 45, making use of Eqs. 15, yields

$$M_{x_2}'' + \frac{M_{z_2}'}{R} + \left(\Delta\kappa_y M_{z_1}\right)' = 0 \tag{46a}$$

$$M_{y_2}''' + \frac{M_{y_2}'}{R^2} + \left(\Delta\tau M_{x_1}\right)'' - \left(\Delta\kappa_x M_{z_1}\right)'' + \left(\Delta\tau V_{y_1}\right)' + \frac{\Delta\tau M_{x_1}}{R^2} - \frac{\Delta\kappa_x M_{z_1}}{R^2}$$

$$+ \frac{\Delta\kappa_x V_{y_1}}{R} = 0 \tag{46b}$$

$$M_{z_2}'' - \frac{M_{x_2}'}{R} - \left(\Delta\kappa_y M_{x_1}\right)' = 0 \tag{46c}$$

and the boundary conditions

$$M_{x_2} + u_2' M_{z_1} = M\,, \qquad M_{y_2} + v_2' M_{z_1} = 0\,, \qquad B_2 = B \quad \text{at } z = 0 \tag{47a}$$

$$M_{x_2} + u_2' M_{z_1} = \eta M\,, \qquad M_{y_2} + v_2' M_{z_1} = 0\,, \qquad B_2 = \beta B \quad \text{at } z = L \tag{47b}$$

Eq. 46b is of the same form as Eq. 27a. Using similar arguments to those used above in reducing the order of Eq. 27a, Eq. 46b can be written as

$$M_{y_2}'' + \left(\Delta\tau M_{x_1}\right)' - \left(\Delta\kappa_x M_{z_1}\right)' + \left(\phi_2 V_{y_1}\right)' = 0 \tag{48}$$

If as before the approximation is made to neglect state 1 deflections while retaining the state 1 internal stress resultants and

Reproduced with permission of the copyright owner. Further reproduction prohibited without permission.

using the moment curvature relations, Eqs. 19 and 20, a set of deflection amplification equations results which are identical to Eqs. 35. In addition, the following boundary conditions are obtained

$$EI_x v_2'' - u_2' M_{z_1} = -M \qquad EI_y u_2'' + v_2' M_{z_1} = 0$$

$$EI_w\left(\phi_2'' + \frac{v_2''}{R}\right) = B \qquad \text{at } z = 0 \tag{49a}$$

and

$$EI_x v_2'' - u_2' M_{z_1} = -\eta M \qquad EI_y u_2'' + v_2' M_{z_1} = 0$$

$$EI_w\left(\phi_2'' + \frac{v_2''}{R}\right) = \beta B \qquad \text{at } z = L \tag{49b}$$

which are the same as Eq. 41 but for the addition of a right hand side. Thus a deflection amplification analysis leads to the same governing equations as the departure analysis, with the difference being that the deflection amplification boundary conditions are non-homogeneous while the departure boundary conditions are homogeneous. Additional discussion of the relationship between these two forms of analysis will be presented in Chapter 3.

Reproduced with permission of the copyright owner. Further reproduction prohibited without permission.

3. NUMERICAL RESULTS

3.1 Method of Solution

In order to illustrate the influence of the significant parameters on the critical loads, it is convenient to nondimensionalize the preceding equations. Eqs. 35 may be written in nondimensional form by introducing the following parameters.

$$M^* = \frac{M}{(M_{cr})_{st}} \quad , \quad B^* = \frac{B}{L(M_{cr})_{st}} \quad , \quad \bar{u} = \frac{u_2}{L} \quad , \quad \bar{v} = \frac{v_2}{L}, \quad \bar{\Phi} = \Phi_2, \quad \bar{z} = \frac{z_2}{L} \tag{50}$$

where $(M_{cr})_{st}$ is the critical moment for lateral-torsional buckling of a simply supported straight girder of length L loaded by equal end moments given by

$$(M_{cr})_{st} = \frac{\pi}{L}\sqrt{EI_y\left[\pi^2\frac{EI_w}{L^2} + GK_T\right]} \tag{51}$$

Using Eqs. 50 and incorporating Eqs. 26, Eqs. 35 become

$$\gamma_1\bar{u}^{IV} + \alpha^2\gamma_1\bar{u}'' + M^*\left[F_1'\bar{\Phi}' + F_1\bar{\Phi}'' + \alpha F_1'\bar{v}' + \alpha F_1\bar{v}'' + F_2'\bar{v}'' + F_2\bar{v}''' - \alpha F_2'\bar{\Phi} - \alpha F_2\bar{\Phi}' + F_3\bar{\Phi}' - \gamma_5 F_4\bar{v}'''\right] = 0 \tag{52a}$$

$$(\gamma_2 + \alpha^2\gamma_3)\bar{v}^{IV} + \alpha\gamma_3\bar{\Phi}^{IV} - \alpha^2\gamma_4\bar{v}'' - (\alpha\gamma_2 + \alpha\gamma_4)\bar{\Phi}'' - M^*\left[F_2'\bar{u}'' + F_2\bar{u}''' + \alpha^2F_2'\bar{u} + \alpha^2F_2\bar{u}' - \gamma_5F_4\bar{u}''' - \alpha^2\gamma_5F_4\bar{u}'\right] = 0 \tag{52b}$$

$$\gamma_3\Phi^{IV} + \alpha\gamma_3\bar{v}^{IV} - \gamma_4\bar{\Phi}'' - (\alpha\gamma_2 + \alpha\gamma_4)\bar{v}'' + \alpha^2\gamma_2\bar{\Phi} + M^*\left[F_1\bar{u}'' + \alpha^2F_1\bar{u}\right] = 0 \tag{52c}$$

Reproduced with permission of the copyright owner. Further reproduction prohibited without permission.

where

$$F_1(\bar{z}) = \{[\sin \alpha(1 - \bar{z}) + \eta \sin \alpha\ \bar{z}]/\sin \alpha\} ,$$

$$F_2(\bar{z}) = \{[\cos \alpha(1 - \bar{z}) - \eta \cos \alpha\ \bar{z}]/\sin \alpha\} + \frac{\eta-1}{\alpha} ,$$

$$F_3 = \eta-1, \qquad F_4 = \beta-1, \qquad \alpha = \frac{L}{R} \tag{53a}$$

$$\gamma_1 = \frac{EI_y}{L(M_{cr})_{st}} , \quad \gamma_2 = \frac{EI_x}{L(M_{cr})_{st}} , \quad \gamma_3 = \frac{EI_w}{L^3(M_{cr})_{st}} ,$$

$$\gamma_4 = \frac{GK_T}{L(M_{cr})_{st}} , \quad \gamma_5 = \frac{B^*}{M^*} . \tag{53b}$$

and the primes now refer to differentiation with respect to the nondimensional arc length parameter $\bar{z}$.

The parameter γ_5, as defined in Eq. 53b, can be written as

$$\gamma_5 = 2\left(\frac{\sigma_w}{\sigma_B}\right)\left(\frac{\gamma_3}{\gamma_2}\right)\left(\frac{L}{b}\right) \tag{54}$$

where b is the flange width, and σ_w and σ_B are the warping normal stress and the bending normal stress, respectively, at the edge of the flanges. The ratio σ_w/σ_B is perhaps more physically meaningful than the ratio B^*/M^*.

Similarly, the boundary conditions for simple supports can be nondimensionalized as

$$\bar{u}\Big|_{\bar{z}=0,1} = \bar{v}\Big|_{\bar{z}=0,1} = \bar{\phi}\Big|_{\bar{z}=0,1} = 0 \tag{55a}$$

Reproduced with permission of the copyright owner. Further reproduction prohibited without permission.

$$\gamma_2 \bar{v}'' - M^* \bar{u}' \left(F_2 - \gamma_5 F_4\right) = 0$$

$$\gamma_1 \bar{u}'' + M^* \bar{v}' \left(F_2 - \gamma_5 F_4\right) = 0$$

$$\bar{\phi}'' + \alpha \bar{v}'' = 0 \qquad \text{at } \bar{z} = 0,1 \tag{55b}$$

For the limiting case of fixed ends, used to approximate a continuous girder, the boundary conditions become

$$\bar{u}\Big|_{\bar{z}=0,1} = \bar{v}\Big|_{\bar{z}=0,1} = \bar{\phi}\Big|_{\bar{z}=0,1} = 0 \tag{56a}$$

$$\bar{u}'\Big|_{\bar{z}=0,1} = \bar{v}'\Big|_{\bar{z}=0,1} = \bar{\phi}'\Big|_{\bar{z}=0,1} = 0 \tag{56b}$$

For the deflection amplification approach, the boundary conditions above are replaced by the following expressions

$$\bar{u}\Big|_{\bar{z}=0,1} = \bar{v}\Big|_{\bar{z}=0,1} = \bar{\phi}\Big|_{\bar{z}=0,1} = 0 \tag{57a}$$

$$\gamma_2 \bar{v}'' - M^* \bar{u}' \left(F_2 - \gamma_5 F_4\right) = -M^*$$

$$\gamma_1 \bar{u}'' + M^* \bar{v}' \left(F_2 - \gamma_5 F_4\right) = 0$$

$$\gamma_3 \left(\bar{\phi}'' + \alpha \bar{v}''\right) = B^* \qquad \text{at } \bar{z} = 0 \tag{57b}$$

and

$$\gamma_2 \bar{v}'' - M^* \bar{u}' \left(F_2 - \gamma_5 F_4\right) = -\eta M^*$$

$$\gamma_1 \bar{u}'' + M^* \bar{v}' \left(F_2 - \gamma_5 F_4\right) = 0$$

$$\gamma_3 \left(\bar{\phi}'' + \alpha \bar{v}''\right) = \beta B^* \qquad \text{at } \bar{z} = 1 \tag{57c}$$

Reproduced with permission of the copyright owner. Further reproduction prohibited without permission.

Solutions to these equations were obtained using Finite Differences. First order central differences were used and the resulting system of linear equations was generated and solved on a UNIVAC 1108 computer. For the determination of critical loads, Eqs. 52 and the boundary conditions in Eqs. 55 or 56 are appropriate. The corresponding linear system is of the form

$$[A]\{x\} = \{0\} \tag{58}$$

where [A] is a square matrix of coefficients and is a function of the load parameter M^* and $\{x\}$ is a column vector of unknown displacements, namely the $\bar{u}$, $\bar{v}$, $\bar{\phi}$ displacements at each node point along $\bar{z}$. The fundamental critical value of M^* is that value of M^* for which

$$|A| = 0 \tag{59}$$

This critical value was determined using a simple search procedure with the determinant being calculated by pivotal condensation.

It should be noted that due to the complicated form of the boundary conditions in Eqs. 55, it is not possible to factor out the critical parameter, M^*, and put the linear system of equations 58 into the standard form of a linear eigenvalue problem. Thus the search procedure approach is manditory.

For the solution of the deflection amplification formulation, Eqs. 52 and the boundary conditions in Eqs. 57 are appropriate. The corresponding linear system in this case is nonhomogeneous and of the form

$$[A]\{x\} = \{b\} \tag{60}$$

Reproduced with permission of the copyright owner. Further reproduction prohibited without permission.

where [A] and {x} are defined as above and {b} is a column vector containing constant terms which result from the right hand sides of the boundary conditions, Eqs. 57. In this case it is possible to obtain unique values of {x} for a given value of M^*. In this way load-deflection curves were obtained by inverting [A] using a Gauss elimination scheme and multiplying through by $[A]^{-1}$, as follows

$$\{x\} = [I]\{x\} = [A][A]^{-1}\{x\} = [A]^{-1}\{b\} \tag{61}$$

Once load-deflection curves are obtained it is possible to calculate internal stress resultants from the constitutive relationships, Eqs. 22 and Eq. 40. These equations are nondimensionalized and the derivatives of $\bar{u}$, $\bar{v}$, and $\bar{\phi}$ necessary for substituting into them are obtained from {x} using central differences.

3.2 Determination of Critical Loads

In order to establish the convergence of the search procedure and the Finite Difference formulation, several cases of central angle and moment gradient were investigated using N = 10, 20, 30, 40, where N is the number of grid spaces along the length of the member. The results are shown in Table 1. On the basis of these results, it was decided to use N = 30 for the determination of critical loads. This results in a matrix [A] of order 87 x 87. An average search procedure for determining one critical load using N = 30 requires less than a minute of computation time on the UNIVAC 1108.

It is impossible to obtain results for the critical loads from Eq. 58 with $\alpha = 0^\circ$. For this value $F_1(\bar{z})$ and $F_2(\bar{z})$, defined by Eqs. 53a,

Reproduced with permission of the copyright owner. Further reproduction prohibited without permission.

become indeterminate. In addition, even if the correct functional expressions for the case of a straight girder subjected to equal end moments were substituted, Eq. 52b would become uncoupled from Eqs. 52a and 52c and take on the form

$$\gamma_2 \bar{v}^{IV} = 0 \tag{62}$$

Eq. 62 leads to the trivial solution $\bar{v} = 0$ when the transverse loads on the girder are zero. Thus this case should be represented by two simultaneous differential equations in $\bar{u}$ and $\bar{\phi}$ which would result in a Finite Difference formulation with [A] being 58 x 58 for $N = 30$. Rather than reformulating the analysis for this case, which represents a straight girder, it was decided to use results obtained for $\alpha = 0.0001$ radians. Note that values obtained for M^*_{cr} using $\alpha = 0.0001$ radians were essentially the same as published values for straight girders and provided a check on the computer program.

To establish the effect of curvature on the value of M^*_{cr}, the value of M^* at which $|A| = 0$, cases were run for several values of central angle and L/b ratio, the length of the girder divided by the flange width. The case of equal end moments and a typical set of cross-section parameters were used. The results obtained for these calculations are shown in Table 2. They indicated that the effect of curvature is small; the largest reduction in M^*_{cr} from the straight case was 4.9% for a central angle of 60° and L/b = 30. This case obviously does not represent dimensions typical of those encountered in practical curved plate girders. Note that the value of M^*_{cr} increases for $\alpha = 90°$. This occurs since the functions $F_1(\bar{z})$ and $F_2(\bar{z})$ are trigonometric functions, periodic in α, which change character when $\alpha = 90°$.

Reproduced with permission of the copyright owner. Further reproduction prohibited without permission.

In a similar manner, the effect on the critical moment of applied end bimoments acting in addition to equal end moments was found to be small as shown in Table 3. Three values of bimoment gradient $\beta = +1, 0, -1$, were considered in these calculations. The magnitude of the bimoment used was such that the ratio of warping to bending stresses at the ends of the girder was 0.5. As noted above the value of M^*_{cr} increases for $\alpha = 90°$.

To investigate the effects of moment gradient on buckling, three values of η, $\eta = +1, 0, -1$, were considered. Critical moments obtained for $L/b = 10, 30$ for the straight case ($\alpha = 0.0001$ radians) and for $\alpha = 60°$ are given in Table 4. Note that the results in Tables 2, 3 indicate that the largest difference between the straight and curved cases occurs at $\alpha = 60°$. The results presented in Table 4 indicate that the effect of moment gradient is essentially the same for both straight and curved girders.

The influence of the boundary conditions, i.e. pinned supports, Eqs. 55, versus fixed supports, Eqs. 56, on the critical moment is shown in Table 5. The results in Table 5 indicate that the critical loads for the case of fixed supports, obtained using Eqs. 56, increase considerably with an increase of curvature. This is to be expected since the fixed girder, in addition to not bending as much as the corresponding straight girder, is also better able to resist the applied torque, which increases with an increase of curvature.

In summary, it was established that as an Euler buckling problem, the critical loads determined for a curved girder loaded normal to the plane of curvature are essentially the same as those for a corresponding straight girder subjected to the same loading. The effect of curvature on the behavior of plate girders will be demonstrated in a more meaningful fashion within the context of the deflection amplification approach.

Reproduced with permission of the copyright owner. Further reproduction prohibited without permission.

3.3 Deflection Amplification Problem

When a curved girder is loaded by end moments and bimoments, the girder deflects downward, deflects laterally and twists from the beginning of loading. The linear theory obtained using Dabrowski's equations (11) does not predict a lateral deflection for girders of doubly symmetric cross-section. As a consequence it does not predict an internal moment about the y axis. When the additional terms are included in the bending equations for a curved girder, as in the deflection amplification approach, this internal moment can be calculated. In Figs. 4, 5, and 6 the distributions of M_x^*, M_y^*, and B^* along the length of a curved girder are shown. These values were nondimensionalized with respect to the critical moment for the straight beam as follows: $M_x^* = M_x/(M_{cr})_{st}$, $M_y^* = M_y/(M_{cr})_{st}$. These figures also indicate which part of the internal bimoment is caused by applied end moments and which part is caused by applied end bimoments. The plots were drawn for an applied end moment equal to 60% of the critical straight beam moment, i.e. $M^* = 0.6$. The distributions shown in Fig. 4 are for the case of equal applied end moments. The applied bimoments were such that the ratio of warping stress to bending stress at the end of the girder, σ_W/σ_B, is -0.5. The distributions shown in Figs. 5 and 6 are for the same σ_W/σ_B ratio, but for loading with a gradient on end moments and end bimoments, respectively. The distributions of M_x^* and B^* for all three cases are similar in shape, but larger in magnitude than the corresponding distributions obtained using the linear solution (11). Note that the internal bimoment caused by applied end moments is considerably larger than that caused by applied end bimoments. At the ends of the girder the applied end moments do not cause an internal bimoment and the internal bimoment is equal to the applied end bimoment.

Reproduced with permission of the copyright owner. Further reproduction prohibited without permission.

For convenience in studying the growth of deflections and internal stress resultants with load, the following discussion will concern itself with midspan values of these quantities resulting from loading by equal end moments and bimoments. The deflections of a girder with a central angle of 30° subjected to equal end moments only were evaluated using the deflection amplification equations. Results for this case are shown in Fig. 7, along with the vertical deflection and the angle of twist given by the linear theory, denoted as $\bar{v}_D$ and $\bar{\phi}_D$. A lateral displacement $\bar{u}$ occurs as soon as the moments are applied and increases rapidly with load. At $M^* \simeq 0.3$, the vertical displacement $\bar{v}$ and the angle of twist $\bar{\phi}$ depart from the values given by the linear theory, $\bar{v}_D$ and $\bar{\phi}_D$, and begin to increase rapidly.

To indicate the difference between the values of $\bar{v}$ and $\bar{\phi}$ obtained from the deflection amplification problem in Chapter 2 and those given by the linear theory, the ratios of $\bar{v}/\bar{v}_D$ and $\bar{\phi}/\bar{\phi}_D$ at midspan were determined for several cases. The results are shown in Fig. 8 for $\alpha = 5°$, 30° and $\sigma_W/\sigma_B = 0, -0.5$. Note that the effect of the applied end bimoment on $\bar{v}$ is considerable for the smaller central angle but in the other cases is insignificant. The reason for this is that the internal bimoment developed by the applied end bimoments is opposite in sign to the internal bimoment developed by the applied end moments. The latter is smaller for smaller central angles and has less effect in cancelling out the internal bimoment due to applied end bimoments.

The influence of applied end bimoment on the $\bar{u}$, $\bar{v}$ and $\bar{\phi}$ displacements is shown in Figs. 9, 10, and 11 respectively. They are again graphed for $\alpha = 5°$, 30° and $\sigma_W/\sigma_B = 0, -0.5$. These results are also presented in

Reproduced with permission of the copyright owner. Further reproduction prohibited without permission.

Table 6, which includes values for $\sigma_W/\sigma_B = -0.1, -0.3$ as well. It should be noted that the applied end bimoments which produce a negative stress ratio σ_W/σ_B at the ends are applied in such a way that the top flange is bent back toward the center of curvature, i.e. the outside edge of the top flange goes into compression. This corresponds to a negative end bimoment for use in the boundary condition equations, Eqs. 57b and c, and in the differential equations, Eqs. 52. The internal bimoment produced by the applied end moments is opposite in sign to this, i.e. it produces tension on the outside edge of the top flange. It is clear from these cases that applied end bimoment tends to slow down the build up of deflections due to applied end moment.

The effects of applied end moments and bimoments on internal stress resultants are also of interest. For the case of a curved girder loaded by equal end moments, graphs showing the growth of the internal stress resultants M_x^*, M_y^* and B^* with increasing applied end moment M^* are presented in Figs. 12 and 13. The growth of M_x^* is linear for the range of M^* shown, but the growth of M_y^* and B^* become nonlinear at $M^* \simeq 0.3$ and increase rapidly. This implies a growth in bimoment stresses and the existence of a rapidly growing lateral bending stress. In Fig. 14, the same data is presented but it is ratioed to the values obtained using the linear theory. Since the linear solution does not predict an internal bending moment M_y, the ratio M_y/M_x^D was used. As with the notation for displacements, M_x^D and B^D denote the values given by the linear theory using formulas presented by Dabrowski (11).

The results of this section and of Section 3.2 indicate that although the critical values obtained from an Euler stability analysis differ little from those obtained for straight girders, the deflection behavior and

Reproduced with permission of the copyright owner. Further reproduction prohibited without permission.

build up of stress in a curved girder differs considerably from that predicted by the linear theory. Immediately upon loading a curved girder, lateral displacements and lateral bending effects take place. These effects grow nonlinearly and quite rapidly. If a girder were designed using the linear theory, the combined stress state caused by bending about the x axis and by flange bending due to internal bimoment would be considered. From the results of the deflection amplification solution, it is evident that stresses due to lateral bending about the y axis are present as well, and that the stresses caused by flange bending are larger than predicted by the linear theory. Design based on the linear theory, therefore, considers only part of the existing stress state. It is possible that, if failure occurred, it might be considered as caused by instability in the Euler sense.

The results discussed up to this point are valid only in the elastic range. Before extending the discussion to the inelastic range and considering the effects of residual stresses, a comparison will be made with experimental results in Chapter 4. In Chapter 5 the results will be extended and put in terms applicable to design use.

Reproduced with permission of the copyright owner. Further reproduction prohibited without permission.

4. SIMPLIFIED ANALYSIS AND COMPARISON WITH TESTS

4.1 Development of Simple Model

It is of interest to attempt to find a simple way of obtaining the distribution of stress in a curved girder rather than going through a complete deflection amplification analysis. It is natural to use in such an attempt, the state 1 values for internal stress resultants and deflections. Considering the assumptions employed in deriving the governing differential equations, Eqs. 35, this is seen to be equivalent to using results obtained from the linear theory. Certainly one possibility involves simply considering projections of the internal bending moment, M_{x_1}, and torque, M_{z_1}, about the y_1 axis as equal to the internal lateral bending moment. Using Eqs. 2 for direction cosines of the state 1 axes, this leads to the expression

$$M_{y_{SM}} = -M_{x_1}\phi_1 - M_{z_1}v_1' \tag{63}$$

where $M_{y_{SM}}$ denotes the internal lateral bending moment given by this simple model. This simple model is shown in graphic terms in Fig. 15. It can be further extended, as indicated in the figure, to an equivalent lateral load on the curved girder equal to $q_{x_{SM}} = M''_{y_{SM}}$. Using the moment curvature relationship, Eq. 22b, and Eq. 20b which expresses the curvature in terms of displacements, this approach leads to the differential equation

$$EI_y\left(u_2^{IV} + \frac{u_2''}{R^2}\right) = q_{x_{SM}} \tag{64}$$

Substituting in Eq. 64 the definition of $q_{x_{SM}}$ and Eq. 63, gives in terms of state 1 expressions

$$EI_y\left(u_2^{IV} + \frac{u_2''}{R^2}\right) = -\left[M_{x_1}\phi_1 + M_{z_1}v_1'\right]'' \tag{65}$$

Reproduced with permission of the copyright owner. Further reproduction prohibited without permission.

This equation can be nondimensionalized using the usual definitions as

$$\gamma_1\left[\bar{u}^{IV} + \alpha^2\bar{u}''\right] + \left[\bar{M}_x^*\bar{\phi}_D + \bar{M}_z^*\bar{v}_D\right]'' = 0 \qquad (66)$$

In order to test the validity of this simple model, an investigation was made to check the degree of linearity present in the results obtained from complete deflection amplification analyses. Results were obtained for the midspan stresses developed in girders subjected to applied end moments and bimoments. The moment and bimoment gradient was zero for these cases, $\eta = \beta = 1$. Cases were run for L/b = 10, 20 and 30 and for $\sigma_W/\sigma_B = -0.5$ (compression on outside edge of the top flange at the ends of the girder due to applied bimoment). Results are shown in Fig. 16 for straight girders ($\alpha = 0.0001$ radians) and in Fig. 17 for girders curved to a central angle of 30°. The bending stress at the extreme fiber of the bottom flange, σ_B , is positive (tension) for both girders. The radial stress on the outer edge of either flange, σ_R, is negative (compression) for the straight girder, Fig. 16, and positive (tension) for the curved girder, Fig. 17. The warping stress at the outer edge of the top flange, σ_W, is also positive (tension) for the straight girder and negative (compression) for the curved girder.

Note that the deflection amplification results yield radial stresses even for a girder of negligible curvature. The reason for this is that an angle of twist and consequently a radial moment is produced due to the applied end bimoment. Note also that the radial stress and the warping stress tend to bend the top flange toward the center of curvature for the straight case, and away from center of curvature for $\alpha = 30°$. This occurs since the only internal bimoment and torque for the straight case are those caused by the applied end bimoments which are negative.

Reproduced with permission of the copyright owner. Further reproduction prohibited without permission.

A comparison of the results in Figs. 16 and 17 indicates that the warping stresses, and the radial stresses, are considerably greater for the curved girder than for the straight girder. The bending stresses are very nearly the same. The bending stresses and warping stresses increase approximately linearly with M^* up to the value $M^* = 0.3$. This is not surprising since the $\bar{v}$ and $\bar{\phi}$ deflections on which these stresses depend are also approximately linear in this range, as can be seen in Figs. 10 and 11. For $\alpha = 30°$ the bending and warping stresses at $M^* = 0.3$ are well beyond any reasonable yield stress. These results imply that the simple model developed using the solutions for $\bar{v}_D$ and $\bar{\phi}_D$ from the linear theory, might be valid in the elastic range. It should be noted that the effect of changing L/b is not as great as it appears at first glance in these figures. The load parameter M^* depends on $(M_{cr})_{st}$ which is different for different L/b ratios.

An alternate method of obtaining a simple model involves replacing v_2 and ϕ_2 in Eqs. 35 by v_1 and ϕ_1. This has the effect of uncoupling the system of equations. The deflection u no longer affects the calculation of v and ϕ in Eqs. 35b and c. Once v_1 and ϕ_1 are obtained they can be substituted into Eq. 35a and u_2 can be calculated. If this is done Eq. 35a becomes

$$EI_y\left[u_2^{IV} + \frac{u_2''}{R^2}\right] + \left[M_{x_1}\phi_1' + \frac{M_{x_1}v_1'}{R} + M_{z_1}v_1'' - \frac{M_{z_1}\phi_1}{R}\right]' + V_y\phi_1' = 0 \qquad (67)$$

From the state 1 equilibrium equations, Eqs. 23, it is evident that

$$V_{y_1} = M_{x_1}' + \frac{M_{z_1}}{R} \qquad (68a)$$

$$M_{z_1}' = \frac{M_{x_1}}{R} \qquad (68b)$$

Reproduced with permission of the copyright owner. Further reproduction prohibited without permission.

$$M''_{x_1} + \frac{M'_{z_1}}{R} = M''_{x_1} + \frac{M_{x_1}}{R^2} = 0 \qquad (68c)$$

Using Eqs. 68, it is possible to reduce Eq. 67 to the form

$$EI_y\left[u_2^{IV} + \frac{u_2''}{R^2}\right] + \left[M_{x_1}\phi_1 + M_{z_1}v_1'\right]'' = 0$$

which is identical to Eq. 65. Thus it is seen that the assumption that the radial stress can be approximated by the projection of the internal moment and torque at state 1 and the assumption that the v_2 and ϕ_2 deflections can be approximated by v_1 and ϕ_1 in the elastic range are equivalent.

Making use of results given by the linear theory for M_{x_1}, M_{z_1}, ϕ_1 and v_1', $M_{y_{SM}}$ as given by Eq. 63 was calculated for several cases. For equal end moments and bimoments, with $\sigma_W/\sigma_B = -0.5$, the stresses due to $M_{y_{SM}}$ were calculated and a comparison was made with results from the deflection amplification analysis. This comparison is presented in Table 7 and shows that for $\alpha = 5°$, $15°$ and at load values up to $M^* = 0.3$, the simple model gives results which are within 10% of the results from the deflection amplification analysis. If a limit of $M^* = 0.2$ is imposed the results are within 3%.

In the next section a comparison with experimental tests will be discussed. For the elastic loads considered in this comparison, M^* does not exceed 0.1 and it is evident that the simple model gives adequate results.

4.2 Comparison with Experiments

In an attempt to check the validity of the results obtained from the deflection amplification analysis and also the simple model discussed in the previous section, a comparison was made with the results of

Reproduced with permission of the copyright owner. Further reproduction prohibited without permission.

lateral buckling tests conducted on horizontally curved plate girders (21). Comparisons of calculated and measured internal stresses were made for two plate girder tests.

A sketch of the test setup and the dimensions of the test specimens are shown in Fig. 18. The single span, simply supported girders were loaded by concentrated loads at the third points. Lateral movement at the load points was restrained by the bracing system shown. Two girders were tested and both steel and aluminum braces were employed. Strain gages were placed on the outside edge of the flange tips at Sections 1 and 2 shown in the figure. Strain gages were also placed on the braces in order to measure the brace forces. A complete description of the fabrication of the girders, the test setup, and the test procedures is available elsewhere (21).

Assuming the lateral braces at the load points to be rigid, i.e. that the angle of twist ϕ is zero at these points, the portion of the girder between the load points acts like a simply supported girder subjected to equal end moments and bimoments. The magnitudes of these end moments and bimoments at the brace points for a particular value of the concentrated load P were obtained from the linear theory (11). This was done by superimposing results for a simply supported girder subjected to two concentrated loads and two concentrated torques (developed in the braces) at the third points. The magnitudes of these torques were determined from the condition that the rotation at the brace points equals zero. Using these end moments and bimoments, the internal stresses at the gage locations were computed using the deflection amplification analysis and the simple model. It is important to note that the applied end bimoments are negative (tending to bend

Reproduced with permission of the copyright owner. Further reproduction prohibited without permission.

the top flange inward toward the center of curvature). Stresses obtained from the deflection amplification analysis, the simple model, and the values measured in the test are presented in Table 8.

The experimental values were measured on reload cycles after the girders had been loaded and unloaded several times in order to wipe out the effect of residual stresses due to fabrication. The behavior of the girders on these reload cycles was therefore elastic. The total stress, obtained by multiplying the measured strains by the elastic modulus, E = 29,750 ksi, was separated into bending, warping and radial components. This was done by assuming that a uniform stress across each flange was developed due to bending, that a linearly distributed stress was developed across each flange due to warping which tended to bend the top flange over the center portion outward and the bottom flange inward toward the center of curvature, and that a linearly distributed stress was developed across each flange due to radial bending, which tended to bend both flanges outward away from the center of curvature. The uniform stress due to bending was taken as the average of the tip stresses for each flange. In general this uniform stress was not the same for the top and bottom flanges. The reason for this is that the web may deform and fail to pick up its share of the bending stress. The top and bottom flanges may then pick up additional stresses. This effect occurs in straight girders, where it predominantly effects the compression flange, and is discussed by Basler (22). For the sake of comparing with computed stresses the average of the values obtained from each flange was used for the bending stress.

Once the bending stress is subtracted from the total stress for each flange, there remains on each flange a linearly distributed stress

Reproduced with permission of the copyright owner. Further reproduction prohibited without permission.

which is due to the combined effects of warping and radial bending. These both tend to bend the top flange outward away from the center of curvature. The stress on the outside edge of the top flange consequently is the sum of σ_W and σ_R. The stress due to warping tends to bend the bottom flange inward toward the center of curvature, while the stresses due to radial bending tend to bend the bottom flange outward away from the center of curvature. The stress on the outside edge of the bottom flange consequently is the difference between σ_W and σ_R. Thus σ_W and σ_R can be separated out simply by solving two simultaneous equations.

The values presented in Table 8 for σ_B, σ_W and σ_R from the tests were averaged over several reload cycles. For example in computing σ_W at Section 1 for the 15 kip load, four values were averaged which ranged from 6.58 ksi to 8.10 ksi. It should be noted that scatter such as this was observed for many of the readings. Thus the test values should not be considered as exact values that can be readily duplicated.

The stresses calculated using the deflection amplification approach and the simple model are essentially identical. The bending stresses obtained in the tests are lower (by about 10%) than the calculated values. The most likely reason for this is that the torque beams, used to prevent twist at the supports, may have contributed some restraint to bending as well. The computed warping stresses are lower (by about 25%) than obtained from the tests. The computed radial stresses are much lower (about 80%) than obtained from the tests. It is likely that the applied bimoments, calculated as discussed above, are smaller algebraically than the bimoments actually developed in the tests at the load points. There

Reproduced with permission of the copyright owner. Further reproduction prohibited without permission.

are several reasons why this might be so. The loads were applied against bearing pads which were placed on the top flange of the girders. It is possible that this arrangement caused some restraint to warping and a consequent decrease (algebraically) in the bimoment at the load points. Also the warping stresses under the load are very sensitive to any eccentricity of the load. For example, the linear theory gives σ_w = +58.07 ksi (tension on outside edge of top flange) at the brace point due to concentrated loads of 10 kips. For rigid braces, concentrated torques of 55.0 kips-in. must be applied to bring the girder back to the zero twist position. The warping stress due to the concentrated torques is σ_w = -11.77 ksi/kip-in. X 55.0 kip-in. = -64.8 ksi at the brace point. Thus the actual warping stress is -64.8 + 58.1 = -6.7 ksi due to both effects. If the concentrated loads were applied at a 0.25" eccentricity (toward the center of curvature) there would be an additional concentrated torque of 2.5 kip-in. generated. The warping stress due to the concentrated torque would become σ_w = -11.77 ksi/kip-in. X 57.5 kip-in. = -67.6 ksi, and the actual warping stress would become -67.6 + 58.1 = -9.5 ksi. Thus a 0.25" eccentricity results in a 42% decrease (algebraically) in warping stress at the brace points. It is clear that any small eccentricity would have a large effect on the warping stresses. Finally, the braces that were used in the test did not function as rigid braces as assumed. As mentioned above, a rigid brace would generate 5.5 kip-in. of concentrated torque per kip of concentrated applied load. The forces in the braces were measured during the test and the resulting concentrated torques generated averaged about 3.75 kip-in. of concentrated torque per kip of concentrated applied load.

Reproduced with permission of the copyright owner. Further reproduction prohibited without permission.

In order to investigate the effect of the braces, the elastic analysis was repeated, this time using concentrated torques of 3.75 kip-in. per kip of the concentrated applied load, i.e. twisting the girder back to an angle of twist that is greater than zero at the braces. It is important to note that in this case the applied end bimoments are positive (tending to bend the top flange outward away from the center of curvature). The stresses obtained using this approach are presented in Table 9. The calculated bending stresses obtained are approximately the same as before. However, in this analysis, the calculated warping stresses are very high (about 400%) and the calculated radial stresses are also high (by about 50%) compared to the test values. It is likely, considering the trends shown in Tables 8 and 9, that the effects of warping restraint under the loads and possible eccentricities in the applied loading combine to give a loading picture in between the two cases that have been discussed. It is evident from the 10% error in matching the bending stresses and from the uncertainty in establishing the bimoment at the load points, that the appropriate moments and bimoments applied to the portion of the girder between braces are essentially unknown. Note that these values were not measured in the tests.

With this in mind, a third approach to obtaining a meaningful comparison was considered. The moments and bimoments at the brace points were assigned values which result in bending and warping stresses at Section 1 which match the test results closely. The comparison was then made between computed radial stresses and the test results. This comparison at Section 1 is presented in Table 10. In this case the results were computed using the simple model, which

Reproduced with permission of the copyright owner. Further reproduction prohibited without permission.

has previously been shown to be quite accurate. This comparison shows the computed radial stress to be low (by about 75%) compared to the test results.

Before any attempt is made to draw conclusions from any of these comparisons, it is important to note the significance of another effect which was observed in the tests. There was a significant amount of cross-sectional deformation of the test specimens, even in the elastic range. This is of considerable importance since all the previous calculated results are based on beam theory which assumes that there is no cross-sectional deformation. In order to make the comparisons more meaningful, an attempt was made to assess the effect of cross-sectional deformation on the stresses.

Consider a section of a curved girder subjected to equal end moments and bimoments as shown in Fig.19a. If the top flange is cut away as shown in Fig.19b, it is not in equilibirum unless the component of the thrust in the radial direction is balanced by a uniformly distributed radial load which must be transmitted to the flange by the web. When the assumption is made that the cross-section will not deform, as in beam theory, it is implied that the web does in fact generate this uniformly distributed radial load. If the web is not strong enough to generate this radial load, the flange is forced to generate a considerable part of this load by deformation. Both the flange and the web bend outward as if loaded by a uniformly distributed radial load as shown in Fig.19c and the cross-section deforms. In the process there is an additional linearly distributed stress developed in the flange. The webs of the test girders were thin ($d/t_w = 156$), and even considering the effect of transverse stiffeners in an approximate

Reproduced with permission of the copyright owner. Further reproduction prohibited without permission.

manner, calculations showed that an additional linearly distributed stress could be expected in the top flange of approximately 0.25 ksi per kip of concentrated load. These calculations were performed assuming the flange could be considered as a fixed-fixed straight beam loaded with a uniform load of $\sigma_B A_f/R$ kips/in. which is seen in Fig. 19 to be the radial load required for equilibrium. The same effect occurs for the bottom flange. It, however, is bent inward and has, due to arch effects, a slightly better ability to resist this bending. Hence an additional linearly distributed stress is developed which is opposite and slightly less than that developed in the top flange. Thus the stresses due to crosssectional deformation are distributed across the flanges in much the same way as the stresses due to warping.

None of the comparisons discussed above match the radial stress very well. It should be realized that the bending, warping and cross-sectional deformation stresses (which are of an order of magnitude of 50% of the warping stresses), greatly predominate over the radial stresses. In fact the radial stresses are of the same order of magnitude as the experimental errors in these other stresses in the elastic range considered. Of course these radial stresses will grow quite fast as deflections, and consequently the angles of projection (v', ϕ) increase and may be of considerable importance in the inelastic range.

The most important conclusion that can be drawn from looking at the test results, therefore, is that it is impossible to neglect the effects of cross-sectional deformations in any further treatment of the lateral buckling problem. This effect will be included in the extension of these results into the inelastic range presented in the next chapter. The significance of the radial stresses in the inelastic range will also be investigated.

Reproduced with permission of the copyright owner. Further reproduction prohibited without permission.

5. DESIGN APPLICATIONS

5.1 General

In actual bridge applications, curved girders are braced at several locations along the total span length. The moment diagrams for such girders display regions of moment gradient which are functions of the various live load positions. Such a situation is depicted in Fig. 20a. Because of the variability due to live load position and the complexity of analyzing the entire system, it was decided to isolate a single length of such a girder system between brace points. This single span will be considered to be simply supported. The moments and bimoments transmitted to this girder from the side spans resulting from continuity will be taken conservatively as equal on each end. The values of these moments and bimoments may be obtained from an analysis of the entire girder and brace system treated either as a grid system or a continuous system if the bridge deck is included by using linear theory. Thus the model to be used for determining bracing spacing requirements has been reduced to a simply supported girder subject to equal end moments and bimoments as shown in Fig. 20b. The study of such a model will yield conservative results for the actual bridge system.

It is desirable to take a conservative approach as well in evaluating the effects of cross-sectional deformation. Since the moment has been taken as constant, the flange thrust $\sigma_B A_f$ is also constant. Reasoning as discussed above in Section 4.2, if the ability of the web to resist lateral load is neglected and the girder is taken as straight for this calculation, the additional stresses in the flange can be evaluated by applying a uniformly distributed load $\sigma_B A_f/R$ as in Fig. 19 to the flanges of the girder. This load should be applied along the entire span length

Reproduced with permission of the copyright owner. Further reproduction prohibited without permission.

of the girder, i.e. to the braced length under consideration as well as the adjacent side spans, Fig. 21a. This is equivalent to considering the flange of the isolated span as a fixed-fixed beam subject to a uniformly distributed load. This situation is realistic if the moment diagram is relatively constant over several bracing spaces. To determine the degree of conservatism inherent in this approximation, the moment diagram in Fig. 21b was considered. This situation corresponds to the case in which the moment drops off to zero at the ends of the adjacent braced spans. Calculations show that the moment at the center of the middle span for the loading in Fig. 21b is 92% of the moment obtained considering the flange as a single span fixed-fixed beam. Thus the latter approach is conservative although not unduly so and will be used in the evaluation of stress due to cross-sectional deformation.

The effect of radial bending will also be included in the analysis of the isolated portion of the girder between brace points.

Thus the model to be used for determining lateral bracing spacing will be that shown in Fig. 20b with cross-sectional deformation and radial bending effects calculated as discussed above. Criteria for lateral bracing spacing and size will be developed, and put in a form suitable for design use.

The variation of the stress at the inner edge (toward the center of curvature) of the compression flange along the simply supported girder is shown in Fig. 22. Stresses due to the bending moment, bimoment or flange moment, radial bending and cross sectional deformation are shown separately. The bending moment produces a uniform compressive stress across the flange width ($\sigma = Mc/I$) which is essentially constant along the curved span length for equal end moments. The end moments also produce warping normal stresses

Reproduced with permission of the copyright owner. Further reproduction prohibited without permission.

which vary linearly across the flange width and along the span length as shown in Fig. 22b. These stresses are compressive stresses at the inner edge of the compression flange. In an actual girder the bimoment at the bracing points may be either positive or negative as shown in Fig. 22c. In both cases the bimoment at midspan is less than the applied end value. A positive bimoment will cause compression on the inner edge of the compression flange whereas a negative bimoment will cause tension. Both positive and negative bimoments were therefore considered in this study. Stresses produced by this bimoment are obtained from the following relationship (11).

$$\sigma_W = \frac{B\omega}{I_w} \tag{69}$$

For a doubly symmetric plate girder Eq. 69 becomes

$$\sigma_W = B \frac{6}{b^2 t_f (d + t_f)}$$

If the concept of flange moment M_f is used and each flange is treated as a rectangular beam to obtain the warping stresses, the flange moment is related to the bimoment as follows

$$\frac{B\omega}{I_w} = \frac{M_F(b/2)}{\frac{1}{12} t_f b^3}$$

$$M_F = \frac{B}{d + t_f} \tag{71}$$

In the remaining discussion this warping stress will be expressed as a percentage of the bending stress, σ_W/σ_B. Either the bimoment or flange moment concept may be used to calculate these warping stresses.

Reproduced with permission of the copyright owner. Further reproduction prohibited without permission.

The variation of the stresses due to radial bending is shown in Fig. 22d. The radial bending effect which is analogous to the entire girder bending as an arch in the horizontal plane produces compressive stress on the inner edge of the compression flange. The stress variation across the flange width is linear as shown.

The stresses due to deformation of the cross section are also compressive along the inner edge on the compression flange over the center portion of the girder. Since the flange was treated as a fixed-fixed beam in determining the stresses produced by this effect, compressive stresses occur along the outer edge of the flange over the portion of the girder near the ends.

Numerical values of the stresses produced by the various effects noted above are related to the following cross sectional and geometrical properties of the girder:

A_w/A_f , d/t_w , t_f/t_w , L/b and $\alpha = L/R$.

It was possible to nondimensionalize all the equations used in this study in terms of these parameters. The ratio of the applied end moment to bimoment or the moment to flange moment ratio was also expressed nondimensionally in terms of σ_w/σ_B . Thus general results covering a wide range of girder proportions were obtained and it was not necessary to analyze a large number of specific girder cross sections in developing the results presented herein. In order to insure that the entire range of practical curved plate girders was considered, the following ranges were used for these parameters:

$$0.5 \leq A_w/A_f \leq 2 \quad , \quad 40 \leq d/t_w \leq 165 \quad , \quad t_f/t_w = 3$$

$$0 < L/b \leq 36 \qquad 0° < \alpha \leq 20° \qquad -0.5 \leq \sigma_w/\sigma_B \leq 0.5$$

Reproduced with permission of the copyright owner. Further reproduction prohibited without permission.

The range for A_w/A_f covers most plate girders built today. The lower limit of web slenderness ratio equal to 40 represents a rolled beam section and the value of 165 is the limit permitted by AASHO for an A36 plate girder. A survey of existing curved bridges indicates that $t_f/t_w = 3$ represents an average value. The range of L/b or bracing spacing to flange width is the same as presently permitted by AASHO for A36 steel. The upper limit of 20° used for the central angle or the ratio of bracing spacing to the radius of the girder $L/R = 0.35$ obviously is considerably larger than any practical value (25). This value was used in order to illustrate the effect of curvature in a highly curved beam. Considerably smaller values will be used in developing the design recommendations in Chapter 6. The ratio of warping to bending stress is significantly affected by the number of transverse diaphragms used in a curved plate girder bridge. The efficient use of diaphragms would limit this ratio to less than 0.25. A value of 0.5 was used, however, and may be considered an absolute upper limit for practical curved bridges. For composite construction the deck will greatly increase the warping torsional rigidity of the girder cross section and thus decrease the warping stress σ_w (32). During construction, however, under wet concrete loading the plate girder section will act alone in resisting the dead load and high warping normal stresses may develop. It is advisable therefore, that the bracing spacing required for this condition also be checked in the design process.

Residual stresses will also affect the load-deformation response of curved plate girders. In this study, effects produced by residual stresses due to either heat curving or flame cutting and welding (26) were included.

Reproduced with permission of the copyright owner. Further reproduction prohibited without permission.

5.2 Elastic Behavior

The complete mathematical model developed in Chapter 2 and the simplified model in Chapter 4 are directly applicable in the elastic range or as long as the stress is less than the yield stress. Since the computational effort for the simple model is considerably easier, it was used for the elastic analysis. The numerical results in Section 3.3 for the deflection amplification problem, however, indicated that the angle of twist and the bimoment produced by the bending moment increased nonlinearly as the applied end moment increased and became very large at $(M_{cr})_{st}$ i.e. $M^* \approx 1$ (Figs. 8, 14). In order to take this effect into account in the simple model, the following amplification factor was used

$$\text{Amplification Factor} = \frac{1 - 0.86M^* + 0.4M^{*2}}{1 - M^*} \tag{72}$$

Eq. 72 was developed from the amplification on bimoment in Fig. 14 and the angle of twist in Fig. 8. This amplification factor was applied to the bimoment at midspan produced by the bending moment and the term $M_x\phi$ in the radial moment $M_{y_{SM}}$. Since the internal bimoment produced by an applied end bimoment is related to the angle of twist, Eq. 72 was also applied to this effect. Note that for $M^* \leq 0.3$ the factor in Eq. 72 is less than 7%. The quantities used in the simple model computations when M^* was less than 0.3 were essentially the values from linear theory (11).

The idealized case of a girder with no initial residual stress was considered first. For a given ratio of applied end moment to bimoment (σ_w/σ_B) the value of the end moment required to produce yielding was determined. The following procedure was used for these computations:

Reproduced with permission of the copyright owner. Further reproduction prohibited without permission.

1. Select a value of applied moment $M^* = M/M_{cr}$.
2. Determine the applied end bimoment associated with this moment for the particular ratio of σ_W/σ_B.
3. Compute the internal moment at the center of the girder due to this applied end moment. Compute the internal bimoment at the center and ends of the girder due to the applied moment and bimoment using linear theory and the amplification factor in Eq. 72.
4. Compute the bending and warping stresses at the center and ends of the girder produced by the applied moment and bimoment.
5. Using the deformations obtained from linear theory ($\bar{v}_D, \bar{\phi}_D$ - Ref. 11), and the linear theory internal forces, M_{x_1} and M_{z_1}, compute the lateral bending moment $M_{y_{SM}}$ using Eq. 63. The amplification factor in Eq. 72 was applied to $M_x\phi$ in this computation. Compute the radial stresses at the center and ends of the girder produced by this moment.
6. Compute the stresses at the center and ends of the girder due to deformation of the cross section by treating each flange as a fixed-fixed rectangular beam loaded with a force of $\sigma_B A_f/R$ kips/in.
7. Add the stresses from steps 4, 5, 6 and compare with the yield stress. This comparison was made at both the center and ends of the girder.
8. Repeat the procedure for another value of applied moment until the total stress in step 7 equals the yield stress. After determining this value of M required to produce yielding, divide by the section modulus of the girder and denote the resulting stress by σ_f.

Reproduced with permission of the copyright owner. Further reproduction prohibited without permission.

Results from this analysis are shown in Figs. 23,24,25 and Table 11. In view of step 8, the ordinates in Figs. 23,24,25 (σ_f/σ_y) represent the ratio of the applied end moment or the moment obtained by the designer in the analysis of the structure required to produce yielding of the curved beam to the yield moment under pure bending, $M_y = \sigma_y S$.

The results in Fig. 23 for $d/t_w = 165$ indicate that a substantial decrease in σ_f/σ_y occurs as L/b increases. With $A_w/A_f = 0.5$ and $\sigma_w/\sigma_B = 0$, σ_f/σ_y decreases from a value of 0.844 at $L/b = 5$ to 0.318 at $L/b = 35$. A similar decrease occurs for $A_w/A_f = 2.0$ and for the case of an applied bimoment. For both the case of applied end moment only, $\sigma_w/\sigma_B = 0$, as well as applied moment and bimoment, $\sigma_w/\sigma_B = 0.5$, increasing the value of web to flange area decreases the moment required to produce yielding. The values of σ_f/σ_y for the case of an applied moment and bimoment are obviously less than those for applied moment only as expected. The results for $d/t_w = 40$ in Fig. 23 are similar to those for $d/t_w = 165$. In this case, however, the reduction of σ_f/σ_y with increasing L/b is less. With $A_w/A_f = 0.5$ and $\sigma_w/\sigma_B = 0$, for example, σ_f/σ_y decreases from 0.861 at $L/b = 5$ to 0.567 at $L/b = 35$.

The ratio of the St. Venant to the warping torsional rigidity of the girder is related to both A_w/A_f and d/t_w. As d/t_w increases, the ratio GK_T/EI_w decreases or the warping torsional rigidity predominates. Conversely as A_w/A_f increases, the ratio GK_T/EI_w increases and the St. Venant torsional rigidity becomes more important. Thus as indicated in Fig. 23, as d/t_w increases from 40 to 165 and GK_T/EI_w decreases the initial yield moment becomes more sensitive to bracing spacing of L/b. In either case as A_w/A_f increases σ_f/σ_y decreases for a particular L/b.

Reproduced with permission of the copyright owner. Further reproduction prohibited without permission.

Since a curved beam bends and twists under applied load, the influence of the various cross sectional properties on this behavior or equivalently on the loads required to produce initial yield should be similar to the effect of these properties on the lateral buckling moment for a straight beam. The critical moment for a straight beam in bending is

$$M_{cr} = \frac{\pi}{L}\sqrt{EI_y GK_T}\sqrt{1 + \pi^2 EI_w/GK_T} \tag{73}$$

Expressing the properties of the cross section in terms of the dimensions as follows

$$I_y = A_f b^2/6 \tag{74a}$$

$$K_T = A_f/3\ [2t_f^2 + (A_w/A_f)t_w^2] \tag{74b}$$

$$I_w = I_y d^2/4 = A_f b^2 d^2/24 \tag{74c}$$

Equation 73 becomes

$$\frac{\sigma_{cr}}{\sigma_y} = \frac{\pi^2}{4(L/b)^2}\left(\frac{E}{\sigma_y}\right)\sqrt{\frac{1}{\left(3 + \frac{A_w}{2A_f}\right)^2} + \frac{4\left(\frac{A_w}{A_f}\right) + 8\left(\frac{t_f}{t_w}\right)^2}{\left(3 + \frac{A_w}{2A_f}\right)^2\left(\frac{d}{t_w}\right)^2}\frac{(L/b)^2}{(1+\nu)\pi^2}} \tag{75}$$

As A_w/A_f increases σ_{cr}/σ_y in Eq. 75 decreases. Similarly as d/t_w increases the second term under the square root in Eq. 75 decreases and σ_{cr}/σ_y becomes more sensitive to L/b. This behavior is similar to that discussed above for initial yield of the curved beam

The results in Fig. 24 for $\alpha = 20°$ are similar to those in Fig. 23. The values of σ_f/σ_y are substantially lower, however, due to the increased effect of curvature. As noted previously this value of α is considerably greater than any practical case for curved bridges.

Reproduced with permission of the copyright owner. Further reproduction prohibited without permission.

The influence of the direction of the end bimoment, +B or -B, is illustrated in Fig. 25 and Table 11. Because the stresses due to the bimoment, radial bending and cross sectional deformation combine differently at the flange tips at the center and ends of the girder, it is possible that yielding may begin at either the center or end cross section. This situation is analagous to that for beam columns (9) in which two design formulas must be checked because of this same possibility. Consider Fig. 25a for the case of a positive applied end bimoment. The stress due to the applied end moment M_x is constant along the girder. This bending moment also produces warping stresses as shown in Fig. 22b which are quite high at the center of the girder. The magnitude of these stresses increases as L/b increases. The applied end bimoment also produces warping stresses as shown in Fig. 22c. The warping stress at the center of the girder due to this effect is less than that at the ends. As L/b increases the warping stress at the center due to the end bimoment decreases. Radial bending and deformation also produce warping type stress as shown in Fig. 22d,e. At the center cross section all these stresses add on the inner edge of the flange. At the end cross section the compressive stress due to deformation of the cross section occurs on the outer edge of the flange while the applied positive end bimoment produces compression on the inner edge. The most highly stressed point is therefore the inner edge of the flange at the center cross section and yielding initiates at this point. As L/b increases, the warping stress at the center section due to moment increases rapidly and yielding always occurs at the center. The situation is somewhat different with a negative applied end bimoment in Fig. 25b. Note in this case the warping stresses at the center cross section due to the end

Reproduced with permission of the copyright owner. Further reproduction prohibited without permission.

bimoment are tension on the inner edge of the flange (Fig. 22c). These stresses therefore subtract from the warping stresses produced by the applied end moment. At the end cross section the compressive stress due to the end bimoment and deformation of the cross section add on the outer edge of the flange. For low values of L/b the outer edge of the flange at the end cross section is the most highly stressed point and yield occurs at the ends. As L/b increases the warping stress at the center cross section due to the end moment increases rapidly while those due to the end bimoment decrease. At $L/b \simeq 25$ the total compressive stress on the inner edge at the center cross section exceeds that on the outer edge at the end cross section and yielding occurs at midspan as L/b increases. Note that the yield curve in the region $25 < L/b \leq 35$ is concave downward to a considerable extent. This occurs since the moment required to produce yielding approaches the critical moment for the straight beam which is low for these values of L/b and the amplification factor in Eq. 72 becomes significant causing the curve to decrease rapidly.

As indicated in Table 11, for a negative flange moment and $\alpha = 2°$, initial yield occurred at the ends of the girder except for one case. With a positive flange moment, however, the midspan cross section yielded first. For $\alpha = 2°$ the direction of the flange moment becomes more important as L/b, d/t_w and A_w/A_f increase. In most cases the yield moment is higher when the applied flange moment is negative or causes compression on the outer edge of the flange at the end. This is as expected since a negative flange moment may be visualized as bending the flange toward the center of curvature which counteracts the effects of lateral outward flange bending produced by deformation of the cross section and the radial moment. For $d/t_w = 165$ this effect becomes quite signi-

Reproduced with permission of the copyright owner. Further reproduction prohibited without permission.

ficant as L/b increases. As α increases to 20° the influence of the direction of the flange moment is more important at the lower values of L/b. For this high curvature the ratio of d/t_w becomes less important and the ratio of the yield moments for the two directions of flange moment are similar for $d/t_w = 40$ and 165.

The influence of curvature on the yield moment is shown in Fig. 26 for a positive and negative flange moment. Although the curved beam equations used in the analysis (11) don't reduce directly to the equations for a straight beam, it was possible to approach this case by setting $\alpha \simeq 0°$. The lowest value of α for which reasonable results were obtained was $\alpha = 1 \times 10^{-6}$ radians. For this case the ratio of σ_f/σ_y was equal to one with equal end moments and zero flange moment, $\sigma_w/\sigma_B = 0$, as expected. This was true for all values of L/b, d/t_w and A_w/A_f for which M^* was less than one since a straight beam under equal end moments will obviously yield only when the end moment reaches M_y i.e. $\sigma_f/\sigma_y = 1$. With an applied flange moment which produces $\sigma_w/\sigma_B = 0.5$, the value of σ_f/σ_y was 0.667 for $\alpha = 1 \times 10^{-6}$ and $L/b \simeq 0$. Since the bending stress at the flange tip in this case is two thirds of the total stress $[\sigma = \sigma_B(1 + \sigma_w/\sigma_B)$, $\sigma_w/\sigma_B = 0.5 \rightarrow \sigma_B = 2/3\sigma]$, this was also as expected. With an applied flange moment the value of σ_f/σ_y decreases as L/b increases, as shown in Fig. 26. As L/b increases additional radial bending occurs and reduces σ_f/σ_y.

The influence of curvature on σ_f/σ_y is apparent in Fig. 26. Obviously as curvature increases, the applied end moment required to produce yielding decreases. This decrease is less significant for a negative flange moment, particularly for lower curvatures, as may be seen by comparing the results for $\sigma_w/\sigma_B = +0.5$ and $\sigma_w/\sigma_B = -0.5$.

Reproduced with permission of the copyright owner. Further reproduction prohibited without permission.

The percentage contributions of the various effects, bending, warping, radial moment, and deformation of the cross section to the total stress at the flange tip are of interest. Results for $\alpha = 1 \times 10^{-6}$ rad. and $\alpha = 20°$ are shown in Figs. 27 and 28 respectively. After determining the end moment required to produce yielding at the flange tip, the stress due to each effect was then computed. The ratio of this stress to σ_y or the percentage contribution of each effect as a function of L/b is shown in these figures.

For the straight beam in Fig. 27, there is no contribution due to deformation of the cross section since $\sigma_B A_f/R = 0$ at $R = \infty$. For $d/t_w = 40$, the girder is torsionally stiff and the warping stress at midspan due to applied end bimoment is considerably reduced (Fig. 22). The radial bending stress at midspan is smaller than this reduction, consequently the total stress at the ends of the girder is higher than at midspan and yielding occurs at the ends. The percentage contributions of warping and bending for this case are slightly affected as L/b increases due to the amplification factor on bimoment. For $L/b < 5$ the percentage contributions of bending and flange moment are approximately 66.7% and 33.3% as discussed previously. With $d/t_w = 165$, as L/b increases, however, the radial bending effect becomes more significant. The analysis presented herein thus predicts radial bending even for the case of an approximately straight beam with an extremely large radius of curvature and an end bimoment or flange moment. This occurs since the twist ϕ produced by this bimoment interacts with the applied end moment in accordance with Eq. 63 to produce a radial bending moment $M_{y_{SM}}$.

Reproduced with permission of the copyright owner. Further reproduction prohibited without permission.

For $\alpha = 20°$ in Fig. 28, the influence of deformation of the cross section is more significant than the effect of radial bending. The contribution of the flange moment or warping is also significant, and the stresses produced by this effect predominate over the bending stresses. As d/t_w decreases the warping contribution decreases and the contribution due to deformation of the cross section increases. This occurs since decreasing d/t_w implies that the flange area A_f be increased in order to keep A_w/A_f constant as was done in Fig. 28. Increasing the flange area will thus increase the deformational force $\sigma_B A_f/R$.

For practical bridge girders the presence of residual stresses due to fabrication will cause yielding to occur at lower values of σ_f/σ_y than discussed above since these residual stresses add to the applied stresses. The influence of residual stresses for a welded girder with $\alpha = 2°$ is indicated in Table 12. The residual stress pattern used for this case is presented elsewhere (26). The results indicate that residual stresses may lower the initial yield moment from 7% to 25%. The effect of residual stresses becomes more important as L/b decreases. The largest reductions occurred in the practical range of L/b from 5 to 15. Values are not given in Table 12 for a heat curved girder. Since the residual compressive stresses nearly equal to the yield stress exist in the compression flange of a heat curved girder (26), yielding will commence for extremely low values of applied end moment.

5.3 Inelastic Behavior

The equations derived in this report as well as the curved beam equations based on linear theory are only directly applicable in the elastic range. After the stress anywhere in the girder reaches the yield stress, modifications must be introduced to account for inelastic action. Because residual stresses cause yielding at very low values of the applied

Reproduced with permission of the copyright owner. Further reproduction prohibited without permission.

load and since test results (21) have indicated that failure or unloading of a curved plate girder does not occur at initial yield, it is necessary to extend the results in the previous section into the inelastic range.

The equations in Chapter 2 were derived on the basis of equilibrium considerations and are therefore valid in the inelastic range provided the influence of yielding on the stiffness properties I_x, I_w, I_y and K_T is taken into account. This would require an incremental type solution in which the spread of yielding along the length of the girder is taken into account (4).

In order to eliminate this complication, a simplification was introduced in the inelastic range. It was assumed that yielding takes place at a single cross section and the accompanying plastification of the cross section occurs at this cross section only i.e., the plastic hinge length was taken to be zero. It was also assumed initially that failure would occur when this cross section was fully yielded or a plastic hinge developed. In slender web straight plate girders encountered in bridges, the compression area of the web is not fully effective in resisting bending (22). Recent tests indicated that this same effect occurs in curved plate girders (21). For straight girders, it was determined (22,33) that the full plastic moment could only develop if the web slenderness ratio is low. It was further determined that for very slender webs, only a portion of the web is effective in carrying compressive stress due to bending. The girders considered in this study have web slenderness ratios that range from 40 to 165. At the higher end of this scale, there is some reduction in the ability of the web to carry compressive stress. However, without detailed information on the behavior of curved web panels near ultimate strength and the resulting redistribution of stress over the cross section it is difficult to evaluate such reduction. In view of some of the conservative factors which are built

Reproduced with permission of the copyright owner. Further reproduction prohibited without permission.

into the ultimate strength model such as completely neglecting the contribution of the web in resisting the flange thrust, it was decided to consider the full web as effective in bending. Instability or unloading due to local buckling is neglected. This implies that the compression flange width-thickness ratio is the same as that for a compact section ($b/t_f \leq 17.5$ - ref. 26). If a girder is non-compact, local and lateral buckling are interrelated. This relationship will be discussed in Chapter 6 in formulating design recommendations.

For the ultimate strength model the following procedure was used to determine the value of the end moment required to cause a plastic hinge to form for a given ratio of the applied flange moment to bending moment at the end of the girder:

1. Given L/b, d/t_w, A_w/A_f and α. Since t_f/t_w is assumed to be 3.0, this completely determines the geometry of the girder.
2. Assume values for the widths of the fully plastic stress blocks in the flanges at the plastic hinge.
3. Compute the depths of the fully plastic stress blocks in the web from equilibrium ($\int_A \sigma dA = 0$).
4. Compute the values of bending moment M_x, flange moment M_F, and radial moment $M_{y_{SM}}$ associated with the fully plastic stress distribution obtained in steps 2 and 3.
5. Using the equilibrium expression from linear theory calculate the applied end moment necessary to produce the bending moment at the assumed hinge. Divide this by $(M_{cr})_{st}$ to obtain M^*.
6. Using the value of M^* obtained in step 5, calculate the value of the flange moments at the hinge attributable to deformation

Reproduced with permission of the copyright owner. Further reproduction prohibited without permission.

of the cross section. Subtract this value from the value obtained in step 4 to determine the value of the flange moments due to internal bimoment. Making use of the amplification factor, Eq. 72, described earlier, calculate the value of the flange moment at the hinge attributable to applied end moment. Subtract this value from the value due to internal bimoment determined above, obtaining the value of the flange moment attributable to applied end bimoment alone. Using this value, determine the ratio of the applied end flange moment to the applied end moment, using the relationships of the linear theory and the amplification factor.

7. For the applied end moment expressed by M^* and the flange moment determined in step 6, calculate the radial moment, $M_{y_{SM}}$, using the simple model relationship, linear theory and the amplification factor. Compare this value with the value obtained in step 4. Divide the difference between the two values obtained by the value of the applied end moment and consider this a measure of accuracy.
8. Repeat steps 2 to 7 for all possible values for the widths of the fully plastic stress blocks in step 2. Record the information obtained for a desired range of ratios of applied end flange moment to bending moment and for an acceptable measure of accuracy.
9. Do steps 2 through 8 considering the hinge to be first at midspan of the girder and second at the end cross section of the girder. For a given ratio of applied end flange moment to bending moment, the location giving the lowest value of M^* is considered to govern.
10. For an acceptable loading configuration, calculate the ratio σ_f/σ_y corresponding to the governing value of M^*, as calculated previously

Reproduced with permission of the copyright owner. Further reproduction prohibited without permission.

for initial yield. If this value is greater than the value given by the AASHO expression (10) for inelastic lateral torsional buckling of a straight girder, the AASHO value is considered to govern.

11. For a given ratio of applied end flange moment to bending moment which may be expressed as the end ratio of warping to bending stress calculated elastically, σ_W/σ_B , steps 1 through 10 may be repeated for different ratios of L/b in the range 0-36 as was done for initial yield.

Before discussing the results obtained using this procedure, it is useful to discuss the effects of the various simplifications on the final value of the ultimate load and consider some limitations on this procedure. There are several factors which tend to make this procedure unconservative. As discussed above, the full web is not effective in resisting compression due to bending as is assumed in the procedure. Also, the assumption has been made that normal stresses predominate over shearing stresses to the extent that shearing stresses have been neglected not only in the ultimate strength calculation but indeed in this entire analysis. Since there is an interaction between the formation of a plastic hinge due to shearing stresses and a plastic hinge due to normal stresses it is unconservative to simply neglect this interaction. Lastly, the assumption is made that the girder acts elastically everywhere but at the plastic hinge which has zero length. If the spread of yielding were considered, cross-sectional properties such as EI_x , EI_y , EI_w and GK_T would be reduced over part of the region which is now considered elastic and as having elastic properties. In addition the amplification factor, which was developed for elastic analysis, is such that it gets very large at the

Reproduced with permission of the copyright owner. Further reproduction prohibited without permission.

elastic buckling moment. This elastic buckling value was taken as identical with $(M_{cr})_{st}$ as indicated by the results discussed in Chapter 3. Actually this factor should get very large at the inelastic buckling moment for a curved beam which is unknown. It is conceivable that the straight beam inelastic buckling value is a good approximation to this value, on the assumption that the behavior in the inelastic range will be quite similar to the behavior in the elastic range. There is no solid evidence to support such an assumption however. All these factors tend to cause the procedure to give a value of σ_f/σ_y that is too large.

There are also several factors which make this analysis conservative. First of all the procedure used to isolate a girder between supports and to evaluate the effects of cross sectional deformation, which was discussed in the beginning of this chapter, is conservative. Also, the development of a plastic hinge at one cross section does not necessarily constitute failure of the entire structure since a redistribution of load is possible. This redistribution, however, requires that the girder possess sufficient rotation capacity at the hinge location. The dimensions of practical curved plate girders are usually less than required in order to obtain this rotation capacity and so the assumption is made that failure is approximated at the formation of the first hinge. However, even if a plate girder does not have the rotation capacity to form a mechanism, it does have some additional strength due to redistribution of stress after the first hinge is formed and to neglect this is conservative. Lastly, if a value of σ_f/σ_y corresponding to the formation of the first hinge as calculated using this procedure was greater than the value given by the straight beam inelastic lateral torsional buckling formula given by AASHO (10), it was replaced by this value. This of course is necessary because the moment which causes a straight

Reproduced with permission of the copyright owner. Further reproduction prohibited without permission.

girder to deflect very quickly and fail due to the geometric build up of deflections associated with buckling is undoubtedly larger than the moment required to cause the same kind of behavior in a curved girder. It may not, as in the elastic range, be very much larger however. The interaction between action of this type and the gradual build up of stress in the model as considered should lead to the same failure moment, and of course should be considered. However, the AASHO formula used only allows values of σ_f/σ_y less than one, even for very low values of L/b. It neglects, for adequately braced sections, the fact that the girder can be loaded beyond M_y, indeed, in some cases, to the fully plastic moment M_p. To neglect this extra strength is, of course, conservative.

Since there are factors which tend to make the final result obtained using the procedure outlined above either too high or too low, the only way to judge the adequacy of the procedure is to check its performance against experimental results. Such a comparison is made in Chapter 6, and indicates that the procedure yields results which are conservative but not unduly so, and thus represents an adequate approximation to the ultimate strength of curved plate girders.

The procedure was used as outlined above since not every specific combination of bending moment, flange moment and radial moment corresponds to a plastic hinge. It was thus more efficient computationally to specify the final stress picture (yield stress distribution of the plastic hinge) and work back to determine the end moments and flange moments rather than increment the end loading until a plastic hinge forms. It is a limitation on this procedure that for certain configurations of geometry and end loading, the stress resultants at the location considered for a hinge are in such a ratio as not to correspond to any possible hinge. This doesn't mean that for these configurations a physical girder would not reach its

Reproduced with permission of the copyright owner. Further reproduction prohibited without permission.

ultimate strength as the end loads are increased, but simply that some (perhaps small) non-zero hinge length is required to cause the ratios of internal stress resultants at the hinge to match up with those from the rest of the girder. For this reason only central angles up to 6° and L/b ratios up to 25 are considered in the following discussion of results rather than α values up to 20° and L/b up to 35 as used for the initial yield results discussed previously. Note that these values cover the range of parameters encountered in practical girders.

The interaction between the results of the ultimate strength procedure described above and the inelastic straight girder lateral buckling results expressed by AASHO (10) as

$$\frac{\sigma_f}{\sigma_y} = \left[1 - 3\left(\frac{L}{b}\right)^2 \frac{\sigma_y}{\pi^2 E}\right] \tag{76}$$

is shown in Fig. 29. In this figure results are shown for a girder with $A_w/A_f = 1.3$ and $d/t_w = 165$ loaded by end moments. At $\alpha \simeq 0°$, the ultimate strength procedure leaving out step 10, yields the result that the girder will fail at the shape factor, 1.11, the ratio of fully plastic moment to the yield moment, regardless of L/b. This is a reasonable result coincident with simple plastic design for a simply supported straight girder subjected to equal end moments. For this case the AASHO curve which is based on buckling considerations governs and is shown as the solid $\alpha = 0°$ curve. At $\alpha = 2°$, the ultimate strength procedure yields values of σ_f/σ_y which are higher than those given by Eq. 76 until L/b reaches 15. Thus it is cut off by the AASHO curve and is shown as the solid $\alpha = 2°$ curve. At $\alpha = 6°$, the ultimate strength procedure yields results which are below the AASHO curve except at very low values of L/b. Note that the dotted curves all approach $\sigma_f/\sigma_y = 1.11$ as L/b approaches zero.

Reproduced with permission of the copyright owner. Further reproduction prohibited without permission.

It is important to note that the AASHO expression, Eq. 76, does not depend on cross sectional geometry or on applied end bimoment. Thus the interaction shown in Fig. 29 is not exactly the same as it would be at a different value of d/t_w or A_w/A_f, or if a bimoment loading were considered. The AASHO curve was developed using the philosophy that the top flange of a girder acts as a column in buckling to the side laterally and it agrees well with test results for straight girders. Considering this there is no reason to expect that the form of the AASHO relationship should necessarily be the same as the form of the ultimate strength results using the procedure as outlined above.

Results are presented in Fig. 30 for $\alpha = 2°$ showing the reduction in ultimate strength, expressed as σ_f/σ_y, with increasing L/b. This figure is comparable to the initial yield results for the same girder geometry and loading shown in Fig. 23. Consider first the curves for $d/t_w = 165$. As in Fig. 23 the curves for the case of applied end bimoment, $\sigma_W/\sigma_B = 0.5$, are lower than those for $\sigma_W/\sigma_B = 0$. However, while in Fig. 23 the curves for $A_w/A_f = 2.0$ are always lower than the corresponding curves for $A_w/A_f = 0.5$, the ultimate strength curves in Fig. 30 are higher at low L/b values for $A_w/A_f = 2.0$ than for $A_w/A_f = 0.5$, and then cross and are lower for high L/b values. In calculating the initial yield curves it was necessary to find the value of applied end moment that would cause an internal moment at either midspan or the end of the girder that equaled the yield moment. In making the ultimate strength calculation it is necessary to do very much the same thing but the value that the internal moment must equal is not a value depending solely on geometry as is the yield moment, but is the hinge moment which depends on geometry and also on the ratios of flange moment to bending

Reproduced with permission of the copyright owner. Further reproduction prohibited without permission.

moment required at the hinge which depend nonlinearly on the value of the end loads. This fact accounts for the difference in behavior between the curves in Fig. 30 and those in Fig. 23. For $d/t_w = 40$, all the curves are cut off by the AASHO curve at high L/b values and all but the curve for $A_w/A_f = 0.5$ and $\sigma_W/\sigma_B = 0.5$ are cut off for low L/b values. At $d/t_w = 40$ the girder has considerable torsional rigidity and the ultimate strength curves do not drop off as fast with L/b as they do for $d/t_w = 165$. Consequently they are higher than the AASHO curve which doesn't depend on any geometric properties except L/b.

Results for the same cases with a central angle of 6° are shown in Fig. 31. For both values of d/t_w the curves with $A_w/A_f = 0.5$ are lower than those for $A_w/A_f = 2.0$. Due to the larger central angle the curves at $d/t_w = 40$ are now for the most part below the AASHO cut off and behave similarly to those at $d/t_w = 165$. The computational procedure did not yield results at $d/t_w = 165$ and $A_w/A_f = 2.0$ for L/b greater than 15 for the case of an applied end bimoment corresponding to $\sigma_W/\sigma_B = 0.5$ and greater than 20 for $\sigma_W/\sigma_B = 0$. This is due to the limitation on the procedure caused by the assumption of a zero hinge length as discussed above.

Figure 32 indicates the influence of the direction of the applied end bimoment on the ultimate strength. It is comparable to Fig. 25 which demonstrated the same effect for initial yield. The same general trend is apparent in that a positive bimoment reduces the strength of the girder more than a negative bimoment.

The influence of curvature on ultimate strength is shown in Fig. 33. This is comparable to Fig. 26 which shows the same effect for initial yield. For $\sigma_W/\sigma_B = 0.5$ the curves indicate a gradual reduction in the

Reproduced with permission of the copyright owner. Further reproduction prohibited without permission.

ultimate strength with curvature. Note that the values of σ_f/σ_y for $L/b = 5$ and $L/b = 0$ on the curves for $\alpha = 0°$ (these are of course the same for + or - σ_w/σ_B) are below the values according to AASHO. This is due to the fact that twisting occurs due to the applied bimoment and hence some radial moment is developed. Because of this there is an internal flange moment as well as bending moment at the hinge and the curves would not approach the simple shape factor for pure bending as $L/b \to 0$. For $\sigma_w/\sigma_B = 0$, the curves do this as is indicated in Fig. 29. The $\alpha = 0°$ curve is then cut off by the AASHO requirement until $L/b = 25$ where it falls below the AASHO value. For $\sigma_w/\sigma_B = -0.5$, the curve for $\alpha = 2°$ behaves similar to this. It is below the AASHO curve at $L/b = 5$, coincides with the AASHO curve until $L/b = 20$ and then drops off below the AASHO value. In this case the hinge was formed first at the end of the girder for $L/b = 5$. As mentioned above, when a curve is close to the AASHO curve it may cross it several times since there is no reason why the shapes of the ultimate strength curves developed herein should be the same as the AASHO curve which is derived from a different philosophy.

In Figs. 34 and 35 the contributions of the bending moment, bimoment, radial moment and flange moment due to cross sectional deformation at the ultimate strength of the girder are shown for $\alpha \approx 0°$ and $\alpha = 6°$. In order to make these plots comparable to those for initial yield, Figs. 27 and 28, the contributions are in terms of the elastic stresses calculated for the end loads corresponding to the formation of the first hinge. These are fictitious since the stress is in reality equal to the yield stress at the hinge and is distributed over the cross section differently. The fictitious total stress, which is of course greater than the yield stress, is denoted as σ_p.

Reproduced with permission of the copyright owner. Further reproduction prohibited without permission.

For $\alpha \approx 0°$ and $d/t_w = 165$, the results are straight-forward. Since the ultimate strength load is higher than the initial yield load, the amplification factors affecting radial moment and bimoment are larger and thus their contribution to the total stress is higher than it is in Fig. 27. They are in the same proportion to each other as before. For $\alpha \approx 0°$ and $d/t_w = 40$, the results are identical to those for initial yield in Fig. 27 up to $L/b = 10$. For these values of L/b failure occurs at the ends of the girder. At values of L/b greater than 10 some radial moment is developed due to the applied end bimoment and failure takes place at midspan. Radial stresses were not significant at initial yield where the loads were of course lower. The contribution of warping to the total stress actually decreases as L/b increases from 10 to 25. The reason for this is that the warping stress is due entirely to applied end bimoment. The midspan bimoment due to an applied end bimoment decreases with an increase of L/b. The amplification factor tends to reverse this effect but evidently there is still a net decrease for this case. For the $\alpha = 6°$ case, there is of course a decrease in the contribution of bending stress, an increase in the contributions of warping and radial stress and the development of a significant contribution due to cross sectional deformation. At $d/t_w = 40$ the girder is stiffer in torsion and the contribution of radial and warping stresses is reduced slightly and the contribution of bending and cross sectional deformation stresses is increased slightly over the $d/t_w = 165$ case.

It is important to realize some of the implications in both the initial yield and ultimate strength development of the nonlinearity in the relationship between the loads and the stresses at failure. The ratio of midspan flange moment to applied end flange moment is nonlinearly dependent on load.

Reproduced with permission of the copyright owner. Further reproduction prohibited without permission.

Take for example a girder with $\alpha = 6°$, $A_w/A_f = 0.5$, $d/t_w = 165$ and $L/b = 15$, subjected to end moments and bimoments such that the end ratio of $\sigma_W/\sigma_B = 0.5$. At low loads where amplification is essentially negligible and where the radial stress is negligibly small, the ratio of the flange moment in the top flange at midspan to applied end flange moment (neglecting cross sectional deformation) is 3.3. This is the value that would be obtained from a linear analysis. At initial yield considering the effects of radial moment and cross sectional deformation and the effects of the amplification, the total flange moment in the top flange at midspan becomes 4.45 times the applied end flange moment. Finally at ultimate strength this ratio increases to 5.05. If a designer in the course of his calculations were to use a fixed ratio for this value, the results obtained could be quite inaccurate.

In Chapter 6 a comparison will be made between the results obtained for the initial yield and ultimate strength analyses using the procedures discussed above and some experimental results. Design formulas based on these results will be determined.

5.4 Bracing Forces

After determining lateral bracing spacing, the bracing members must be designed to carry the appropriate forces induced in the bracing system. In a buckling analysis no calculable stress is induced in the brace. For straight girders, therefore, bracing forces were determined empirically or on the basis of an assumed deflected shape after buckling (28). For the curved girder, however, lateral deflections occur from the beginning of loading as indicated in Chapter 3 and it is possible to calculate brace forces directly. Before proceding, however, it is necessary to define what is meant by lateral bracing.

Reproduced with permission of the copyright owner. Further reproduction prohibited without permission.

For the purposes of this report a lateral brace will be defined as a structural member whose purpose is to resist the radial thrust force component developed by the compression flange. If the single span girder in Fig. 20 represents a portion of a curved plate girder between cross diaphragms, these diaphragms must resist the forces developed at the supports. Due to the applied end moment and bimoment a torque M_z results at the ends. For a truss type diaphragm this torque or couple produces forces in the top and bottom chord members of the diaphragm. This torque and the resulting diaphragm forces may be computed from a grid analysis of the entire bridge (31). The diaphragm chord members will also resist the end reactions produced by the radial moment $M_{y_{SM}}$ and the flange force $\sigma_B A_f/R$. Thus the diaphragm will not only function as a grid member in transfering load from one girder to another girder but will also act as lateral bracing. In view of the above definition of a lateral brace, the bracing forces considered herein will include only the force due to $M_{y_{SM}}$ and $\sigma_B A_f/R$, i.e. the force which the member must carry in addition to any forces induced due to the structural action not associated with bracing the compression flange. Note that at the brace points the girder segments on either side of the brace will produce a force in the brace and the total brace force will be approximately twice that produced by the single span girder segment considered herein. If the moment diagram is not constant over the adjacent braced spans this force would be less than twice as large.

Brace forces due to radial bending and cross sectional deformation from the initial yield analysis are given in Table 13 for $\alpha = 2°$ (L/R = 0.035) and $\alpha = 20°$ (L/R = 0.35) for several values of A_w/A_f and d/t_w. These forces were nondimensionalized and expressed as a percentage of the compression flange force $\sigma_B A_f$. Note that since the force due to deformation of

Reproduced with permission of the copyright owner. Further reproduction prohibited without permission.

the cross section is given by $(\sigma_B A_f/R$ Kips/in.$)L/2$, the nondimensional brace force due to this effect is simply $L/2R$ and is independent of A_w/A_f and d/t_w. The radial forces in each case are less than the forces due to deformation of the cross section. As L/b, A_w/A_f, d/t_w and σ_w/σ_B increase the radial forces also increase. It is interesting to note that for $L/R = 0.035$ the brace forces due to deformation of the cross section are quite close to the empirically determined value of 2% of the flange force which is presently used for designing braces for straight beams in buildings.

Bracing forces corresponding to the ultimate strength analysis in Section 5.3 are given in Table 14. The trends in the bracing forces for this case are similar to those for initial yield although the values are somewhat larger. This is reasonable of course since they are calculated the same way but at higher values of the end loads.

It is of interest to compare the brace forces for $\alpha = 2°$ with those determined by Lay (28) for straight beams using simple plastic design. In order to compare these values it is necessary to express the results in Table 14 in terms of the total brace force divided by $\sigma_y A_f$. This was done for $L/R = 0.035$. The brace force determined by Lay increases as the span decreases (and the rotation capacity increases) and also increases linearly with the flange force $\sigma_B A_f$. For a W10 x 25 A36 steel beam with $A_w/A_f = 1.03$ braced at $L/b = 8.3$, Lay obtained a force of 3.2% $\sigma_y A_f$. To compare with this value, the brace forces in Table 14 were multiplied by two to take the adjacent spans into account. For $L/b = 10$ and $L/R = 0.035$ with $\sigma_w/\sigma_B = 0$, these values are somewhat larger than that determined by Lay. This is understandable since both this analysis and that by Lay are based on ultimate strength concepts. Obviously as the curvature L/R

Reproduced with permission of the copyright owner. Further reproduction prohibited without permission.

increases from the straight case to L/R = 0.035 one would expect the brace force to increase.

Design values for brace forces at both initial yield and ultimate strength will be developed in Chapter 6.

Reproduced with permission of the copyright owner. Further reproduction prohibited without permission.

6. DESIGN RECOMMENDATIONS

6.1 General

In developing a design formula for the allowable compression flange stress in a curved girder it is advantageous to express this relationship in the following form

$$F_{bc} = F_{bs}\rho \tag{77}$$

In Eq. 77 F_{bc} represents the stress in the curved beam, F_{bs} the stress in the equivalent length straight beam and ρ the effects of curvature. The factor ρ should reduce to unity when $\sigma_w/\sigma_B = 0$ as L/R approaches zero or the radius of curvature becomes infinite. The existing AASHO formula will be used for F_{bs}, i.e.

$$F_{bs} = 0.55F_y\left[1 - 3\left(\frac{L}{b}\right)^2 \frac{F_y}{\pi^2 E}\right] \tag{78}$$

Using Eq. 78 with $0.55F_y$ will result in the same factor of safety for a curved girder as presently used for straight girders which is reasonable. The results in Chapter 5 indicate that ρ will be a function of the following parameters:

$$\rho = \rho(A_w/A_f,\ d/t_w,\ L/b,\ \alpha = L/R,\ \sigma_w/\sigma_B) \tag{79}$$

It will be shown later that the factor ρ is independent of yield stress and is the same for the various grades of structural steel.

As noted previously, the terms A_w/A_f and d/t_w relate the St. Venant and warping torsional rigidities of the girder cross section.

Reproduced with permission of the copyright owner. Further reproduction prohibited without permission.

Since the percentage contribution of each of these rigidities to the total torsional rigidity of the cross section varies with the type of section (beam vs. girder), it was necessary to use two formulas for allowable stress for bending members in buildings in order to reflect this fact (9). For the sections commonly used in bridges, the warping torsional rigidity or the lateral bending rigidity of the compression flange usually predominates (22). For this case, the dependence of ρ in Eq. 79 on A_w/A_f and d/t_w may be neglected to achieve a simplified design formula. This is consistent with the current AASHO allowable stress formula for straight beams which neglects these two factors (10,22). The factor ρ will therefore be developed from the results in Chapter 5 for a specific value A_w/A_f and d/t_w.

The results in Chapter 5 indicated that the values of σ_f/σ_y were related to A_w/A_f and d/t_w. The relationship between A_w/A_f, d/t_w and the flange proportions may be expressed as

$$\frac{A_w}{A_f} = \frac{dt_w}{bt_f} = \frac{(d/t_w)}{(b/t_f)}\left(\frac{t_w}{t_f}\right)^2 \qquad (80)$$

Note that specifying b/t_f amd d/t_w in Eq. 80 fixes A_w/A_f. With b/t_f = 17, 23 and d/t_w = 40, 165 the following values of A_w/A_f result

d/t_w	b/t_f	A_w/A_f		
		$t_f/t_w = 1$	$t_f/t_w = 2$	$t_f/t_w = 3$
40	17	2.35	0.59	0.26
	23	1.74	0.44	0.29
165	17	9.70	2.42	1.08
	23	7.17	1.79	0.79

Reproduced with permission of the copyright owner. Further reproduction prohibited without permission.

The value of $b/t_f = 17$ is close to the value for a compact section in which local buckling will not occur prior to full yielding of half of the flange (26) and $b/t_f = 23$ is the present AASHO limiting value for A36 girders. In deriving the curvature correction factor ρ the following values will be used: $A_w/A_f = 1.0$, $d/t_w = 150$. This gives $b/t_f = 16.7$ with $t_f/t_w = 3$. These values are quite close to the average values of $A_w/A_f = 1.3$, $d/t_w = 147$, $b/t_f = 17.2$ and $t_f/t_w = 3$ determined from a survey conducted by the authors of 28 curved girder bridges.

The range of curvature will be $0 \leq L/R \leq 0.1$. The value of L/R of 0.1 corresponds to an included angle between braces of 5.7°. The total central angle between supports for an average curved bridge (25) is about 5°. Even for the maximum central angle of 30° determined from this survey, with diaphragms located less than 25 ft. apart the value of L/R would be less than the upper limit of 0.1 selected in this study.

The curvature factor ρ in Eq. 77 will be determined for two conditions. The first condition will be for a girder with no residual stresses and failure will be defined as initial yield of the most highly stressed fiber i.e. the flange tip. The second condition will be based on the ultimate strength concept in Section 5.3 in which failure occurs when the compression flange is fully yielded. The appropriate condition to be used for design specifications will be discussed andmay be evaluated on the basis of comparisons with test results from the CURT project. The influence of local buckling on this final design recommendation will also be considered.

Reproduced with permission of the copyright owner. Further reproduction prohibited without permission.

Equation 77 in its most general form should be applicable to unsymmetric (about the bending axis) as well as symmetric plate girders. Equation 78 for the straight girder is applicable to both symmetric and unsymmetric girders. Although Eq. 78 was derived for symmetric girders it was extended to unsymmetric girders in view of the fact that lateral buckling involved only consideration of the compression flange treated as a column. The writers believe that Eq. 77 which will be based on the results presented herein for symmetric cross sections will also apply for unsymmetric cross sections. Consideration of the four effects influencing ρ will confirm this. For a singly symmetric girder loaded by end moments and bimoment, lateral deflections in the plane of curvature will result in addition to vertical deflections and twist (11). The radial bending derived in Chapter 2 on the basis of a second order analysis produces a similar effect. Since the moment and bimoment at the brace point or the ends of the single span model used in this report were assumed to be those calculated on the basis of linear theory using a grid analysis, these values will incorporate the effects of single symmetry assuming the appropriate moment-curvature relationships are used in the grid analysis (11). The fourth effect considered herein, the lateral flange thrust producing deformation of the cross section, will be affected if the compression flange is larger than the tension flange. Since the thrust equals $\sigma_B A_f/R$, increasing the flange area will increase this force. The ability of the flange to resist this force, however, will also increase since the section modulus of the flange about the vertical axis will increase. Although it is not possible to determine the resultant effect produced by increasing A_f since the value of

Reproduced with permission of the copyright owner. Further reproduction prohibited without permission.

σ_B for an unsymmetric girder will probably also be different from that in a symmetric girder, the increased flange rigidity should compensate for any increase in flange thrust for practical bridge girders.

For composite construction the compression flange in the positive moment region is continuously laterally braced by the concrete deck and no stress reduction to account for lateral buckling is required. Note, however, that the tension flange will be subjected to additional flange bending due to deformation of the cross section. Since this effect is not usually taken into account in design, formulas for limiting the tension flange stress in composite construction will also be developed. In the negative moment region near interior supports in continuous bridges, the results herein are directly applicable if the contribution of the slab to the moment of inertia of the girder is neglected due to cracking.

6.2 Initial Yield

Studies by Culver and Nasir (26) showed that local buckling occurred at loads quite close to those at which the outer edge of the flange tip yielded due to the combined warping and bending stress for girders with b/t_f less than certain values. These results are indicated in Table 15. In determining the values of the nondimensional local buckling moments M/M_y listed, the effects of residual stresses due to fabrication were included. Also listed in Table 15 are the values of the moment required to produce initial yield at the flange tip, neglecting residual stress, for the corresponding ratios of σ_W/σ_B. Since the warping and bending stresses are linearly related, the values of the nondimensional initial yield moment are simply $M/M_y = 1/(1 + \sigma_W/\sigma_B)$.

Reproduced with permission of the copyright owner. Further reproduction prohibited without permission.

The yield moments, neglecting residual stress, and the local buckling moments in Table 15 are quite close. Thus if the bending stress or bracing spacing L/b which involves lateral buckling considerations is based on the initial yield results obtained in Chapter 5 neglecting residual stress, the results in Table 15 indicate that local buckling and lateral buckling would occur almost simultaneously, i.e. the factor of safety against both effects would be the same. This is reasonable even though the local buckling moments are slightly less than the initial yield moments for some cases in Table 15, e.g. A441 welded girder. These differences are within the range of accuracy of the local buckling analysis since the material properties in the inelastic range are not known exactly. It must also be noted that the residual stress pattern used in this analysis was not exact and would vary somewhat from one girder to another. Similar small differences have been neglected in establishing design requirements for straight girders.

If the compression flange width-thickness ratio is small enough it is possible to fully plastify the entire flange before local buckling occurs. In this case the ultimate strength determined in Section 5.3 could be realized. Use of the initial yield condition for determining bracing spacing in this case would be unduly conservative. It is therefore advisable to relate the allowable bending stress to the width-thickness ratio of the flange. Design formulas for non compact girders with b/t_f values similar to those presently used for straight beams will be given in this section. Design formulas for compact girders will be developed in Section 6.3.

A summary of limiting values of the compression flange width-thickness ratios based on local buckling given in various specifications as well as

Reproduced with permission of the copyright owner. Further reproduction prohibited without permission.

those determined for curved girders is given in Table 16. All the appropriate specification formulas have been converted to psi. The AASHO formula (10) has been expressed in terms of the yield stress using $f_b = 0.55F_y$. The tabulated values of b/t_f for the various yield stress values were taken directly from these references. Note that for noncompact sections the AASHO values of b/t_f and those proposed for load factor design are less than those presently allowed for buildings using the AISC Specification. For compact sections, the values proposed for load factor design differ slightly from the corresponding AISC values. This is due to the approximations involved in developing a simple formula for design use. The values determined for compact curved girders (26) are less than both of these values and the difference increases as F_y increases. For F_y = 50,000 psi. The value of $b/t_f = 13.0$ is 10% less than the load factor value. In view of the fact that the inelastic material properties, particularly the shear modulus G_{st}, on which these values for curved beams are based are not known that accurately and since the conservative assumption of uniform moment over the local buckling length was used in the analysis it is reasonable, for the sake of uniformity, to adopt the values of b/t_f used for load factor design for compact sections.

The formulas for allowable stress or bracing spacing presented in this section which are based on the initial yield concept in Section 5.2 will therefore apply to non compact girders with $3200/\sqrt{F_y} \leq b/t_f \leq 4400/\sqrt{F_y}$. In view of the fact that initial yielding of the flange tip drastically reduces the local buckling strength of the girder (26) and there is very little increase in the local buckling moment above the yield moment for this entire range of b/t_f (see Table 15) a single formula will be deter-

Reproduced with permission of the copyright owner. Further reproduction prohibited without permission.

mined for this range of b/t_f. The use of a transition formula which permits an increase in allowable stress as b/t_f is decreased from $4400/\sqrt{F_y}$ to $3200/\sqrt{F_y}$ (9,33) is not advisable for curved beams.

The results in Chapter 5 indicate that the values of σ_f/σ_y for both initial yield and ultimate strength decrease substantially at high values of L/b. For this reason it is proposed that the bracing spacing be limited to $L/b \leq 25$. Although this limit is less than $L/b = 36$ presently permitted for straight bridges, (A36 steel), it is doubtful that curved bridges designed with $L/b > 25$ would be economical in view of the significant warping or flange bending stresses which would occur with such large diaphragm spacing. This upper limit is also reasonable if the maximum diaphragm spacing of 25 ft. presently used for straight bridges is adopted for curved bridges, i.e. assumming a minimum flange width equal to 1 ft. then $(L/b)_{max} = 25$.

In order to develop a design formula, the initial yield curves for A36 steel girders in Figs. 36, 37 and 38 were determined using the approach discussed in Section 5.2. Note that the range of σ_W/σ_B was between +0.5 and -0.5. A trial and error process was then used to develop a simple design formula. In order to illustrate the effect of the lateral flange bending stress, the curvature correction factor ρ was separated into two parts and Eq. 77 was rewritten as

$$F_{bc} = F_{bs}\rho_B\rho_w \tag{81}$$

The first part, ρ_B, applies to the bending stress and the second, ρ_w, to the lateral flange bending or warping stress.

To determine ρ_B, the curves for $\sigma_W/\sigma_B = 0$ were replotted and the variation with L/R and L/b determined. In view of Eq. 77, the curves

Reproduced with permission of the copyright owner. Further reproduction prohibited without permission.

in Figs. 36, 37 38 were divided by the AASHO value of F_{bs} in Eq. 78 before replotting.

After determining the influence of L/R and L/b for $\sigma_w/\sigma_B = 0$, the factor ρ_w for the influence of the lateral flange bending stress was determined by a similar trial and error process. In view of the different influence of a positive or negative flange moment at the brace points, it was necessary to derive two values for ρ_w depending upon the direction of M_F.

The final values obtained for these correction factors are

$$F_{bc} = F_{bs}\rho_B\rho_w \tag{82}$$

where

$$\rho_B = \frac{1}{1 + (L/R)(L/b)[1 - \frac{L/b}{500}]} \tag{83}$$

$$\rho_w = \frac{1}{1 + (F_w/F_{bc})[1 - \frac{L/b}{75}]} \tag{84}$$

$$\rho_w = \frac{0.95 + (L/b)/[30 + 8000(0.1 - L/R)^2]}{1 - 0.6(F_w/F_{bc})} \tag{85}$$

For the case in which the applied flange moment at the ends of the girder causes compression on the flange tip toward the center of curvature, positive bimoment Fig. 22, Eqs. 83 and 84 should be used in Eq. 82. For the case in which lateral flange bending produces compression at the outer flange tip on the ends of the girder, Eq. 82 must be checked using Eq. 83 and 84 and also Eqs. 83 and 85. In this case the smallest value of F_{bc} should be used.

Reproduced with permission of the copyright owner. Further reproduction prohibited without permission.

In deriving Eqs. 83, 84 and 85 every attempt was made to obtain simple equations. Since this involved curve fitting the exact results in Figs. 36, 37 and 38, these equations contain some approximation. This is indicated in Table 17. The exact results, those obtained using Eqs. 83, 84, 85 and the percent differences are shown in this Table. Note that in most cases the percent differences are quite small in the practical range. For high values of the warping stress ratio σ_w/σ_B the design equations are slightly unconservative. This is acceptable in view of the conservatism built into the analytical model. Although the design equations become quite conservative for $L/R = 0.1$ and $L/b = 25$, this is reasonable since this range is beyond values encountered in most practical bridges. For these high values it is not unreasonable to introduce additional conservatism. These differences and consequently the approximations in the design equations, in the writers opinion, are acceptable for design purposes. Although more accurate formulas over the entire range of parameters could probably be derived, they would be more complicated than Eqs. 83, 84 and 85. Note that if limitations were applied to the range of values of some of the parameters e.g. $|\sigma_w/\sigma_B| \leq 0.2$, it may be possible to simplify these equations further.

For design purposes, it is useful to present the correction factors ρ in graphical or tabular form to eliminate the necessity of evaluating Eqs. 83, 84, 85. These values are given in Tables 18 and 19 and Figs. 39 and 40. Figures 39 and 40 were drawn quite accurately and values sufficiently accurate for design use may be scaled directly from these figures.

It should be noted that the correction factors in Eqs. 83, 84 and 85 take into account several effects. Since Eq. 82 refers to the allowable stress at the ends of the braced segment or the diaphragm locations, the

Reproduced with permission of the copyright owner. Further reproduction prohibited without permission.

increase in stress at the center of this braced length due to curvature effects is included in ρ. The second order radial bending effects as well as deformation of the cross section are also included in these factors.

As indicated, Figs. 36, 37 and 38 were developed for A36 steel with σ_y = 36 ksi. Since the AASHO formula used to derive Eq. 82 depends on σ_y it was necessary to determine if the same correction factor in terms of L/R, L/b and σ_w/σ_B was applicable to steels with different yield stress values. Results similar to those in Figs. 36, 37 and 38 were therefore obtained for σ_y = 50 ksi. These results are shown in Table 20a. They indicate that the initial yield curves were affected by the value of the yield stress. This occurs because of the nonlinearity in the analytical model. Since the end loads required to produce yielding increase nonlinearly the ratio of σ_f/σ_y is not independent of the value of the yield stress. The AASHO formula, F_{bs} Eq. 82, also varies with yield stress. The variation of σ_f/σ_y with yield stress level from the analytical solution and the ratio $F_{bs}/0.55F_y$ using the AASHO formula is shown in Table 20. Note that the variation of $F_{bs}/0.55F_y$ is similar to that for σ_f/σ_y. Although the variations are not identical it is sufficiently accurate for design purposes to neglect this fact. Thus Eq. 82 is applicable to the various grades of steel provided the appropriate value of F_y is used to determine F_{bs} in Eq. 78.

In summary, the results in this section may be expressed as the following design recommendation:

> "For horizontally curved plate girders in which the compression flange plate width to thickness is in the range determined by the formula:
>
> $$3200\sqrt{F_y} < b/t_f \leq 4400\sqrt{F_y} \qquad \text{(a)}$$

Reproduced with permission of the copyright owner. Further reproduction prohibited without permission.

The average unit stress in the compression flange shall not exceed

$$F_{bc} = F_{bs}\rho_B\rho_w \qquad (b)$$

at the location of the cross diaphragms, where

$$F_{bs} = 0.55F_y\left[1 - 3\left(\frac{L}{b}\right)^2\frac{F_y}{\pi^2 E}\right] \qquad (c)$$

$$\rho_B = \frac{1}{1 + (L/R)(L/b)[1 - \frac{L/b}{500}]} \qquad (d)$$

$$\rho_w = \frac{1}{1 + (F_w/F_{bc})[1 - \frac{L/b}{75}]} \qquad (e)$$

$$\rho_w = \frac{0.95 + (L/b)/[30 + 8000(0.1 - L/R)^2]}{1 - 0.6(F_w/F_{bc})} \qquad (f)$$

L = Length in inches of the unsupported compression flange between cross diaphragms.

R = Radius of curvature in inches to the web of the girder.

b = Total flange width in inches.

In Eqs. e and f, F_w represents the stress at the diaphragm location due to lateral flange bending. The ratio F_w/F_{bc} shall be taken as negative if F_w is compression on the flange tip further away from the center of curvature and positive if F_w is compression on the flange tip closest to the center of curvature. If F_w/F_{bc} is positive Eq. e shall be used in Eq. b for ρ_w. If F_w/F_{bc} is negative, Eq. b shall be evaluated using Eqs. e and f and the smaller value obtained for F_{bc} shall govern.

The allowable stress in Eq. b shall be computed using the larger of the two bending moments and the two flange moments at either end of the braced flange.

In no case shall $|F_w/F_{bc}|$ exceed 0.5 and L/b shall not exceed 25.

Eq. b shall be checked for both live load and erection conditions."

Reproduced with permission of the copyright owner. Further reproduction prohibited without permission.

6.3 ULTIMATE STRENGTH

As discussed in Section 6.2, the formulas for allowable stress based on the ultimate strength concept presented in this section will apply to compact girders i.e. girders with $b/t_f \leq 3200/\sqrt{F_y}$. Limiting the width-thickness ratio of the compression flange to this value will insure that the ultimate moment will be reached prior to the occurrence of local buckling.

The ultimate strength curves for A36 steel girders in Figs. 41, 42 and 43 were determined using the approach discussed in Section 5.3. A trial and error process similar to that discussed for the initial yield case was then used to determine a simple design formula. In this case the following result was obtained

$$F_{bc} = F_{bs}\rho_b\rho_w \tag{86}$$

where

$$\rho_b = \frac{1}{1 + (L/R-0.01)^2\, L/b \left[1 + \frac{L/b}{6}\right]} \tag{87}$$

$$\rho_w = 0.95+18(0.1-L/R)^2-\frac{(F_w/F_{bc})\left[0.3-0.1(L/R)(L/b)\right]}{\rho_B F_{bs}} \tag{88}$$

The correction factor ρ_w in Eq. 86 is valid for both positive and negative bimoment i.e. σ_w/σ_B + or -. If, however, the product $\rho_B\rho_w$ in Eq. 86 exceeds one, then the total correction factor should be set equal to unity and the allowable stress F_{bc} equals the AASHO value F_{bs}. In this case it was not necessary to determine two values for σ_w depending upon the direction of the flange moment.

Reproduced with permission of the copyright owner. Further reproduction prohibited without permission.

The approximations involved in Eqs. 87, 88 as compared to the exact ultimate strength results are indicated in Table 21. The per cent differences are similar to those in Table 17. Again the design formula compares quite well with the exact result for the practical range of L/b and L/R.

The results in Table 20b indicate that the influence of the value of the yield stress on Eq. 86 for ultimate strength is similar to that discussed previously for the case of initial yield. Consequently Eq. 86 may be used for any grade of steel provided the appropriate AASHO value is used for F_{bs}.

The curvature correction factors ρ_B and ρ_w in Eqs. 87 and 88 are presented in tabular and graphical form in Tables 22, 23 and Figs. 44, 45.

The curvature correction factor ρ defined previously takes into account the additional stress produced by radial bending and deformation of the cross section. In addition, the increase in stress due to bending and warping torsion which occurs at the center of the braced span due to the applied end loads was accounted for. Thus, ρ may be considered as a stress amplification factor which accounts for curvature effects. In composite construction, the stresses in the compression flange which is supported by the slab will be small. The cross sectional deformation stress due to $\sigma_B A_f/R$ will probably be negligible. The tension flange, however, will be subjected to an increase in stress due to deformation of the cross section. It therefore seems reasonable to limit the total tension flange stress (warping plus bending) at the diaphragm locations for this case. Due to composite action, initial yield does not constitute failure for such a member (35, 36) and indeed load factor design takes into account the fully plastic stress distri-

Reproduced with permission of the copyright owner. Further reproduction prohibited without permission.

bution in proportioning composite members subjected only to bending (33). In view of this it is proposed that the total tension flange stress at the brace points for composite girders be limited using the ultimate strength analysis developed herein, Eq. 86. Since the shape factor for a composite beam M_{ult}/M_y is greater than that for an individual plate girder, it is reasonable to increase the factor 0.55 F_y in Eq. 78 to 0.60 F_y. It is not possible, at this time, to evaluate the factor of safety inherent in this approach since the ultimate strength of composite beams subjected to combined bending and torsion is not known. It is anticipated, however, that studies currently under way in this area (34) may be used to evaluate this procedure at a later date.

In summary, the results in this section may be expressed as the following design recommendation:

"For horizontally curved plate girders in which the compression flange plate width to thickness does not exceed the value determined by the formula:

$$b/t_f \leq 3200/\sqrt{F_y} \qquad (g)$$

The average unit stress in the compression flange shall not exceed

$$F_{bc} = F_{bs}\,\rho_B\rho_w \qquad (h)$$

at the location of the cross diaphragms where

$$F_{bs} = 0.55\,F_y\left[1-3\left(\frac{L}{b}\right)^2\frac{F_y}{\pi^2 E}\right] \qquad (i)$$

$$\rho_B = \frac{1}{1+(L/R-0.01)^2\,L/b\left[1+\frac{L/b}{6}\right]} \qquad (j)$$

$$\rho_w = 0.95 + 18\,(0.1-L/R)^2 - \frac{F_w/F_{bc}\left[0.3-0.1(L/R)(L/b)\right]}{\rho_B F_{bs}} \qquad (k)$$

L = Length in inches of the unsupported compression flange between cross diaphragms

Reproduced with permission of the copyright owner. Further reproduction prohibited without permission.

R = Radius of curvature in inches to the web of the girder

b = Total flange width in inches

In Eq. k, F_w represents the stress at the diaphragm location due to lateral flange bending. The ratio F_w/F_{bc} shall be taken as negative if F_w is compression on the flange tip further away from the center of curvature and positive if F_w is compression on the flange tip closest to the center of curvature.

If the product $\rho_B\rho_w$ exceeds one then a value of unity shall be used for this product in Eq. h and the straight girder allowable stress will apply.

The allowable stress in Eq. h shall be computed using the larger of the two bending moments and the two flange moments at either end of the braced flange.

In no case shall $|F_w/F_{bc}|$ exceed 0.5 and L/b shall not exceed 25.

Eq. h shall be checked for both live load and erection conditions."

"For horizontally curved plate girders in composite bridges, the average unit stress in the tension flange shall not exceed

$$F_{bc} = F_{bs}\rho_B\rho_w \qquad (1)$$

at the location of the cross diaphragms where

$$F_{bs} = 0.60\ F_y \left[1-3\left(\frac{L}{b}\right)^2 \frac{F_y}{\pi^2 E} \right] \qquad (m)$$

ρ_B, ρ_w, are given by Eq. j and k respectively.

The allowable stress in Eq. l shall be computed using the larger of the two bending moments and the two flange moments at either end of the braced flange.

In no case shall $|F_w/F_{bc}|$ exceed 0.5 and L/b shall not exceed 25.

Eq. l shall be checked for both live load and erection conditions."

Reproduced with permission of the copyright owner. Further reproduction prohibited without permission.

6.4 BRACING REQUIREMENTS

In determining bracing requirements for straight girders (28) both strength and stiffness requirements were developed. Stiffness requirements were necessary since lateral movements at the brace points affected the effective braced length used in deriving bracing spacing formulas. For the analysis considered herein only strength requirements or the axial force which the brace must be designed to carry will be necessary. Since no effective length factor was used in determining the failure loads, lateral movement at the braces will not effect the formula for F_{bc}. In fact the stresses produced by radial bending would decrease due to lateral movement of the braces. The stresses due to deformation of the cross section would increase somewhat at the center of the braced length and decrease at the brace points due to brace flexibility since the flange would no longer act as a fixed-fixed beam. Since the moment was assumed constant over both the braced length considered and the adjacent braced lengths, the conservatism introduced by neglecting the beneficial effects of moment gradient should be sufficient to compensate for any changes in these deformational stresses. Note that the bracing stiffness for the case in which the transverse diaphragms brace the compression flange is taken into account in the grid analysis used to determine the design moment and bimoment at the brace points (31).

To develop design formulas, compression flange bracing forces were calculated as discussed in Chapter 5 for several values of L/b, L/R and σ_w/σ_B. Results obtained from these calculations are plotted in Fig. 46 for the initial yield case and Fig. 47 for the ultimate strength analysis. The brace force was divided by the normal force in the flange, $\sigma_B A_f$, in

Reproduced with permission of the copyright owner. Further reproduction prohibited without permission.

plotting these figures. The sign convention used for these figures considers a brace force directed radially outward i.e. compression in a brace on the convex side of the girder as positive. The dotted line L/2R in these figures represents the brace force due to deformation of the cross section. Since the uniform thrust per unit length due to this effect is $\sigma_B A_f/R$ kips/in, Fig. 19, the corresponding brace force is simply $(\sigma_B A_f/R)(L/2)$.

Referring to Fig. 46 with L/b=5 note that the bracing force divided by $\sigma_B A_f$ exceeds L/2R (contribution due to flange thrust) as L/R increases. The brace force for a positive bimoment is larger than that for a negative bimoment. In most cases the force exerted on the brace is directed radially outward, brace force/$\sigma_B A_f$ is positive. Obviously the flange thrust $\sigma_B A_f/R$ in Fig. 19 tends to drive the compression flange outward and braces on the convex side of the girder are in compression. For very low values of L/R in Fig. 46 with L/b=5 and σ_w/σ_B=0.5 the brace force reverses and is tension, brace force/$\sigma_B A_f$ is negative. This trend is due to the term $M_x\phi$ in Eq. 63 i.e. the radial bending effect. For L/R=0 and σ_w/σ_B=0 i.e. the straight beam, the brace forces reduce to zero as expected.

For L/b=20 in Fig. 46 the brace forces are somewhat higher than for L/b=5 as expected. The difference between the nondimensional forces and L/2R is also greater due to the increased effect of the radial bending moment M_{ySM}. This effect also causes the variation of brace force with L/R to be more nonlinear in the lower range of L/R than for L/b=5. For σ_w/σ_B negative, negative brace forces also occur as discussed above.

The brace force curves for the ultimate strength analysis in Fig. 47 are similar to those for initial yield. As expected, the nondimensional

Reproduced with permission of the copyright owner. Further reproduction prohibited without permission.

forces are somewhat higher. Note that these forces have been divided by $\sigma_B A_f$ or the flange force due to the applied end moment and not by $\sigma_y A_f$.

The braces in Fig. 20a will be subjected to forces produced by both spans on either side of the brace point. Since the forces considered thusfar refer only to the brace forces produced by the single span model in Fig. 20b, the effect of the adjacent spans must be taken into account. If the moment diagram is assumed to vary over the braced span and the two adjacent spans as shown in Fig. 21b, the reactions at the two interior braces will be 1.82 times as large as those for a single span. If the moment were constant over the adjacent spans as well as the braced spans the brace forces would be 2.2 times those for the single span. These values are simply the ratios of the interior reactions for a three span beam loaded as in Fig. 21b or a three span uniformly loaded beam to the reactions for a single span uniformly loaded fixed-fixed beam. In view of this comparison, it is suggested that the brace forces discussed previously be multiplied by two to account for the adjacent spans.

It should be noted that these brace forces may be small in comparison to the forces induced in these members due to grid action of the structure. Consequently they may not affect the final size of the bracing member selected in design. A similar situation sometimes occurs in designing bracing members used in buildings (28).

The brace forces discussed above are produced by the compression flange. These forces are oriented perpendicular to the curved centerline of the girder. Since they develop from the flange thrust it is advisable to attach the braces directly to the compression flange. Connecting the braces to the web would require that this brace force be transferred from the flange to the web and then into the brace. This would result in high localized web bending stresses in the vicinity of the brace. If the

Reproduced with permission of the copyright owner. Further reproduction prohibited without permission.

brace is not attached directly to the flange, but to a transverse stiffner attached to the web, it is recommended that this stiffener be welded to the compression flange. The stiffener weld should be designed to transfer the brace force.

The force developed in the brace by the girder to which the brace is attached must be transmitted through the brace to the adjacent girder at the other end of the brace. Due consideration must be given to the manner in which this force is transmitted from one girder to another and the corresponding stresses produced in the structure.

An attempt was made to derive simple formulas for bracing forces suitable for design use similar to those developed for allowable stress. Although some formulas were obtained they were not sufficiently accurate over the entire practical range and were too complicated for design use. The results for bracing forces are therefore given in tabular form in Table 24 and Table 25.

The nondimensional percentage brace forces in Table 24 should be used for noncompact girders designed using Eq. b for allowable stress. To obtain the design force for the compression flange brace, the values in Table 24 should be multiplied by $F_{bc}A_f/100$. Note that these values include the effects of the adjacent spans mentioned above. As indicated in the table, if the sign of the tabular value is positive the force exerted by the girder on the brace is directed radially outward. For a negative value the force is directed radially inward. For values of L/R, F_w/F_{bc} or L/b not listed in Table 24 the brace force may be obtained using linear interpolation between the values given.

For compact sections designed using Eq. h the brace forces given in Table 25 should be used.

Reproduced with permission of the copyright owner. Further reproduction prohibited without permission.

Bracing members framing into the tension flange are also subjected to forces in addition to those induced by grid action. In this case the brace force component due to deformation of the cross section is opposite from that associated with radial bending. Thus the total force in the tension flange brace is less than that in the compression flange brace. This is obvious since the net force on the girder in the radial direction is not zero but must equal the reaction due to $q_{x_{SM}}$ in Eq. 64 for equilibrium. The tension flange brace force may be determined using the values in Tables 24 and 25. Subtracting $F_{bc}A_f(L/R)$ from the compression flange brace force will give the component of the total force due to radial bending. The direction of this force, radially outward or inward, is indicated by the resulting algebraic sign e.g. if the result is positive the radial force exerted by the tension flange on the brace is directed away from the center of curvature. To this force must be added algebraically the value $-F_{bc}A_f(L/R)$ to obtain the total tension flange brace force. Again the algebraic sign of this quantity will indicate the direction of the force exerted by the tension flange on the brace.

For specification purposes, brace forces may be presented in tabular form as in Tables 24, 25 or in graphical form. It may also be possible, if certain conservative simplifications are introduced to simply use a single value for the brace force expressed in terms of the flange force $F_{b_c}A_f$ as was done for buildings with the 2% rule discussed in Chapter 5.

Reproduced with permission of the copyright owner. Further reproduction prohibited without permission.

6.5 COMPARISON WITH STATE OF PENNSYLVANIA INTERIM CRITERIA

It is of interest to compare the allowable stress formulas developed in Sections 6.2 and 6.3 with the interim design criteria presently used by the State of Pennsylvania for curved plate girder bridges. A derivation of this interim criteria is given in the Appendix. Before making this comparison, the implications implicit in this interim criteria will be considered.

In developing the interim criteria, the rationale of turning the compression flange force $P=\sigma_B A_f$ to the direction of the chord is not clear. In essence this concept considers curvature in the same light as initial imperfections in a straight beam and thus essentially disregards curved beam theory in which the internal moment and resulting stress distribution are normal to the plane of the cross section. Also the manner in which the cross section resists the radial flange thrust shown in Fig. 19 is ignored. Although a thin web is not capable of resisting this thrust and additional flange bending occurs, turning the compression flange force to the direction of the chord eliminates this factor. The fact that the warping normal stresses due to torsion are simply added to the modified bending stress $\overline{F}_b$ also disregards the interaction between bending and twisting which occurs in curved beams (11). In addition, the influence of the bending and warping rigidities of the girder are not taken into account. Although it is implied in the derivation of the interim criteria that the location at which the maximum stress is to be computed is the brace point or diaphragm location, it is not explicitly stated. Finally, the use of the secant formula in the interim criteria implies that the resulting allowable stresses are based on the occurance of initial yield (24). For some practical girders basing the design concept on initial yield may be quite conservative. This will be illus-

Reproduced with permission of the copyright owner. Further reproduction prohibited without permission.

trated subsequently in a comparison of allowable stresses determined from this criteria with test results (21).

A comparison of the interim criteria with the results of this analysis is shown in Figs. 48, 49 and 50 for L/R=0.01, 0.05 and 0.08. The initial yield and ultimate strength curves were obtained directly from the analysis in Chapter 5 and are not based on the curve fitted formulas developed in sections 6.2 and 6.3. The factor of safety was removed from the interim criteria and the values of σ_f/σ_y plotted represent $\overline{F}_b/0.55\sigma_y=\rho F_b/0.55\sigma_y$.

For the case in which bending and warping stresses exist, $\sigma_w/\sigma_B\neq 0$, two curves have been plotted for the interim criteria. This was done since the manner in which warping or lateral flange bending stresses are taken into account in design using the interim criteria is not clear and two interpretations of this criteria are possible. For example, the interim criteria contains the following two provisions:

1. "The allowable unit stresses $\overline{F}_b$ in the curved compression girder flanges, as an interim design criteria, shall be the allowable AASHO stress F_b modified by the coefficient ρ."
2. "The allowable compressive edge unit stress, i.e. average unit stress $\overline{F}_b$ plus unit stress due to lateral flange bending may be assumed, conservatively F_b or somewhat larger."

These two provisions may be expressed as

$$\overline{F}_b = \rho F_b \tag{89}$$

$$\overline{F}_b + \sigma_w = F_b \tag{90}$$

Eq. 89 which limits the bending stress is clear and no confusion arises. In eq. 90, however, the value used for σ_w is not clear. Expressing the warping stress in this equation in terms of $\overline{F}_b$, eq. 90 may be written as

$$\overline{F}_b + \overline{F}_b\left(\frac{\sigma_w}{\overline{F}_b}\right) = F_b \tag{91}$$

Reproduced with permission of the copyright owner. Further reproduction prohibited without permission.

If in calculating the warping stress σ_w, the value of $\overline{F}_b$ from eq. 89 is used, eq. 91 becomes

$$\overline{F}_b + \rho F_b \left(\frac{\sigma_w}{\overline{F}_b}\right) = F_b \quad \rightarrow \quad \overline{F}_b = F_b \left[1 - \rho \left(\frac{\sigma_w}{\overline{F}_b}\right)\right] \tag{92}$$

If, however, the value of $\overline{F}_b$ is considered to be unknown in calculating the warping stress, eq. 91 can be solved for $\overline{F}_b$ as

$$\overline{F}_b = \frac{F_b}{1 + \sigma_w/\overline{F}_b} \tag{93}$$

Note that the compressive edge stress due to warping must be used in these formulas in order to obtain the maximum total stress i.e. compressive bending stress plus compressive warping stress. Eqs. 92 and 93 have both been plotted in Figs. 48, 49 and 50, and denoted as 1 and 2 respectively.

Referring to Fig. 48 note that the interim criteria and the initial yield criteria presented herein are almost identical for L/R=0.01 and σ_w/σ_B=0. As the curvature increases, however, the interim criteria is above the initial yield criteria with σ_w/σ_B=0, Figs. 49 and 50. When warping stresses are included, the interim criteria is below the initial yield criteria for L/R=0.01 and above initial yield for L/R=0.05 and 0.08. This is not surprising in view of the approximate manner in which warping or lateral flange bending is handled in the interim criteria. Note that in all cases the interim criteria is below the ultimate strength curves obtained from the analysis herein.

Since the method used in deriving the interim criteria is completely different from that used in this report, it is not possible to draw any general conclusions concerning the relationship between these results. Since the results in this report are based on a more rational analysis of curved beam behavior, however, it is reasonable to replace the interim criteria with the requirements developed in Sections 6.2 and 6.3. A com-

Reproduced with permission of the copyright owner. Further reproduction prohibited without permission.

parison with test results further substantiates this conclusion. Such a comparison is shown in Fig. 51.

The interim criteria using eq. 93, the initial yield curve and the ultimate strength curve for a girder with L/R=0.10 are shown in Fig. 51. Test results obtained from two girders with geometric proportions similar to practical girders (b/t_f = 15.4, $d/t_w \simeq 149$, t_f/t_w = 3.2, A_w/A_f = 0.92, L/b = 10) are shown (21). Note that additional tests under the CURT project at higher values of L/b will be conducted and may also be used to evaluate these analytical results. Values of σ_f/σ_y corresponding to initial yield and failure are shown. Test values for initial yield, σ_f/σ_y = 0.563 girder L1 and σ_f/σ_y = 0.547 girder L2, are quite close to the values for both the interim criteria, σ_f/σ_y = 0.587, and the initial yield criteria, σ_f/σ_y = 0.532. The test values corresponding to failure, σ_f/σ_y = 0.938 girder L1 and σ_f/σ_y = 0.926 girder L2, are within 5% of those obtained from the ultimate strength criteria, σ_f/σ_y = 0.880. The test values are approximately 57% greater than those obtained from the interim criteria. It should be noted that the two test girders had compact flanges (26); i.e. $b/t_f < 17.5$ and initial yield did not constitute failure. A survey of twenty-eight existing curved bridges indicated that most of these girders also had compact flanges.

If the two test girders had been designed using the interim criteria the resulting factor of safety against failure would have been

$$\frac{\left(\sigma_f/\sigma_y\right)_{\text{failure}}}{\left(\rho F_b/0.55\sigma_y\right)_{\text{interim}}} = \text{Factor of Safety} \qquad (94)$$

2.91 for girder L1 and 2.87 for girder L2. This factor of safety is considerably greater than that presently used for straight girders (factor of safety = $\sigma_y/0.55\sigma_y$ = 1.80). This large a factor of safety appears unreasonable and could conceivably offset the economic advantages associated

Reproduced with permission of the copyright owner. Further reproduction prohibited without permission.

with curved girders versus straight girders.

The values of ρ_B developed from the analysis herein and presented in Tables 18 and 22 may be compared with those obtained from the interim criteria. Note that the values of ρ in these Tables are independent of σ_y and the design formulas upon which they are based are somewhat simpler than the formula given in the interim criteria. The values of ρ_B herein for the initial yield condition are lower than the interim values. The per cent difference increases with L/b and L/R. Similarly the values of ρ_B for the ultimate strength condition are above the interim criteria and the per cent difference increases with L/R and L/b.

Reproduced with permission of the copyright owner. Further reproduction prohibited without permission.

7. SUMMARY AND CONCLUSIONS

Lateral bending of horizontally curved plate girders was studied. A mathematical model including second order effects which produce radial bending was devised. Using this model the relationship between the lateral bending of curved plate girders and lateral buckling of straight beams was investigated.

Based on the results obtained from the second order model, a simple model characterizing the behavior of curved beams was devised. This simple model included deformation of the cross section which has been observed in tests on curved plate girders. The model was used to study the behavior of curved beams in the elastic and inelastic range. The influence of the geometric proportions of the girder cross section as well as curvature effects were studied. Lateral bracing forces induced in curved bridges were also determined.

Based on results obtained from this simple model, design recommendations for allowable stress in curved girders as a function of the bracing spacing were developed. These recommendations were expressed in terms of formulas suitable for design use. The relationship between local and lateral buckling was taken into account in establishing these results. Design values for lateral brace forces were also determined;

The results obtained from the analysis herein were compared with values presently in use by the State of Pennsylvania for curved bridge design. In addition, comparisons with available test results on curved plate girders were also made.

Reproduced with permission of the copyright owner. Further reproduction prohibited without permission.

8. NOMENCLATURE

A_f = Area of top flange;

A_w = Area of web;

B = Bimoment;

B^* = $B/L(M_{cr})_{st}$

ΔB = Change of bimoment during buckling;

d,b = Depth of web and width of flange of a girder, respectively;

E,G = Modulus of elasticity and shear modulus, respectively;

F_{bc} = Allowable bending stress in curved beam;

F_{bs} = Allowable bending stress in straight beam;

F_w = Normal stress due to lateral flange bending or warping;

F_y = Yield stress;

F_1,F_2,F_3,F_4 = Nondimensional functions used in describing state 1 internal stress resultants;

$f(z)$ = Function of z;

I_w = Warping constant;

I_x,I_y = Moment of inertia about x and y axes, respectively;

K_T = Saint-Venant shearing constant;

L = Arc length of girder;

M,M^F,B = Applied moment, flange moment, and bimoment, respectively;

$\bar{M}_x,\bar{M}_y,\bar{M}_z$ = Reactions at the ends of the girder;

M^*,B^* = Nondimensional applied moment and bimoment, respectively;

M_x^*,M_y^*,M_z^* = $M_x/(M_{cr})_{st}$, $M_y/(M_{cr})_{st}$, $M_z/(M_{cr})_{st}$, respectively;

$(M_{cr})_{st}$ = Critical moment for straight beam;

Reproduced with permission of the copyright owner. Further reproduction prohibited without permission.

m_x, m_y, m_z = Applied distributed moments about x, y, z axes, respectively;

M_x, M_y, M_z = Internal moments about x, y, z axes, respectively;

$M_{y_{SM}}$ = Internal moment as calculated using simple model;

M_x^D, B^D = Internal moment about x axis and bimoment given by linear theory, respectively;

$\Delta M_x, \Delta M_y, \Delta M_z$ = Change in internal moments during buckling;

P = Load in kips applied at each of the third points in the experimental tests;

q_x, q_y, q_z = Applied distributed forces in x, y, z directions, respectively;

$q_{x_{SM}}$ = Equivalent radial load used in simple model;

R = Radius of curvature of girder;

t_f, t_w = Thickness of flange and web of a girder, respectively;

u, v, w, ϕ = Displacements in x,y,z directions and rotation about z axis, respectively;

$\bar{u}, \bar{v}, \bar{\phi}$ = Nondimensional displacements;

$\bar{v}_D, \bar{\phi}_D$ = $\bar{v}$ and $\bar{\phi}$ given by linear theory;

V_x, V_y, V_z = Internal shears in x, y, z directions, respectively;

$\Delta V_x, \Delta V_y, \Delta V_z$ = Change in internal shears during buckling;

x,y,z = Orthogonal curvilinear coordinates;

[A] = Square matrix of coefficients;

$[A]^{-1}$ = Inverse of square matrix [A];

[I] = Identity matrix;

{x},{b} = Column vectors of displacements and loads, respectively;

α = Central angle of girder;

β, η = Nondimensional bimoment and moment gradient parameters, respectively;

$\gamma_1, \gamma_2, \gamma_3, \gamma_4$ = Nondimensional stiffness parameters;

γ_5 = Ratio $B/ML = B^*/M^*$ at the end of a girder;

Reproduced with permission of the copyright owner. Further reproduction prohibited without permission.

κ_x, κ_y = Components of curvature in x and y axes, respectively;

$\Delta\kappa_x, \Delta\kappa_y$ = Change in curvatures during buckling;

σ_w, σ_B = Warping stress and bending stress, respectively;

σ_R = Stresses due to radial bending;

σ_y = Yield stress;

σ_f = Failure stress - initial yield or ultimate strength;

σ_p = Fictitious stress using elastic analysis;

τ = Twist of girder;

$\Delta\tau$ = Change in twist during buckling;

ρ = Curvature correction factor;

ρ_B = Curvature correction factor - bending stress;

ρ_w = Curvature correction factor - warping stress;

Reproduced with permission of the copyright owner. Further reproduction prohibited without permission.

9. APPENDIX

A. Present Bracing Spacing Requirements - State of Pennsylvania

The State of Pennsylvania presently limits the stress in the compression flanges of curved plate girders to (23)

$$\bar{F}_b = \rho F_b \tag{1}$$

where

$\bar{F}_b$ = Allowable average compressive unit stress in the curved flange

F_b = Allowable unit compressive stress as per AASHO Specifications (10)

ρ = correction factor to account for curvature

$$= \frac{1 + 0.25 \sec \alpha}{1 + \bar{\epsilon} \sec \bar{\alpha}} \tag{2}$$

$$\bar{\epsilon} = \frac{1}{4}\left\{1 + \frac{12R}{b}\left(2 - \sqrt{4 - \lambda^2}\right)\right\} \tag{3}$$

$$\alpha = \frac{L}{b}\sqrt{\frac{3F_y}{E}\left\{1 - \left(\frac{L}{b}\right)^2 \frac{3F_y}{\pi^2 E}\right\}} \tag{4}$$

$$\bar{\alpha} = \alpha\sqrt{\rho} \qquad \lambda = \frac{L}{R} \tag{5}$$

b = Flange width, R = radius of flange centerline

L = Spacing of lateral flange supports

The derivation of the above equations is included in this report in order to be able to compare the design philosophy presently used in Pennsylvania to select lateral bracing spacing with that using the mathematical model developed herein. Although the formulas pre-

Reproduced with permission of the copyright owner. Further reproduction prohibited without permission.

sented were taken directly from material provided by the Pennsylvania Department of Transportation, the explanation of their derivation given below is due solely to the authors.

In deriving Eq. 2, use was made of the secant formula. Before proceeding, therefore, the philosophy of the secant formula for straight girders will be reviewed. Consider a portion of a straight girder between lateral braces subjected to equal end moments at the bracing points and denote the uniform stress in the compression flange due to the end moments by F_c. If the girder is assumed to be initially curved and the compression flange is treated as a pinned-end column with initial curvature, the maximum compressive stress (direct stress + bending stress) on the inner edge, toward the center of curvature, of the flange half way between the braces is given by (24)

$$F_{max} = F_c\left\{1 + \frac{ec}{r^2}\sec\ \frac{L}{2r}\sqrt{\frac{F_c}{E}}\right\} \qquad (6)$$

where

- e = initial mid-span deflection normal to the plane of loading prior to loading
- r = radius of gyration of compression flange--$b/\sqrt{12}$
- c = distance to extreme fiber--$b/2$
- L = bracing spacing

Note that the stress F_c is in the direction of the undeformed center-line of the flange i.e., the resultant force produced by these stresses, $P = F_c A_f$, is directed along the straight line connecting the bracing points.

Eq. 6 indicates that the stress F_c calculated using beam theory assuming the girder is straight is increased to F_{max} due to the initial

Reproduced with permission of the copyright owner. Further reproduction prohibited without permission.

curvature. Using the same approach for a curved girder, denoting the flange stress by $\bar{F}_c$ gives

$$\bar{F}_{max} = \bar{F}_c \left\{ 1 + \frac{\bar{e}c}{r^2} \sec \frac{L}{2r} \sqrt{\frac{\bar{F}_c}{E}} \right\} \qquad (7)$$

To be consistent with the straight beam case the stress $\bar{F}_c$ should be directed along the curved centerline axis with no initial imperfections. Note that in solving the curved beam equations (11), the bending stresses are directed along the tangent to the curved centerline. For this case, however, Eq. 7 would not be correct since the flange should then be treated as a circular arch with initial imperfections. In order to simplify the analysis therefore the stress $\bar{F}_c$ is assumed to act in the direction of the chord connecting the ends of the curved flange as shown below

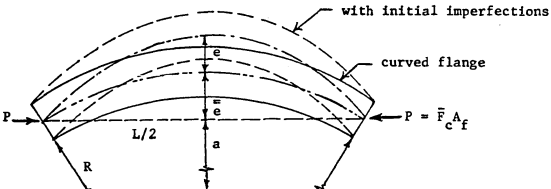

The eccentricity $\bar{e}$ used in Eq. 7, therefore, will be taken as that due to the circular curvature, $\bar{\bar{e}}$, plus the assumed imperfection, e, measured from the ideal circular curved beam as shown. The eccentricity $\bar{\bar{e}}$ is given by

$$\bar{\bar{e}} = R - a = R - \sqrt{R^2 - \left(\frac{L}{2}\right)^2}$$

$$= \frac{R}{2}\left[2 - \sqrt{4 - \lambda^2}\right]; \quad \lambda = L/R \qquad (8)$$

Reproduced with permission of the copyright owner. Further reproduction prohibited without permission.

Using Eq. 8 and the expression for the radius of gyration $r = b/\sqrt{12}$, the quantity $\bar{e}c/r^2$ in Eq. 7 becomes

$$\frac{\bar{e}c}{r^2} = \frac{c}{r^2}\left(e + \bar{e}\right) = \frac{6}{b}\left\{e + \frac{R}{2}\left[2 - \sqrt{4 - \lambda^2}\right]\right\} \qquad (9)$$

Letting $ec/r^2 = 6e/b = 0.25$ as was done in the AASHO formula for straight girders, Eq. 9 becomes

$$\frac{\bar{e}c}{r^2} = 0.25 + \frac{3R}{b}\left[2 - \sqrt{4 - \lambda^2}\right] = \bar{\varepsilon} \qquad (10)$$

Setting the maximum stress in the curved beam equal to that in the straight beam, $\bar{F}_{max} = F_{max}$, and using Eqs. 6, 7 and 10 gives

$$\frac{\bar{F}_c}{F_c} = \frac{1 + 0.25 \sec \frac{L}{2r}\sqrt{\frac{F_c}{E}}}{1 + \bar{\varepsilon} \sec \frac{L}{2r}\sqrt{\frac{F_c}{E}}} = \rho \qquad (11)$$

Eq. 11 gives the ratio of the calculated bending stress in the curved beam, $\bar{F}_c$, to that in the straight beam, F_c, in terms of the parameter ρ. Note that this parameter is also a function of these stresses. In order to reduce ρ to a form which is compatible with the AASHO Specifications for straight girders, F_c, in the secant term will be expressed as

$$F_c = F_y\left[1 - 3\left(\frac{L}{b}\right)^2 \frac{F_y}{\pi^2 E}\right] \qquad (12)$$

Using Eq. 12 the term $L/2r\sqrt{F_c/E}$ in Eq. 11 becomes

$$\frac{L}{2r}\sqrt{\frac{F_c}{E}} = \frac{L}{b}\sqrt{\frac{3F_c}{E}} = \frac{L}{b}\sqrt{\frac{3F_y}{E}\left[1 - \left(\frac{L}{b}\right)^2 \frac{3F_y}{\pi^2 E}\right]} = \alpha \qquad (13)$$

Reproduced with permission of the copyright owner. Further reproduction prohibited without permission.

Similarly the term $L/2r\sqrt{\bar{F}_c/E}$ in Eq. 11 may be written

$$\frac{L}{2r}\sqrt{\frac{\bar{F}_c}{E}} = \bar{\alpha} = \sqrt{\rho}\ \alpha \tag{14}$$

Using Eqs. 13, 14 in Eq. 11 gives

$$\frac{\bar{F}_c}{F_c} = \frac{1 + 0.25 \sec \alpha}{1 + \bar{\epsilon} \sec \bar{\alpha}} = \rho \tag{15}$$

If $\bar{F}_c$ is denoted by $\bar{F}_b$, the allowable average compressive stress in the curved beam and F_c by F_b the allowable compressive stress in a straight girder according to the AASHO Specification, Eq. 15 reduces to Eq. 1.

In the preceeding derivation, $\bar{F}_c$ and $\bar{F}_b$ denoted the stress in the curved girder due to the bending moment about the strong axis of the girder. Due to nonuniform torsion or warping torsion sometimes referred to as cross bending or lateral flange bending additional stresses which vary linearly across the flange width (zero at the flange web juncture) are produced. Presently (23) the total stress at the flange tip $\bar{F}_b$ plus the lateral flange bending stress is limited to F_b.

Reproduced with permission of the copyright owner. Further reproduction prohibited without permission.

10. TABLES AND FIGURES

Reproduced with permission of the copyright owner. Further reproduction prohibited without permission.

Reproduced with permission of the copyright owner. Further reproduction prohibited without permission.

TABLE 1

FINITE DIFFERENCE CONVERGENCE

η	α	N	M^*_{cr}	$M^{*\,ST}_{cr}$
+1	0.0001	10	0.992	1.00
		20	0.998	
		30	0.999	
		40	1.000	
	15°	10	0.987	1.00
		20	0.994	
		30	0.995	
		40	0.996	
-1	0.0001	10	2.718	2.73
		20	2.736	
		30	2.739	
		40	2.740	
	15°	10	2.702	2.73
		20	2.723	
		30	2.727	
		40	2.728	

$L/b = 15$ $d/b = 3$ $d/t_w = 165$ $t_f/t_w = 3$

$\beta = 1$ $\sigma_w/\sigma_B = 0$

TABLE 2

EFFECT OF CURVATURE ON CRITICAL MOMENT

L/b	α	M^*_{cr}
5	0.0001	0.999
	30°	0.984
	60°	0.953
	90°	1.001
30	0.0001	0.999
	30°	0.984
	60°	0.951
	90°	0.991
60	0.0001	0.999
	30°	0.983
	60°	0.951
	90°	0.991

$d/b = 3$ $d/t_w = 165$

$t_f/t_w = 3$ $\eta = \beta = 1$

$\sigma_w/\sigma_B = 0$ $N = 30$

TABLE 3

EFFECT OF BIMOMENT ON CRITICAL MOMENT

β	α	M^*_{cr}
+1	0.0001	0.999
	30°	0.984
	60°	0.951
	90°	0.992
0	0.0001	0.999
	30°	0.984
	60°	0.951
	90°	0.991
-1	0.0001	0.999
	30°	0.984
	60°	0.951
	90°	0.991

$L/b = 15$ $d/b = 3$

$d/t_w = 165$ $t_f/t_w = 3$

$\eta = 1$ $\sigma_w/\sigma_B = 0.5$

$N = 30$

TABLE 4 - EFFECT OF MOMENT GRADIENT ON CRITICAL MOMENT

α	L/b	M^*_{cr} no grad	η	M^*_{cr} grad	M_{cr} grad / M_{cr} no grad
0.0001	10	0.999	0	1.854	1.85
			-1	2.740	2.74
	30	0.999	0	1.851	1.85
			-1	2.736	2.74
60°	10	0.952	0	1.760	1.85
			-1	2.535	2.66
	30	0.951	0	1.757	1.85
			-1	2.532	2.66

$d/b = 3$ $d/t_w = 165$ $t_f/t_w = 3$ $\beta = 1$ $\sigma_w/\sigma_B = 0$ $N = 30$

Reproduced with permission of the copyright owner. Further reproduction prohibited without permission.

TABLE 5 - INFLUENCE OF BOUNDARY CONDITIONS ON CRITICAL MOMENT

α	η	M^*_{cr} fixed	M^*_{cr} pinned	M_{cr} fixed / M_{cr} pinned
0.0001	+1	3.918	0.999	3.92
	-1	10.067	2.739	3.68
30°	+1	5.477	0.984	5.56
	-1	14.742	2.688	5.50
60°	+1	7.371	0.951	7.75
	-1	23.242	2.535	9.20
90°	+1	7.585	0.992	7.65
	-1	28.520	2.274	12.50

$L/b = 15$ $d/b = 3$ $d/t_w = 165$ $t_f/t_w = 3$ $\beta = 1$ $\sigma_w/\sigma_B = 0$

$N = 30$

Reproduced with permission of the copyright owner. Further reproduction prohibited without permission.

TABLE 6 - INFLUENCE OF BIMOMENT ON DEFLECTION (MID SPAN)

$M/(M_{cr})^{ST}$	α	σ_w/σ_B	$\bar{u}$	$\bar{v}$	$\bar{\phi}$
0.1	5°	0.0	-0.000115	0.000493	-0.0109
		-0.1	-0.000102	0.000483	-0.00978
		-0.3	-0.0000773	0.000461	-0.00745
		-0.5	-0.0000523	0.000440	-0.00512
	30°	0.0	-0.000739	0.00411	-0.0694
		-0.1	-0.000726	0.00404	-0.0682
		-0.3	-0.000700	0.00391	-0.0658
		-0.5	-0.000674	0.00378	-0.0634
0.2	5°	0.0	-0.000474	0.000993	-0.0226
		-0.1	-0.000422	0.000970	-0.0202
		-0.3	-0.000319	0.000927	-0.0154
		-0.5	-0.000216	0.000883	-0.0106
	30°	0.0	-0.00305	0.00846	-0.143
		-0.1	-0.00300	0.00832	-0.141
		-0.3	-0.00289	0.00805	-0.136
		-0.5	-0.00278	0.00778	-0.131
0.3	5°	0.0	-0.00113	0.00151	-0.0358
		-0.1	-0.00100	0.00147	-0.0319
		-0.3	-0.000757	0.00140	-0.0243
		-0.5	-0.000512	0.00133	-0.0167
	30°	0.0	-0.00726	0.0133	-0.227
		-0.1	-0.00713	0.0131	-0.223
		-0.3	-0.00688	0.0127	-0.216
		-0.5	-0.00662	0.0123	-0.208
0.4	5°	0.0	-0.00217	0.00204	-0.0517
		-0.1	-0.00193	0.00199	-0.0462
		-0.3	-0.00146	0.00189	-0.0351
		-0.5	-0.000986	0.00179	-0.0241
	30°	0.0	-0.0140	0.0192	-0.330
		-0.1	-0.0138	0.0189	-0.324
		-0.3	-0.0133	0.0183	-0.313
		-0.5	-0.0128	0.0176	-0.301
0.5	5°	0.0	-0.00380	0.00262	-0.0724
		-0.1	-0.00338	0.00255	-0.0647
		-0.3	-0.00256	0.00241	-0.0492
		-0.5	-0.00173	0.00227	-0.0336
	30°	0.0	-0.0247	0.0268	-0.464
		- 0.1	-0.0243	0.0263	-0.456
		- 0.3	-0.0233	0.0255	-0.440
		- 0.5	-0.0225	0.0246	-0.424
0.6	5°	0.0	-0.00642	0.00328	-0.102
		- 0.1	-0.00572	0.00318	-0.0911
		- 0.3	-0.00432	0.00298	-0.0692
		- 0.5	-0.00292	0.00279	-0.0472
	30°	0.0	-0.0420	0.0375	-0.659
		- 0.1	-0.0413	0.0369	-0.647
		- 0.3	-0.0398	0.0357	-0.624
		- 0.5	-0.0383	0.0344	-0.601

$l/b = 15$ $d/b = 3$ $d/t_w = 165$ $t_f/t_w = 3$ $\eta = \beta = 1$ $N = 20$

Reproduced with permission of the copyright owner. Further reproduction prohibited without permission.

TABLE 7 - COMPARISON OF SIMPLE MODEL AND DEFLECTION AMPLIFICATION RESULTS

α	M^*	σ_R^* (Defl. Amp.) (ksi)	σ_R^* (Simple Model) (ksi)	% Difference
5°	0.1	0.509	0.502	1.38
	0.2	2.097	2.010	0.14
	0.3	4.973	4.522	9.03
15°	0.1	2.708	2.712	0.15
	0.2	11.176	10.846	2.96
	0.3	26.547	24.404	8.10

* Midspan

$L/b = 15$ $d/b = 3$ $t_f/t_w = 3$ $d/t_w = 165$

$\eta = \beta = 1$ $\sigma_W/\sigma_B = -0.5$

Reproduced with permission of the copyright owner. Further reproduction prohibited without permission.

Reproduced with permission of the copyright owner. Further reproduction prohibited without permission.

TABLE 8 - TEST COMPARISON - BRACES RIGID

LOAD	Section 1									Section 2								
	Defl. Amp.			Simple Model			Tests			Defl. Amp.			Simple Model			Tests		
(kips)	σ_B	σ_W	σ_R	σ_B	σ_W	σ_R	σ_B	σ_W	σ_R	σ_B	σ_W	σ_R	σ_B	σ_W	σ_R	σ_B	σ_W	σ_R
5.0	6.17	1.95	0.04	6.17	1.95	0.04	5.64	2.49	0.47	6.17	1.62	0.04	6.17	1.62	0.04	5.49	2.16	0.15
7.5	9.26	2.92	0.09	9.26	2.92	0.09	8.00	3.86	0.51	9.26	2.43	0.08	9.26	2.43	0.08	8.06	3.97	0.52
10.0	12.34	3.90	0.16	12.34	3.89	0.16	11.39	4.91	1.02	12.34	3.25	0.14	12.34	3.24	0.14	11.19	4.14	0.29
12.5	15.40	4.89	0.25	15.40	4.87	0.25	13.69	6.05	1.06	15.40	4.06	0.22	15.40	4.05	0.22	13.92	6.19	1.15
15.0	18.51	5.87	0.36	18.51	5.84	0.35	17.26	7.47	1.76	18.51	4.89	0.32	18.51	4.86	0.32	16.90	5.90	0.80

All stresses in ksi.

TABLE 9 - TEST COMPARISON - MEASURED BRACE TORQUE

LOAD	Section 1									Section 2								
	Defl. Amp.			Simple Model			Tests			Defl. Amp.			Simple Model			Tests		
(kips)	σ_B	σ_W	σ_R	σ_B	σ_W	σ_R	σ_B	σ_W	σ_R	σ_B	σ_W	σ_R	σ_B	σ_W	σ_R	σ_B	σ_W	σ_R
5.0	6.19	11.84	0.39	6.19	11.83	0.39	5.64	2.49	0.47	6.19	11.53	0.37	6.19	11.52	0.37	5.49	2.16	0.15
7.5	9.28	17.79	0.89	9.28	17.75	0.89	8.00	3.86	0.51	9.28	17.32	0.83	9.28	17.28	0.83	8.06	3.97	0.52
10.0	12.38	23.76	1.58	12.38	23.66	1.57	11.39	4.91	1.02	12.38	23.13	1.47	12.38	23.05	1.47	11.19	4.14	0.29
12.5	15.47	29.76	2.47	15.47	29.58	2.46	13.69	6.05	1.06	15.47	28.98	2.31	15.47	28.81	2.30	13.92	6.19	1.15
15.0	18.57	35.82	3.56	18.57	35.50	3.54	17.26	7.47	1.76	18.57	34.86	3.33	18.57	34.57	3.31	16.90	5.90	0.80

All stresses in ksi.

TABLE 10- TEST COMPARISON - THIRD APPROACH

LOAD (kips)	Section 1					
	Simple Model			Tests		
	σ_B	σ_W	σ_R	σ_B	σ_W	σ_R
5.0	5.58	2.47	0.06	5.64	2.49	0.47
7.5	8.37	3.71	0.12	8.00	3.86	0.51
10.0	11.16	4.95	0.22	11.39	4.91	1.02
12.5	13.95	6.18	0.34	13.69	6.05	1.06
15.0	16.74	7.42	0.50	17.26	7.47	1.76

All stresses in ksi.

Reproduced with permission of the copyright owner. Further reproduction prohibited without permission.

Reproduced with permission of the copyright owner. Further reproduction prohibited without permission.

TABLE 11 - INFLUENCE OF DIRECTION OF FLANGE MOMENT - INITIAL YIELD

A_w/A_f	d/t_w	L/b	$\alpha = 2°$			$\alpha = 20°$		
			σ_f/σ_y		Ratio	σ_f/σ_y		Ratio
			$\sigma_w/\sigma_b = {}_{(1)}{}^{+0.5}$	$\sigma_w/\sigma_b = {}_{(2)}{}^{-0.5}$	(2)/(1)	$\sigma_w/\sigma_b = {}_{(3)}{}^{+0.5}$	$\sigma_w/\sigma_b = {}_{(4)}{}^{-0.5}$	(4)/(3)
0.5	40	5	0.6148	0.6361*	1.0346	0.3235	0.4442*	1.3731
		10	0.5898	0.6042*	1.0244	0.2359	0.2843	1.2052
		20	0.5684	0.5456*	0.9599	0.1876	0.2017	1.0752
		30	0.5391	0.4938*	0.9160	0.1690	0.1656*	0.9799
	165	5	0.5907	0.6307*	1.0677	0.2979	0.4255	1.4283
		10	0.5183	0.5964*	1.1507	0.1917	0.2371	1.2368
		20	0.3983	0.5263*	1.3214	0.1136	0.1272	1.1197
		30	0.3074	0.4411*	1.4349	0.0330	0.0895	1.0783
2.0	40	5	0.6016	0.6317*	1.0500	0.2985	0.4119	1.3799
		10	0.5730	0.5994*	1.0460	0.2165	0.2570	1.1871
		20	0.5458	0.5396*	0.9886	0.1743	0.1860*	1.0671
		30	0.5107	0.4855*	0.9507	0.1588	0.1637*	1.0309
	165	5	0.5775	0.6308*	1.0923	0.2724	0.3748	1.3759
		10	0.4971	0.5952*	1.1973	0.1709	0.2055	1.2025
		20	0.3670	0.5180*	1.4114	0.0995	0.1099	1.1045
		30	0.2743	0.4033	1.4703	0.0726	0.0774	1.0661

*Initial yield occurred at end cross section.

TABLE 12 - INFLUENCE OF RESIDUAL STRESS ON INITIAL YIELDING OF COMPRESSION FLANGE

σ_w/σ_b	L/b	No Residual Stress	Flame Cut	
		σ_f/σ_y	σ_f/σ_y	% Reduction
0	5	0.8323	0.6265	24.7
	10	0.6963	0.5457	21.6
	15	0.5825	0.4756	18.4
	20	0.4870	0.4132	15.2
	25	0.4078	0.3581	12.2
	30	0.3435	0.3105	9.6
	35	0.2922	0.2701	7.6
0.5	5	0.5839	0.4698	19.5
	10	0.5068	0.4194	17.2
	15	0.4393	0.3736	15.0
	20	0.3811	0.3323	12.8
	25	0.3312	0.2954	10.8
	30	0.2888	0.2629	9.0
	35	0.2532	0.2344	7.4

$d/t_w = 165$ $A_w/A_f = 1.3$ $\alpha = 2°$ $L/R = 0.035$

Reproduced with permission of the copyright owner. Further reproduction prohibited without permission.

TABLE 13 - LATERAL BRACING FORCES - INITIAL YIELD

d/t_w	A_w/A_f	σ_w/σ_B	L/b	Bracing Force L/R = 0.035		Bracing Force L/R = 0.35	
				$\frac{\text{Def. F}}{\sigma_B A_F}$ x 100%	$\frac{\text{Rad. F}}{\sigma_B A_F}$ x 100%	$\frac{\text{Def. F}}{\sigma_B A_F}$ x 100%	$\frac{\text{Rad. F}}{\sigma_B A_F}$ x 100
40	0.5	0	5	1.75	0.04	17.5	0.21
			10		0.14		0.50
			20		0.32		0.89
			30		0.44		1.06
		0.5	5	1.75	0.24	17.5	0.29
			10		0.44		0.58
			20		0.70		0.99
			30		0.84		1.16
	2	0	5	1.75	0.06	17.5	0.28
			10		0.20		0.64
			20		0.50		1.14
			30		0.60		1.35
		0.5	5	1.75	0.28	17.5	0.36
			10		0.54		0.73
			20		0.86		1.25
			30		1.04		1.47
165	0.5	0	5	1.75	0.06	17.5	0.22
			10		0.18		0.53
			20		0.54		1.13
			30		0.94		1.68
		0.5	5	1.75	0.22	17.5	0.28
			10		0.46		0.60
			20		0.92		1.21
			30		1.32		1.76
	2	0	5	1.75	0.08	17.5	0.29
			10		0.26		0.69
			20		0.72		1.47
			30		1.24		2.16
		0.5	5	1.75	0.28	17.5	0.36
			10		0.58		0.77
			20		1.14		1.55
			30		1.66		2.24

Reproduced with permission of the copyright owner. Further reproduction prohibited without permission.

TABLE 14 - LATERAL BRACING FORCES - ULTIMATE STRENGTH

d/t_w	A_w/A_f	σ_w/σ_B	L/b	Bracing Force L/R=0.035			Bracing Force L/R=0.105	
				$\frac{\text{Def.F}}{\sigma_B A_f}$ x100%	$\frac{\text{Rad.F}}{\sigma_B A_f}$ x100%	$\frac{\text{Total F}}{\sigma_y A_f}$ x100%	$\frac{\text{Def.F}}{\sigma_B A_f}$ x100%	$\frac{\text{Rad.F}}{\sigma_B A_f}$ x100%
40	0.5	0	5	1.75	0.05	1.78	5.24	0.15
			10		0.18	1.86		0.45
			20		0.43	1.85		1.00
		0.5	5	1.75	0.32	1.86	5.24	0.37
			10		0.62	2.11		0.79
			20		1.06	2.38		1.45
	2.0	0	5	1.75	0.08	1.81	5.24	0.22
			10		0.25	1.92		0.72
			20		0.64	2.02		1.63
		0.5	5	1.75	0.44	2.16	5.24	0.54
			10		0.85	2.50		1.16
			20		1.46	2.72		2.15
165	0.5	0	5	1.75	0.06	1.79	5.24	0.16
			10		0.23	1.85		0.56
			20		0.93	2.10		1.57
		0.5	5	1.75	0.32	1.75	5.24	0.38
			10		0.71	1.96		0.89
			20		1.64	2.50		1.92
	2.0	0	5	1.75	0.08	1.81	5.24	0.26
			10		0.35	2.02		0.91
			20		1.76	2.77		2.70
		0.5	5	1.75	0.46	2.09	5.24	0.55
			10		1.04	2.48		1.35
			20		2.47	2.74		3.49

Reproduced with permission of the copyright owner. Further reproduction prohibited without permission.

TABLE 15 COMPARISON OF YIELD AND LOCAL BUCKLING MOMENTS

Material	Fabrication Process	b/t_f	σ_w/σ_B	M/M_y Local Buckling	M/M_y Initial Yield*
A36	Welded	23.0	0.00	1.00	1.00
		23.0	0.18	0.83	0.85
		17.6	0.18	0.83	0.85
		23.0	0.40	0.74	0.71
		17.6	0.40	0.75	0.71
		23.0	0.72	0.63	0.58
		17.6	0.72	0.63	0.58
	Heat Curved	23.0	0.00	1.06	1.00
		23.0	0.15	1.00	0.87
		23.0	0.32	0.94	0.76
		23.0	0.50	0.90	0.67
A441	Welded	20.0	0.00	0.93	1.00
		17.2	0.00	0.93	1.00
		17.0	0.00	0.98	1.00
		13.2	0.17	0.87	0.85
		17.0	0.18	0.84	0.85
		20.0	0.19	0.80	0.84
		17.2	0.19	0.80	0.84
		16.8	0.38	0.80	0.72
		13.2	0.38	0.80	0.72
		20.0	0.45	0.67	0.69
		17.2	0.45	0.67	0.69
		13.2	0.67	0.67	0.60
	Heat Curved	20.0	0.00	1.03	1.00
		15.8	0.00	1.04	1.00
		20.0	0.15	0.95	0.87
		15.4	0.15	0.97	0.87
		20.0	0.33	0.90	0.75
		15.3	0.33	0.92	0.75
		15.0	0.52	0.86	0.66
		15.8	0.55	0.81	0.65
		20.0	0.57	0.80	0.64

* Neglecting Residual Stress - $M_y = \sigma_y S$

Reproduced with permission of the copyright owner. Further reproduction prohibited without permission.

Reproduced with permission of the copyright owner. Further reproduction prohibited without permission.

TABLE 16
SUMMARY OF COMPRESSION FLANGE WIDTH - THICKNESS RATIOS

1. Ref. 9 - AISC Specifications (compact section) - $b/t_f \leq 3301/\sqrt{F_y}$
2. Ref. 9 - AISC Specifications (noncompact section) - $b/t_f \leq 6008/\sqrt{F_y}$
3. Ref. 10 - AASHO Specification $b/t_f \leq 4382/\sqrt{F_y}$
4. Ref. 33 - Load Factor Design (compact section) - $b/t_f \leq 3200/\sqrt{F_y}$
5. Ref. 33 - Load Factor Design (noncompact section) - $b/t_f \leq 4400/\sqrt{F_y}$
6. Ref. 26 - Curved Plate Girders

Criteria	b/t_f				
	F_y = 36,000 psi	F_y = 42,000 psi	F_y = 46,000 psi	F_y = 50,000 psi	F_y = 55,000 psi
1	17.4	16.2	15.4	14.8	14.0
2	31.6	29.4	28.0	26.8	25.6
3	23.0	21.0	21.0	20.0	19.0
4	16.8	15.6	15.0	14.4	13.6
5	23.2	21.4	20.6	19.6	18.8
6	17.5	15.0	13.7	13.0	11.5

b= Total flange width, t_f= flange thickness, F_y= psi

TABLE 17
APPROXIMATION INVOLVED IN ALLOWABLE STRESS DESIGN FORMULA-
INITIAL YIELD

L/R	L/b	σ_w/σ_B	σ_f/σ_y		% Difference = (2)-(1) * (1)
			Exact (1)	Design Eq. (2)	
0.01	5	-0.5	0.66	0.73	10.3
		-0.1	0.89	0.89	0
		0	0.95	0.94	-0.6
		0.1	0.86	0.87	0.7
		0.5	0.64	0.65	1.7
	10	-0.5	0.64	0.71	11.2
		-0.1	0.87	0.87	0
		0	0.89	0.88	-1.5
		0.1	0.81	0.81	0
		0.5	0.60	0.63	4.3
	25	-0.5	0.55	0.58	4.8
		-0.1	0.72	0.66	-8.1
		0	0.63	0.62	-2.0
		0.1	0.58	0.59	1.4
		0.5	0.45	0.49	9.8
0.05	5	-0.5	0.62	0.64	3.4
		-0.1	0.82	0.79	-4.1
		0	0.78	0.79	1.8
		0.1	0.72	0.73	1.2
		0.5	0.56	0.55	-2.2
	10	-0.5	0.57	0.57	0
		-0.1	0.67	0.70	4.6
		0	0.63	0.65	2.5
		0.1	0.59	0.60	1.4
		0.5	0.47	0.46	-1.9
	25	-0.5	0.45	0.39	-13.4
		-0.1	0.37	0.37	0
		0	0.36	0.35	-3.0
		0.1	0.35	0.33	-4.9
		0.5	0.30	0.28	-6.8
0.10	5	-0.5	0.57	0.57	0
		-0.1	0.69	0.70	1.2
		0	0.64	0.66	3.5
		0.1	0.60	0.61	1.3
		0.5	0.49	0.46	-6.7
	10	-0.5	0.50	0.48	-4.0
		-0.1	0.49	0.53	8.6
		0	0.46	0.49	5.7
		0.1	0.44	0.45	2.3
		0.5	0.37	0.35	-6.2
	25	-0.5	0.28	0.31	10.9
		-0.1	0.25	0.24	-3.0
		0	0.24	0.23	-5.7
		0.1	0.24	0.22	-10.1
		0.5	0.22	0.18	-17.7

* % Difference negative = Design Eq. Conservative

Reproduced with permission of the copyright owner. Further reproduction prohibited without permission.

TABLE 18 - CURVATURE CORRECTION FACTOR ρ_B FOR ALLOWABLE STRESS-INITIAL YIELD

L/R	L/b										
	7	8	9	10	12	14	16	18	20	22	24
0.008	0.95	0.94	0.93	0.93	0.91	0.90	0.89	0.88	0.87	0.86	0.85
0.010	0.94	0.93	0.92	0.91	0.90	0.88	0.87	0.85	0.84	0.83	0.81
0.014	0.91	0.90	0.89	0.88	0.86	0.84	0.82	0.80	0.79	0.77	0.76
0.018	0.89	0.88	0.86	0.85	0.83	0.80	0.78	0.76	0.74	0.73	0.71
0.022	0.87	0.85	0.84	0.82	0.80	0.77	0.75	0.72	0.70	0.68	0.67
0.026	0.85	0.83	0.81	0.80	0.77	0.74	0.71	0.69	0.67	0.65	0.63
0.030	0.83	0.81	0.79	0.77	0.74	0.71	0.68	0.66	0.63	0.61	0.59
0.034	0.81	0.79	0.77	0.75	0.72	0.68	0.66	0.63	0.61	0.58	0.56
0.038	0.79	0.77	0.75	0.73	0.69	0.66	0.63	0.60	0.58	0.56	0.54
0.042	0.78	0.75	0.73	0.71	0.67	0.64	0.61	0.58	0.55	0.53	0.51
0.046	0.76	0.73	0.71	0.69	0.65	0.62	0.58	0.56	0.53	0.51	0.49
0.050	0.74	0.72	0.69	0.67	0.63	0.60	0.56	0.54	0.51	0.49	0.47
0.060	0.71	0.68	0.65	0.63	0.59	0.55	0.52	0.49	0.46	0.44	0.42
0.080	0.64	0.61	0.59	0.56	0.52	0.48	0.45	0.42	0.39	0.37	0.35
0.120	0.55	0.51	0.49	0.46	0.42	0.38	0.35	0.32	0.30	0.28	0.27
0.160	0.48	0.44	0.41	0.39	0.35	0.31	0.29	0.26	0.25	0.23	0.21
0.200	0.42	0.39	0.36	0.34	0.30	0.27	0.24	0.22	0.21	0.19	0.18
0.240	0.38	0.35	0.32	0.30	0.26	0.23	0.21	0.19	0.18	0.17	0.15

Reproduced with permission of the copyright owner. Further reproduction prohibited without permission.

Reproduced with permission of the copyright owner. Further reproduction prohibited without permission.

TABLE 19 - CURVATURE CORRECTION FACTOR ρ_w FOR ALLOWABLE STRESS - INITIAL YIELD

L/R	σ_w/σ_B	L/b 7	8	9	10	12	14	16	18	20	22	24
0.008	-0.2	0.91	0.92	0.93	0.94	0.96	0.97	0.99	1.01	1.03	1.05	1.07
	-0.1	0.96	0.97	0.98	0.99	1.01	1.03	1.05	1.07	1.08	1.08	1.08
	0.1	0.92	0.92	0.92	0.93	0.93	0.93	0.94	0.94	0.94	0.95	0.95
	0.2	0.85	0.86	0.86	0.86	0.87	0.87	0.88	0.89	0.89	0.90	0.91
0.010	-0.2	0.91	0.92	0.93	0.94	0.96	0.98	1.00	1.02	1.04	1.06	1.07
	-0.1	0.97	0.98	0.99	1.00	1.02	1.04	1.06	1.08	1.08	1.08	1.07
	0.1	0.92	0.92	0.92	0.93	0.93	0.93	0.94	0.94	0.94	0.95	0.95
	0.2	0.85	0.86	0.86	0.86	0.87	0.87	0.88	0.89	0.89	0.90	0.91
0.014	-0.2	0.92	0.92	0.94	0.95	0.97	0.99	1.01	1.03	1.05	1.07	1.09
	-0.1	0.97	0.98	0.99	1.00	1.02	1.04	1.07	1.08	1.08	1.08	1.07
	0.1	0.92	0.92	0.92	0.93	0.93	0.93	0.94	0.94	0.94	0.95	0.95
	0.2	0.85	0.86	0.86	0.86	0.87	0.87	0.88	0.89	0.89	0.90	0.91
0.018	-0.2	0.92	0.93	0.94	0.95	0.98	1.00	1.02	1.04	1.06	1.08	1.10
	-0.1	0.98	0.99	1.00	1.01	1.03	1.05	1.08	1.08	1.08	1.08	1.07
	0.1	0.92	0.92	0.92	0.93	0.93	0.93	0.94	0.94	0.94	0.95	0.95
	0.2	0.85	0.86	0.86	0.86	0.87	0.87	0.88	0.89	0.89	0.90	0.91
0.022	-0.2	0.93	0.94	0.95	0.96	0.98	1.01	1.03	1.05	1.07	1.10	1.12
	-0.1	0.98	0.99	1.00	1.02	1.04	1.06	1.09	1.08	1.08	1.08	1.07
	0.1	0.92	0.92	0.92	0.93	0.93	0.93	0.94	0.94	0.94	0.95	0.95
	0.2	0.85	0.86	0.86	0.86	0.87	0.87	0.88	0.89	0.89	0.90	0.91
0.050	-0.2	0.97	0.99	1.01	1.03	1.06	1.10	1.13	1.17	1.17	1.16	1.16
	-0.1	1.03	1.05	1.07	1.08	1.09	1.09	1.09	1.08	1.08	1.08	1.08
	0.1	0.92	0.92	0.92	0.93	0.93	0.93	0.94	0.94	0.94	0.95	0.95
	0.2	0.85	0.86	0.86	0.86	0.87	0.87	0.88	0.89	0.89	0.90	0.91
0.080	-0.2	1.04	1.06	1.09	1.12	1.17	1.19	1.19	1.18	1.17	1.16	1.16
	-0.1	1.10	1.10	1.10	1.09	1.09	1.09	1.09	1.08	1.08	1.08	1.07
	0.1	0.92	0.92	0.92	0.93	0.93	0.93	0.94	0.94	0.94	0.95	0.95
	0.2	0.85	0.86	0.86	0.86	0.87	0.87	0.88	0.89	0.89	0.90	0.91

TABLE 20 INFLUENCE OF YIELD STRESS ON DESIGN EQUATIONS

(a) Initial Yield

L/R	L/b	σ_w/σ_B	σ_f/σ_y (exact)		%Diff.	$F_{bs}/0.55F_y = 1-3\left(\frac{L}{b}\right)^2 \frac{F_y}{\pi^2}$		%Diff.
			(1) σ_y=50 ksi	(2) σ_y=36 ksi	$\frac{(2)-(1)}{(1)}$ x100	(3) σ_y=50 ksi	(4) σ_y=36 ksi	$\frac{(4)-(3)}{(3)}$ x100
0.01	5	0.1	0.86	0.86	0	0.99	0.99	0
		0	0.95	0.95	0	0.99	0.99	0
		-0.1	0.89	0.89	0	0.99	0.99	0
	10	0.1	0.80	0.81	1.3	0.95	0.96	1.1
		0	0.88	0.89	1.1	0.95	0.96	1.1
		-0.1	0.87	0.87	0	0.95	0.96	1.1
	20	0.1	0.61	0.66	8.2	0.79	0.85	7.6
		0	0.68	0.74	8.8	0.79	0.85	7.6
		-0.1	0.77	0.81	5.2	0.79	0.85	7.6
0.05	5	0.1	0.72	0.72	0	0.99	0.99	0
		0	0.78	0.78	0	0.99	0.99	0
		-0.1	0.82	0.82	0	0.99	0.99	0
	10	0.1	0.58	0.59	1.7	0.95	0.96	1.1
		0	0.62	0.63	1.6	0.95	0.96	1.1
		-0.1	0.67	0.67	0	0.95	0.96	1.1
	20	0.1	0.38	0.41	7.9	0.79	0.85	7.6
		0	0.40	0.43	7.5	0.79	0.85	7.6
		-0.1	0.42	0.45	7.1	0.79	0.85	7.6

(b) Ultimate Strength

L/R	L/b	σ_w/σ_B	σ_f/σ_y (exact)		% Diff.	$F_{bs}/0.55F_y = 1-3\frac{L^2}{b}\frac{F_y}{\pi^2 E}$		% Diff.
			(1) σ_y=50 ksi	(2) σ_y=36 ksi	$\frac{(2)-(1)}{(1)}$ x100	(3) σ_y=50 ksi	(4) σ_y=36 ksi	$\frac{(4)-(3)}{(3)}$ x100
0.01	5	0.1	0.99	0.99	0	0.99	0.99	0
		0	0.99	0.99	0	0.99	0.99	0
		-0.1	0.99	0.99	0	0.99	0.99	0
	10	0.1	0.95	0.96	1.1	0.95	0.96	1.1
		0	0.95	0.96	1.1	0.95	0.96	1.1
		-0.1	0.95	0.96	1.1	0.95	0.96	1.1
	20	0.1	0.79	0.85	7.6	0.79	0.85	7.6
		0	0.79	0.85	7.6	0.79	0.85	7.6
		-0.1	0.79	0.85	7.6	0.79	0.85	7.6
0.05	5	0.1	0.98	0.98	0	0.99	0.99	0
		0	0.99	0.99	0	0.99	0.99	0
		-0.1	0.99	0.99	0	0.99	0.99	0
	10	0.1	0.90	0.90	0	0.95	0.96	1.1
		0	0.92	0.93	1.1	0.95	0.96	1.1
		-0.1	0.95	0.95	0	0.95	0.96	1.1
	20	0.1	0.63	0.70	11.1	0.79	0.85	7.6
		0	0.65	0.72	10 8	0.79	0.85	7.6
		-0.1	0.68	0.75	10.3	0.79	0.85	7.6

Reproduced with permission of the copyright owner. Further reproduction prohibited without permission.

TABLE 21
APPROXIMATION INVOLVED IN ALLOWABLE STRESS DESIGN FORMULA-
ULTIMATE STRENGTH

L/R	L/b	σ_w/σ_B	σ_f/σ_y Exact (1)	σ_f/σ_y Design Eq. (2)	% Diff. = $\frac{(2)-(1)}{(1)}$ *
0.01	5	-0.5	0.95	0.99	4.3
		-0.1	0.99	0.99	0
		0	0.99	0.99	0
		0.1	0.99	0.99	0
		0.5	0.93	0.94	0.9
	10	-0.5	0.95	0.96	1.3
		-0.1	0.96	0.96	0
		0	0.96	0.96	0
		0.1	0.96	0.96	0
		0.5	0.91	0.91	0
	25	-0.5	0.77	0.76	-0.8
		-0.1	0.76	0.76	0
		0	0.76	0.76	0
		0.1	0.77	0.76	-0.8
		0.5	0.67	0.70	4.5
0.05	5	-0.5	0.96	0.99	3.2
		-0.1	0.99	0.99	0
		0	0.99	0.97	-1.9
		0.1	0.98	0.94	-3.7
		0.5	0.87	0.83	-4.2
	10	-0.5	0.96	0.96	0
		-0.1	0.95	0.94	-0.7
		0	0.93	0.92	-1.3
		0.1	0.90	0.89	-0.7
		0.5	0.80	0.79	-0.8
	25	-0.5	0.70	0.72	2.5
		-0.1	0.60	0.65	7.9
		0	0.58	0.63	8.6
		0.1	0.57	0.61	7.5
		0.5	0.50	0.54	8.5
0.10	5	-0.5	0.98	0.99	1.1
		-0.1	0.96	0.90	-6.1
		0	0.93	0.88	-5.8
		0.1	0.90	0.85	-5.4
		0.5	0.80	0.75	-6.1
	10	-0.5	0.90	0.85	-5.4
		-0.1	0.81	0.77	-4.7
		0	0.78	0.75	-3.6
		0.1	0.76	0.73	-3.7
		0.5	0.68	0.65	-4.1
	25	-0.5	0.49	0.38	-22.5
		-0.1	0.44	0.36	-18.2
		0	0.43	0.35	-18.6
		0.1	0.43	0.35	-18.6
		0.5	0.39	0.33	-15.4

* %Diff. negative = Design eq. conservative

Reproduced with permission of the copyright owner. Further reproduction prohibited without permission.

TABLE 22 - CURVATURE CORRECTION FACTOR ρ_B FOR ALLOWABLE STRESS-ULTIMATE STRENGTH

L/R	L/b										
	7	8	9	10	12	14	16	18	20	22	24
0.008	1.00	1.00	1.00	1.00	1.00	1.00	1.00	1.00	1.00	1.00	1.00
0.010	1.00	1.00	1.00	1.00	1.00	1.00	1.00	1.00	1.00	1.00	1.00
0.014	1.00	1.00	1.00	1.00	1.00	1.00	1.00	1.00	1.00	1.00	1.00
0.018	1.00	1.00	1.00	1.00	1.00	1.00	1.00	1.00	0.99	0.99	0.99
0.022	1.00	1.00	1.00	1.00	0.99	0.99	0.99	0.99	0.99	0.99	0.98
0.026	1.00	1.00	0.99	0.99	0.99	0.99	0.99	0.98	0.98	0.97	0.97
0.030	0.99	0.99	0.99	0.99	0.99	0.98	0.98	0.97	0.97	0.96	0.95
0.034	0.99	0.99	0.99	0.98	0.98	0.97	0.97	0.96	0.95	0.94	0.94
0.038	0.99	0.99	0.98	0.98	0.97	0.96	0.96	0.95	0.94	0.93	0.91
0.042	0.98	0.98	0.98	0.97	0.96	0.95	0.94	0.93	0.92	0.90	0.89
0.046	0.98	0.98	0.97	0.97	0.96	0.94	0.93	0.91	0.90	0.88	0.87
0.050	0.98	0.97	0.97	0.96	0.95	0.93	0.91	0.90	0.88	0.86	0.84
0.060	0.96	0.96	0.95	0.94	0.92	0.90	0.87	0.85	0.82	0.80	0.77
0.080	0.93	0.92	0.90	0.88	0.85	0.81	0.78	0.74	0.70	0.67	0.63
0.120	0.84	0.82	0.79	0.76	0.70	0.64	0.58	0.53	0.49	0.45	0.41
0.160	0.75	0.70	0.66	0.63	0.55	0.49	0.43	0.38	0.34	0.30	0.27
0.200	0.65	0.60	0.55	0.51	0.43	0.37	0.32	0.28	0.24	0.21	0.19
0.240	0.55	0.50	0.46	0.41	0.34	0.29	0.24	0.21	0.18	0.16	0.14

Reproduced with permission of the copyright owner. Further reproduction prohibited without permission.

Reproduced with permission of the copyright owner. Further reproduction prohibited without permission.

TABLE 23 - CURVATURE CORRECTION FACTOR ρ_w FOR ALLOWABLE STRESS

ULTIMATE STRENGTH

L/R	σ_w/σ_B	L/b										
		7	8	9	10	12	14	16	18	20	22	24
0.008	-0.2	1.00	1.00	1.00	1.00	1.00	1.00	1.00	1.00	1.00	1.00	1.00
	-0.1	1.00	1.00	1.00	1.00	1.00	1.00	1.00	1.00	1.00	1.00	1.00
	0.1	1.00	1.00	1.00	1.00	1.00	1.00	1.00	1.00	1.00	1.00	1.00
	0.2	1.00	1.00	1.00	1.00	1.00	1.00	1.00	1.00	1.00	1.00	1.00
0.010	-0.2	1.00	1.00	1.00	1.00	1.00	1.00	1.00	1.00	1.00	1.00	1.00
	-0.1	1.00	1.00	1.00	1.00	1.00	1.00	1.00	1.00	1.00	1.00	1.00
	0.1	1.00	1.00	1.00	1.00	1.00	1.00	1.00	1.00	1.00	1.00	1.00
	0.2	1.00	1.00	1.00	1.00	1.00	1.00	1.00	1.00	1.00	1.00	1.00
0.014	-0.2	1.00	1.00	1.00	1.00	1.00	1.00	1.00	1.00	1.00	1.00	1.00
	-0.1	1.00	1.00	1.00	1.00	1.00	1.00	1.00	1.00	1.00	1.00	1.00
	0.1	1.00	1.00	1.00	1.00	1.00	1.00	1.00	1.00	1.00	1.00	1.00
	0.2	1.00	1.00	1.00	1.00	1.00	1.00	1.00	1.00	1.00	1.00	1.00
0.018	-0.2	1.00	1.00	1.00	1.00	1.00	1.00	1.00	1.00	1.01	1.01	1.01
	-0.1	1.00	1.00	1.00	1.00	1.00	1.00	1.00	1.00	1.01	1.01	1.01
	0.1	1.00	1.00	1.00	1.00	1.00	1.00	1.00	1.00	1.01	1.01	1.01
	0.2	1.00	1.00	1.00	1.00	1.00	1.00	1.00	1.00	1.01	1.01	1.00
0.022	-0.2	1.00	1.00	1.00	1.00	1.01	1.01	1.01	1.01	1.01	1.01	1.02
	-0.1	1.00	1.00	1.00	1.00	1.01	1.01	1.01	1.01	1.01	1.01	1.02
	0.1	1.00	1.00	1.00	1.00	1.01	1.01	1.01	1.01	1.01	1.01	1.02
	0.2	1.00	1.00	1.00	1.00	1.00	1.00	1.00	1.00	1.00	1.00	1.00
0.050	-0.2	1.02	1.03	1.04	1.04	1.05	1.05	1.05	1.05	1.05	1.05	1.05
	-0.1	1.02	1.02	1.02	1.02	1.02	1.02	1.02	1.02	1.02	1.02	1.02
	0.1	0.97	0.97	0.97	0.97	0.97	0.97	0.97	0.97	0.97	0.97	0.97
	0.2	0.94	0.94	0.94	0.94	0.94	0.94	0.94	0.94	0.94	0.94	0.94
0.080	-0.2	1.01	1.01	1.01	1.01	1.01	1.01	1.01	1.01	1.00	1.00	1.00
	-0.1	0.98	0.98	0.98	0.98	0.98	0.98	0.98	0.98	0.98	0.98	0.98
	0.1	0.93	0.93	0.93	0.93	0.93	0.93	0.93	0.93	0.93	0.93	0.93
	0.2	0.90	0.90	0.90	0.90	0.90	0.90	0.90	0.90	0.91	0.91	0.91

TABLE 24 - COMPRESSION FLANGE BRACE FORCE DESIGN VALUES - INITIAL YIELD

L/R	$F_w F_{bc}$	L/b										
		7	8	9	10	12	14	16	18	20	22	24
0.008	-0.2	0.52	0.49	0.47	0.44	0.40	0.36	0.32	0.29	0.25	0.21	0.15
	0.0	0.86	0.88	0.90	0.92	0.97	1.02	1.09	1.17	1.26	1.37	1.50
	0.2	1.15	1.21	1.26	1.32	1.44	1.56	1.69	1.82	1.97	2.13	2.31
0.01	-0.2	0.74	0.72	0.69	0.67	0.64	0.62	0.59	0.59	0.59	0.59	0.59
	0.0	1.07	1.09	1.12	1.14	1.20	1.27	1.35	1.44	1.54	1.66	1.81
	0.2	1.36	1.42	1.48	1.54	1.66	1.78	1.92	2.06	2.21	2.37	2.54
0.014	-0.2	1.17	1.15	1.14	1.14	1.13	1.15	1.16	1.19	1.23	1.29	1.37
	0.0	1.50	1.53	1.56	1.60	1.67	1.76	1.86	1.97	2.09	2.23	2.38
	0.2	1.77	1.84	1.90	1.96	2.10	2.23	2.37	2.52	2.67	2.83	2.99
0.018	-0.2	1.60	1.60	1.59	1.59	1.61	1.64	1.69	1.76	1.84	1.94	2.07
	0.0	1.92	1.96	2.00	2.04	2.13	2.24	2.35	2.48	2.62	2.77	2.92
	0.2	2.19	2.26	2.32	2.39	2.53	2.67	2.82	2.98	3.13	3.29	3.44
0.022	-0.2	2.03	2.03	2.04	2.05	2.09	2.14	2.22	2.31	2.43	2.56	2.72
	0.0	2.35	2.39	2.43	2.48	2.59	2.71	2.84	2.98	3.13	3.28	3.43
	0.2	2.60	2.67	2.74	2.81	2.86	3.11	3.27	3.42	3.58	3.74	3.88
0.026	-0.2	2.46	2.47	2.48	2.50	2.56	2.64	2.73	2.85	2.99	3.15	3.33
	0.0	2.77	2.82	2.87	2.92	3.05	3.18	3.32	3.47	3.62	3.78	3.93
	0.2	3.02	3.09	3.16	3.24	3.39	3.55	3.71	3.87	4.03	4.18	4.32
0.030	-0.2	2.88	2.90	2.92	2.95	3.03	3.12	3.24	3.38	3.54	3.72	3.92
	0.0	3.19	3.24	3.30	3.36	3.49	3.64	3.79	3.95	4.11	4.26	4.41
	0.2	3.42	3.50	3.58	3.66	3.82	3.98	4.15	4.31	4.47	4.62	4.75
0.034	-0.2	3.31	3.33	3.36	3.40	3.49	3.60	3.74	3.90	4.08	4.28	4.46
	0.0	3.61	3.67	3.73	3.80	3.94	4.09	4.25	4.42	4.58	4.74	4.89
	0.2	3.84	3.92	4.00	4.08	4.24	4.41	4.58	4.75	4.90	5.05	5.19

Reproduced with permission of the copyright owner. Further reproduction prohibited without permission.

TABLE 24 - con't.

L/R	F_w/F_{bc}	L/b 7	8	9	10	12	14	16	18	20	22	24
0.042	-0.2	4.16	4.17	4.24	4.29	4.41	4.56	4.73	4.92	5.13	5.32	5.49
	0.0	4.45	4.52	4.59	4.66	4.82	4.99	5.17	5.34	5.51	5.67	5.81
	0.2	4.66	4.74	4.83	4.91	5.09	5.27	5.44	5.61	5.77	5.91	6.04
0.050	-0.2	5.00	5.05	5.11	5.17	5.32	5.50	5.70	5.92	6.12	6.31	6.47
	0.0	5.29	5.36	5.44	5.52	5.70	5.88	6.06	6.24	6.41	6.57	6.71
	-.2	5.48	5.57	5.66	5.75	5.93	6.11	6.29	6.46	6.62	6.77	6.89
0.060	-0.2	6.06	6.12	6.19	6.27	6.45	6.66	6.90	7.11	7.31	7.49	7.65
	0.0	6.33	6.41	6.50	6.59	6.78	6.97	7.16	7.35	7.52	7.68	7.82
	0.2	6.50	6.59	6.69	6.78	6.97	7.16	7.35	7.52	7.68	7.82	7.94
0.080	-0.2	8.16	8.24	8.34	8.45	8.69	8.94	9.16	9.38	9.59	9.77	9.92
	0.0	8.40	8.50	8.60	8.70	8.90	9.12	9.32	9.51	9.69	9.85	9.97
	0.2	8.54	8.64	8.74	8.84	9.05	9.24	9.43	9.61	9.77	9.91	10.02
0.12	-0.2	12.31	12.42	12.55	12.68	12.98	13.26	13.51	13.74	13.94	14.11	14.24
	0.0	12.51	12.62	12.73	12.85	13.09	13.32	13.53	13.73	13.91	14.06	14 17
	0.2	12.60	12.71	12.82	12.93	13.15	13.36	13.55	13.73	13.89	14.02	14.12
0.16	-0.2	16.39	16.50	16.63	16.76	17.03	17.31	17.58	17.86	18.12	18.32	18.44
	0.0	16.59	16.71	16.84	16.96	17.21	17.45	17.67	17.87	18.05	18.19	18.29
	0.2	16.65	16.76	16.88	16.99	17.22	17.43	17.63	17.81	17.96	18.09	18.19
0.2	-0.2	20.44	20.56	20.68	20.80	21.05	21.30	21.54	21.77	21.98	22.16	22.31
	0.0	20.65	20.78	20.91	21.04	21.30	21.54	21.77	21.97	22.14	22.28	22.39
	0.2	20.68	20.80	20.92	21.04	21.27	21.48	21.68	21.86	22.02	22.14	22.24
0.24	-0.2	24.49	24.61	24.73	24.85	25.09	25.33	25.55	25.75	25.94	26.09	26.22
	0.0	24.69	24.83	24.97	25.11	25.37	25.61	25.84	26.04	26.21	26.35	26.45
	0.2	24.71	24.83	24.95	25.07	25.31	25.53	25.73	25.91	26.06	26.18	26.28

Reproduced with permission of the copyright owner. Further reproduction prohibited without permission.

Reproduced with permission of the copyright owner. Further reproduction prohibited without permission.

TABLE 25 - COMPRESSION FLANGE BRACE FORCE DESIGN VALUES - ULTIMATE STRENGTH

L/R	F_w/F_{bc}	L/b										
		7	8	9	10	12	14	16	18	20	22	24
0.008	-0.2	0.48	0.45	0.42	0.39	0.33	0.29	0.24	0.19	0.13	0.05	-0.07
	0.0	0.86	0.88	0.90	0.93	0.98	1.05	1.14	1.24	1.39	1.59	1.89
	0.2	1.24	1.32	1.39	1.47	1.63	1.82	2.03	2.30	2.64	3.13	2.85
0.01	-0.2	0.69	0.67	0.64	0.62	0.58	0.55	0.52	0.50	0.48	0.45	0.41
	0.0	1.08	1.10	1.13	1.16	1.23	1.31	1.42	1.55	1.73	1.99	2.37
	0.2	1.46	1.54	1.62	1.70	1.88	2.08	2.32	2.61	2.99	3.52	4.33
0.014	-0.2	1.13	1.11	1.09	1.08	1.07	1.07	1.09	1.12	1.17	1.24	1.35
	0.0	1.51	1.54	1.58	1.62	1.72	1.84	1.99	2.18	2.43	2.78	3.31
	0.2	1.90	1.98	2.07	2.16	2/37	2.60	2.88	3.23	3.68	4.32	4.27
0.018	-0.2	1.56	1.55	1.54	1.54	1.56	1.60	1.66	1.74	1.86	2.04	2.30
	0.0	1.94	1.98	2.03	2.08	2.21	2.37	2.56	2.80	3.12	3.57	4.26
	0.2	2.32	2.42	2.52	2.63	2.86	3.13	3.45	3.85	4.37	4.11	6.18
0.022	-0.2	1.99	1.99	1.99	2.01	2.05	2.13	2.23	2.37	2.56	2.83	3.25
	0.0	2.37	2.42	2.48	2.55	2.70	2.89	3.12	3.42	3.81	4.37	5.21
	0.2	2.75	2.86	2.97	3.09	3.35	3.65	4.00	4.43	4.99	5.75	6.84
0.026	-0.2	2.42	2.43	2.45	2.47	2.54	2.65	2.80	2.99	3.25	3.62	4.19
	0.0	2.80	2.86	2.93	3.01	3.19	3.42	3.69	4.04	4.50	5.16	6.15
	0.2	3.18	3.29	3.41	3.54	3.82	4.14	4.52	4.99	5.57	6.35	7.41
0.030	-0.2	2.85	2.87	2.90	2.93	3.04	3.18	3.36	3.61	3.94	4.42	5.14
	0.0	3.23	3.30	3.38	3.47	3.69	3.94	4.26	4.66	5.20	5.94	6.98
	0.2	3.60	3.72	3.85	3.98	4.29	4.63	5.04	5.52	6.13	6.90	7.92
0.034	-0.2	3.28	3.31	3.35	3.40	3.53	3.70	3.93	4.23	4.64	5.21	6.09
	0.0	3.66	3.74	3.84	3.94	4.18	4.47	4.82	5.25	5.80	6.53	7.52
	0.2	4.02	4.15	4.28	4.43	4.75	5.12	5.54	6.04	6.66	7.42	8.38
0.042	-0.2	4.14	4.19	4.25	4.32	4.51	4.75	5.07	5.46	5.95	6.59	7.44
	0.0	4.52	4.62	4.73	4.85	5.13	5.46	5.85	6.32	6.89	7.59	8.45
	0.2	4.86	5.00	5.16	5.32	5.67	6.17	6.52	7.04	7.65	8.35	9.17

TABLE 25 - con't.

L/R	F_wF_{bc}	L/b										
		7	8	9	10	12	14	16	18	20	22	24
0.050	-0.2	5.01	5.07	5.15	5.25	5.49	5.78	6.14	6.56	7.08	7.69	8.42
	0.0	5.38	5.49	5.61	5.75	6.07	6.43	6.85	7.34	7.90	8.54	9.25
	0.2	5.70	5.86	6.02	6.20	6.58	7.00	7.47	7.99	8.57	9.20	9.87
0.060	-0.2	6.08	6.17	6.28	6.40	6.68	7.02	7.41	7.86	8.36	8.91	9.49
	0.0	6.44	6.57	6.71	6.87	7.22	7.61	8.02	8.54	9.06	9.61	10.15
	0.2	6.75	6.92	7.10	7.28	7.69	8.13	8.61	9.11	9.64	10.17	10.67
0.080	-0.2	8.22	8.35	8.49	8.64	9.00	9.39	9.81	10.24	10.66	11.05	11.38
	0.0	8.55	8.71	8.88	9.06	9.46	9.88	10.32	10.76	11.18	11.55	11.86
	0.2	8.84	9.03	9.23	9.43	9.87	10.32	10.77	11.21	11.61	11.97	12.26
0.12	-0.2	12.47	12.64	12.83	13.02	13.43	13.82	14.18	14.49	14.72	14.88	14.95
	0.0	12.75	12.95	13.15	13.36	13.77	14.17	14.53	14.83	15.07	15.23	15.32
	0.2	13.00	13.21	13.43	13.65	14.08	14.48	14.84	15.15	15.39	15.57	15.68
0.16	-0.2	16.68	16.89	17.10	17.30	17.69	18.03	18.30	18.48	18.57	18.57	18.49
	0.0	16.94	17.15	17.37	17.58	17.98	18.32	18.59	18.79	18.92	18.98	18.98
	0.2	17.16	17.39	17.61	17.83	18.23	18.58	18.87	19.10	19.28	19.42	19.53
0.2	-0.2	20.89	21.12	21.34	21.54	21.90	22.17	22.35	22.42	22.39	22.26	22.04
	0.0	21.13	21.36	21.58	21.79	22.16	22.45	22.66	22.80	22.87	22.88	22.84
	0.2	21.35	21.58	21.81	22.02	22.40	22.72	22.98	23.20	23.40	23.57	23.75
0.24	-0.2	25.11	25.32	25.57	25.77	26.10	26.30	26.39	26.35	26.20	25.94	25.58
	0.0	25.35	25.59	25.82	26.02	26.36	26.62	26.79	26.88	26.92	26.90	26.83
	0.2	25.56	25.81	26.04	26.25	26.63	26.94	27.22	27.47	27.72	27.98	28.27

Reproduced with permission of the copyright owner. Further reproduction prohibited without permission.

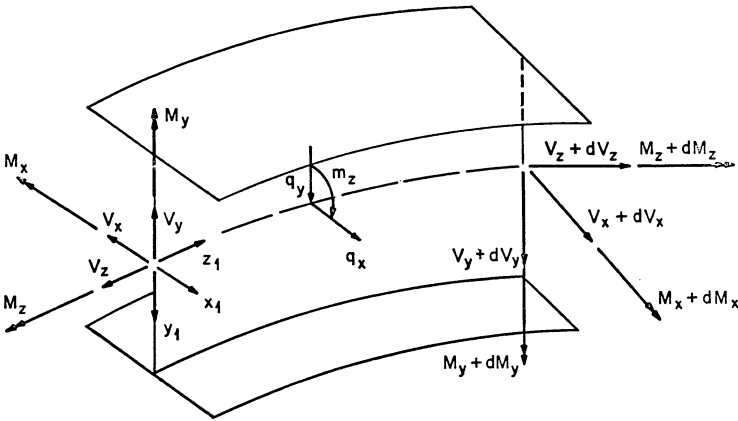

FIG. 1 - ELEMENT OF CURVED PLATE GIRDER

Reproduced with permission of the copyright owner. Further reproduction prohibited without permission.

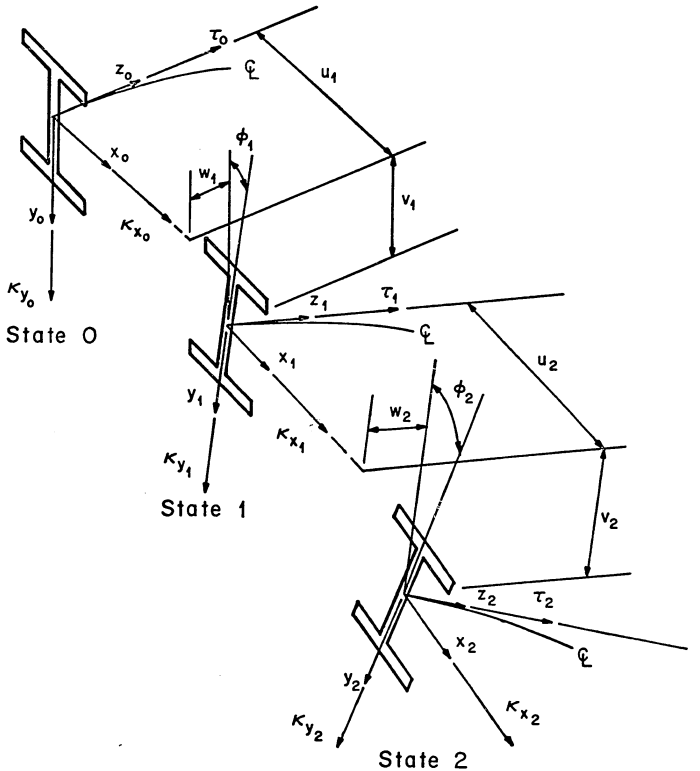

FIG. 2 - DISPLACEMENT COMPONENTS

Reproduced with permission of the copyright owner. Further reproduction prohibited without permission.

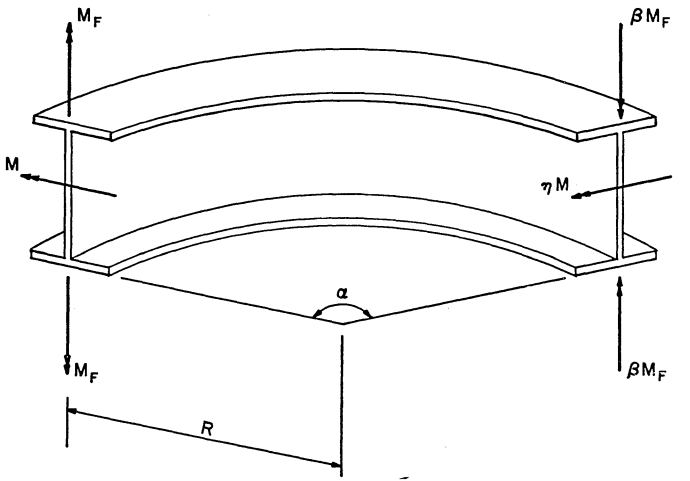

FIG. 3 - CURVED PLATE GIRDER SUBJECTED TO END LOADS

Reproduced with permission of the copyright owner. Further reproduction prohibited without permission.

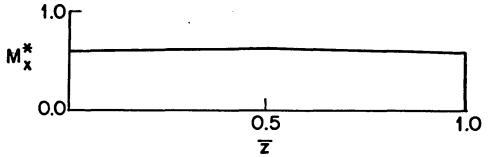

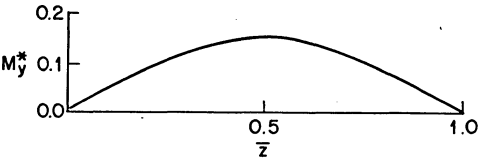

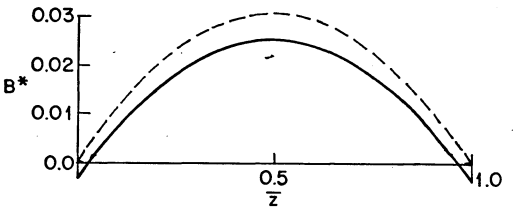

$L/b = 15,\ d/b = 3,\ t_f/t_w = 3, d/t_w = 165,$
$\alpha = 15°,\ \eta = \beta = 1, \sigma_W/\sigma_B = -0.5, M^* = 0.6$

FIG. 4 - INTERNAL STRESS RESULTANTS - NO GRADIENT

Reproduced with permission of the copyright owner. Further reproduction prohibited without permission.

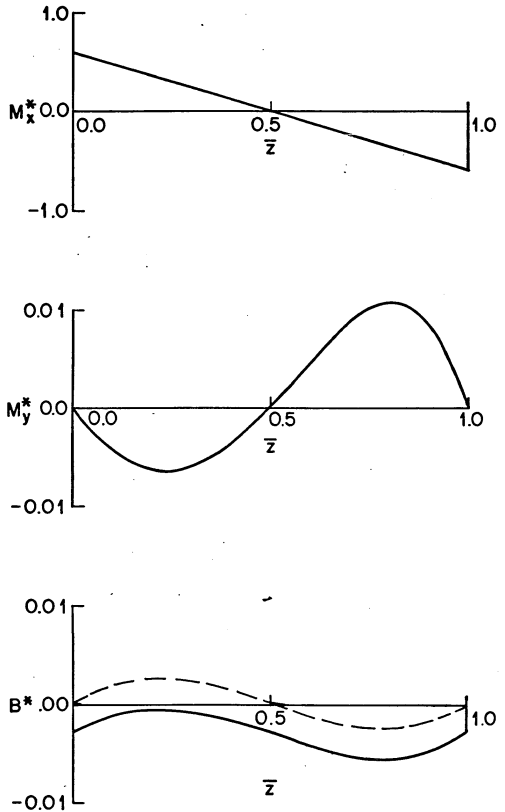

FIG. 5 - INTERNAL STRESS RESULTANTS - GRADIENT ON MOMENT

Reproduced with permission of the copyright owner. Further reproduction prohibited without permission.

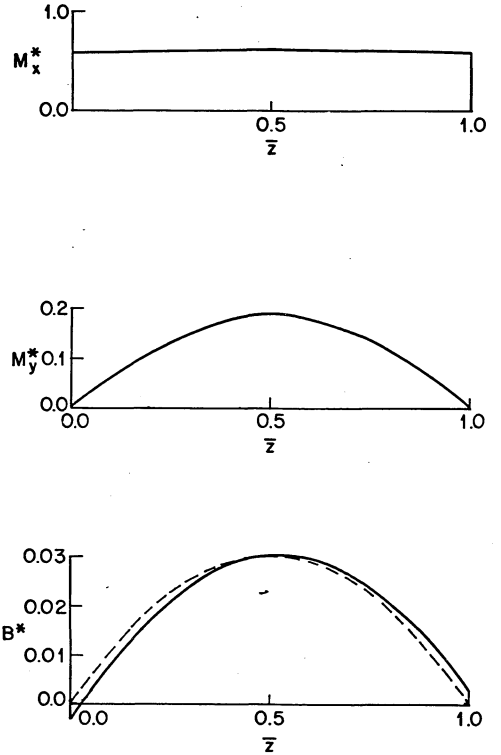

$L/b = 15,\ d/b = 3,\ t_f/t_w = 3,\ d/t_w = 165,$
$\alpha = 15°, \eta = 1, \beta = -1, \sigma_w/\sigma_B = -0.5, M^* = 0.6$

FIG. 6 - INTERNAL STRESS RESULTANTS - GRADIENT ON BIMOMENT

Reproduced with permission of the copyright owner. Further reproduction prohibited without permission.

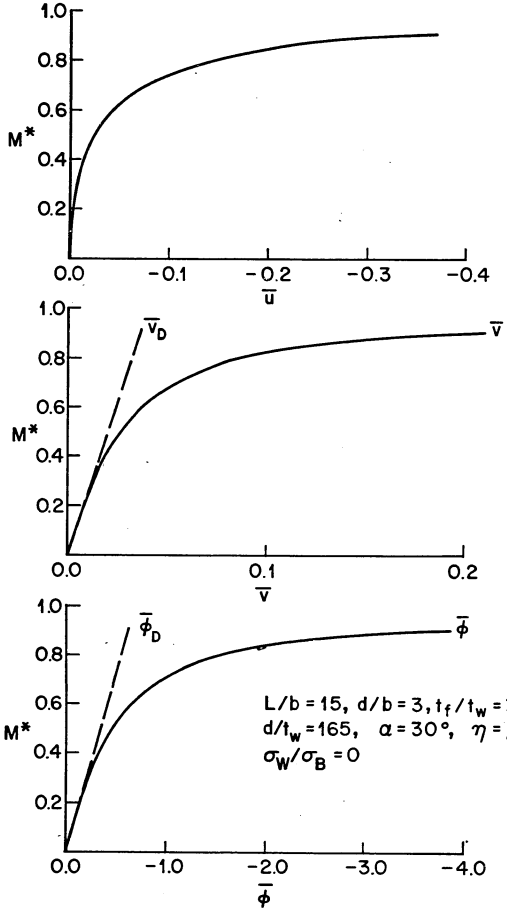

FIG. 7 - COMPARISON OF DEFLECTIONS

Reproduced with permission of the copyright owner. Further reproduction prohibited without permission.

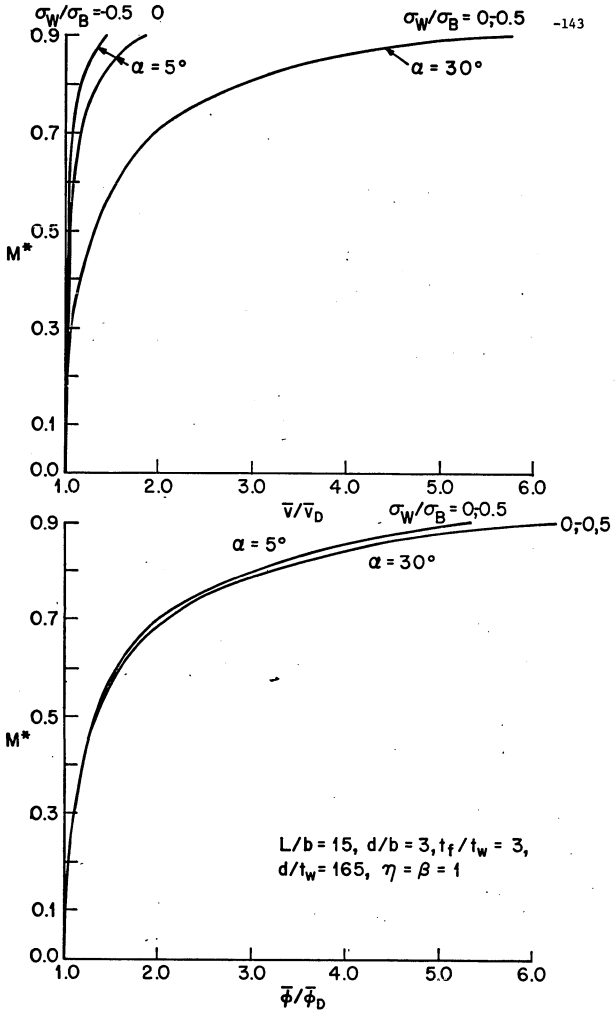

FIG. 8 - DEFLECTION RATIOS

Reproduced with permission of the copyright owner. Further reproduction prohibited without permission.

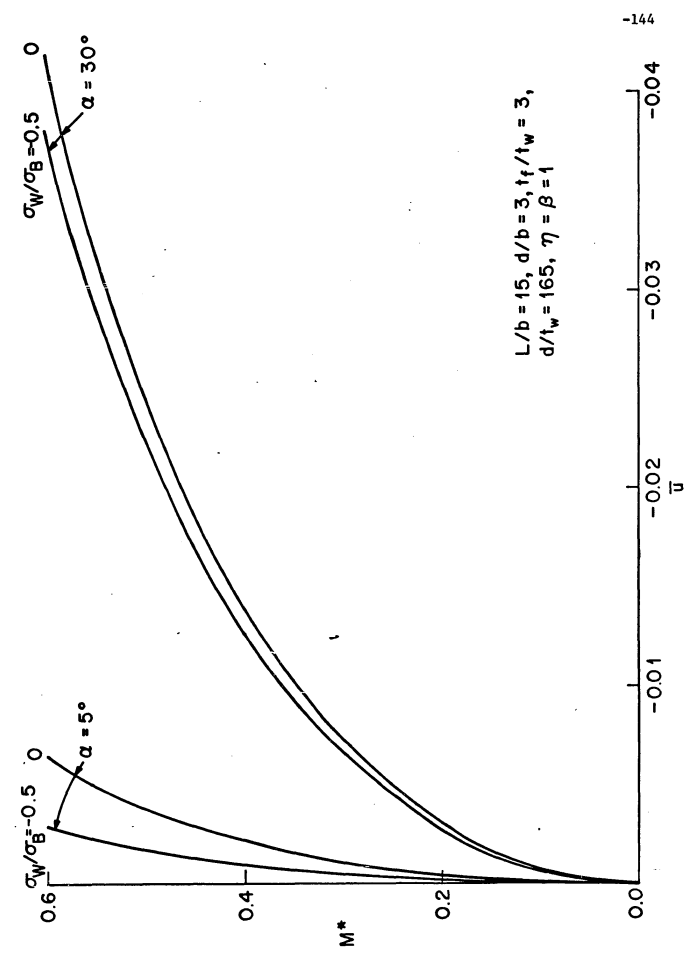

FIG. 9 - LATERAL DEFLECTION AMPLIFICATION

Reproduced with permission of the copyright owner. Further reproduction prohibited without permission.

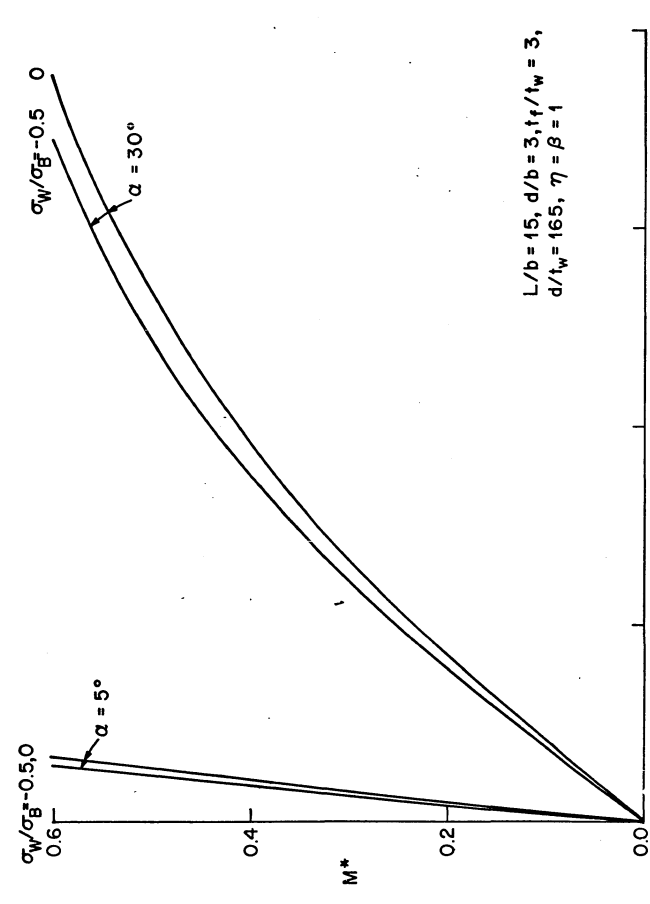

FIG. 10 - VERTICAL DEFLECTION AMPLIFICATION

Reproduced with permission of the copyright owner. Further reproduction prohibited without permission.

Reproduced with permission of the copyright owner. Further reproduction prohibited without permission.

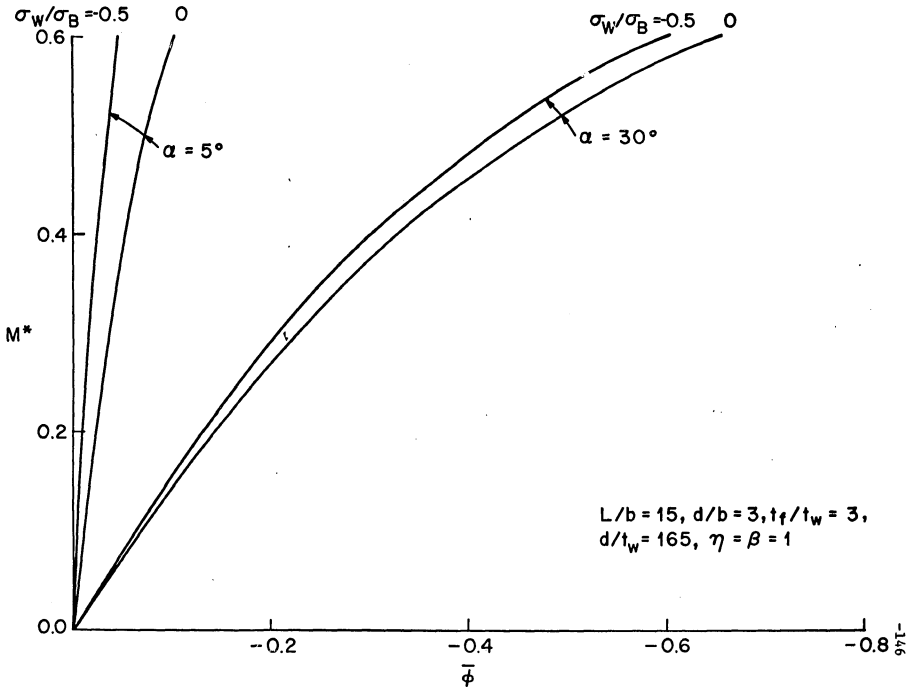

FIG. 11 - AMPLIFICATION OF ANGLE OF TWIST

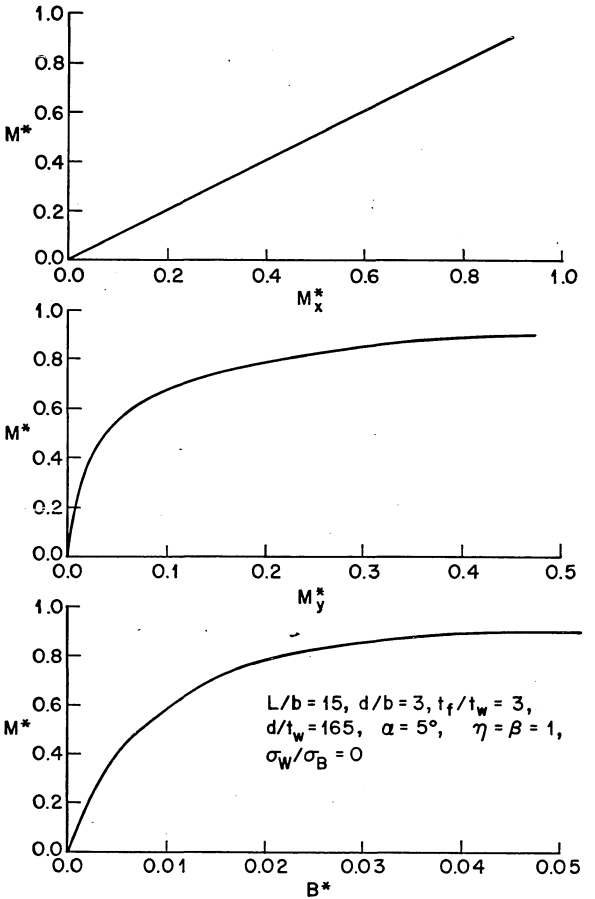

FIG. 12 - GROWTH OF INTERNAL STRESS RESULTANTS WITH LOAD - 5°

Reproduced with permission of the copyright owner. Further reproduction prohibited without permission.

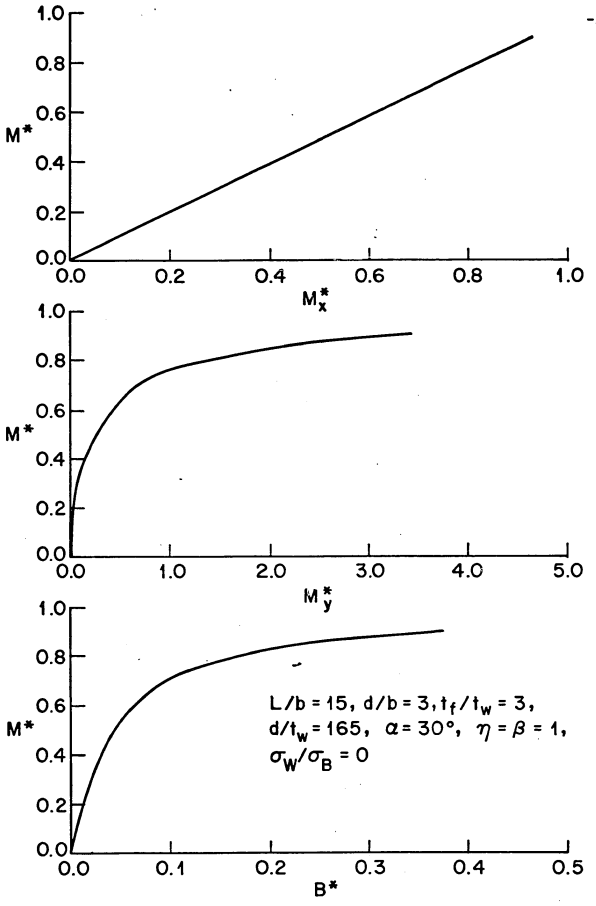

FIG. 13 - GROWTH OF INTERNAL STRESS RESULTANTS WITH LOAD - 30°

Reproduced with permission of the copyright owner. Further reproduction prohibited without permission.

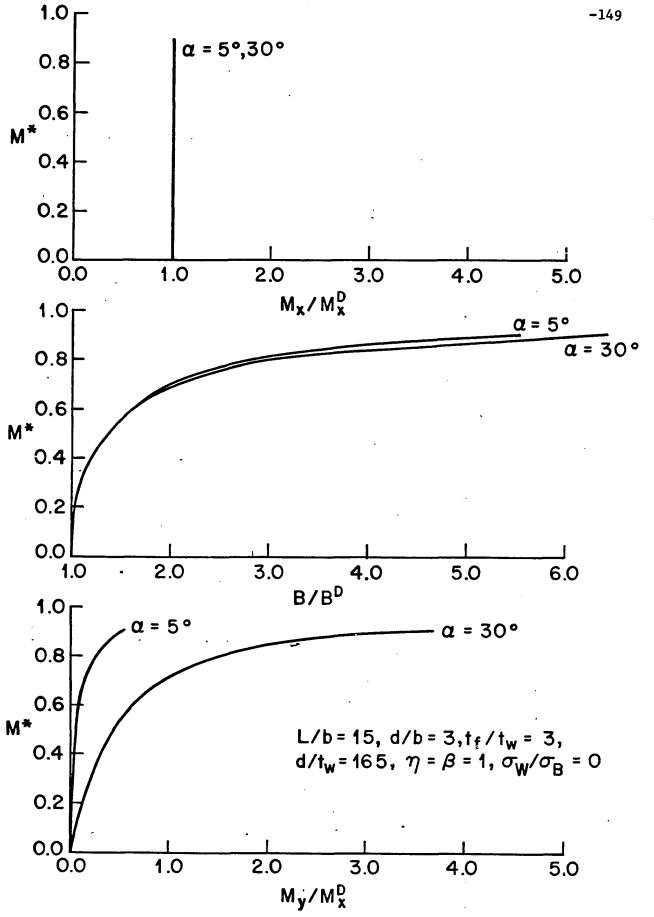

FIG. 14 - RATIO OF INTERNAL STRESS RESULTANTS

Reproduced with permission of the copyright owner. Further reproduction prohibited without permission.

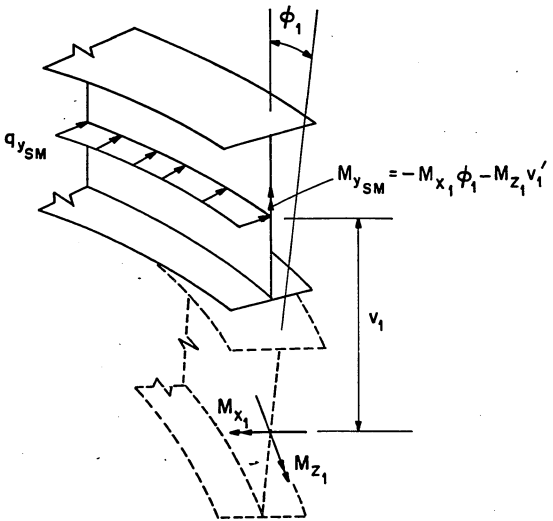

FIG. 15 - PROJECTION OF INTERNAL STRESS RESULTANTS

Reproduced with permission of the copyright owner. Further reproduction prohibited without permission.

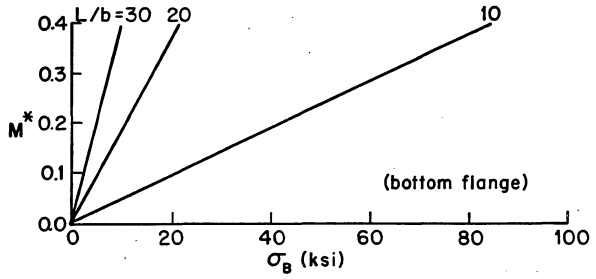

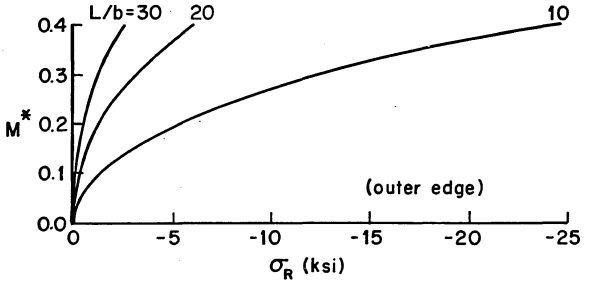

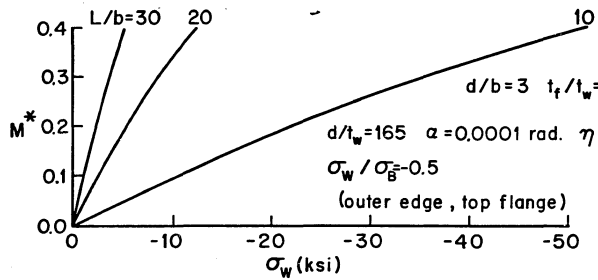

FIG. 16 - GROWTH OF STRESSES WITH LOAD - STRAIGHT CASE

Reproduced with permission of the copyright owner. Further reproduction prohibited without permission.

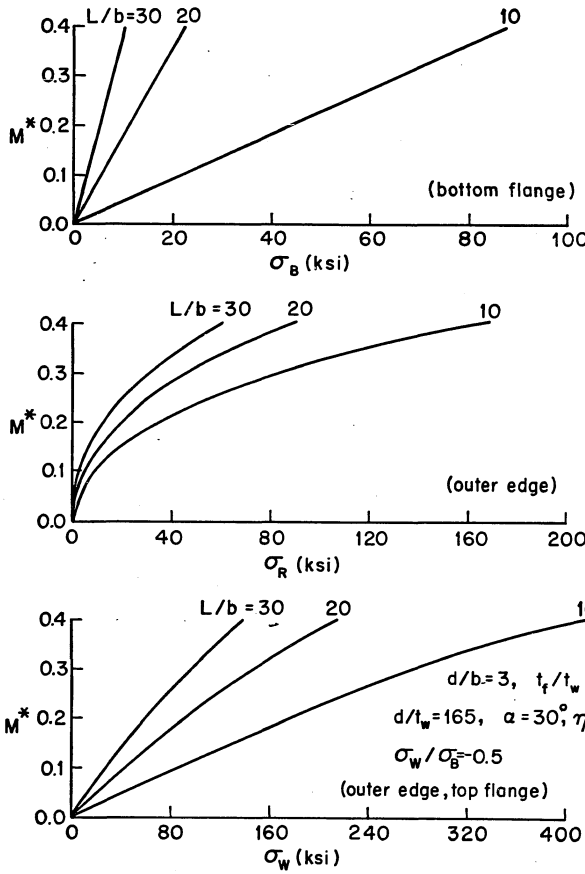

FIG. 17 - GROWTH OF STRESSES WITH LOAD - 30°

Reproduced with permission of the copyright owner. Further reproduction prohibited without permission.

Reproduced with permission of the copyright owner. Further reproduction prohibited without permission.

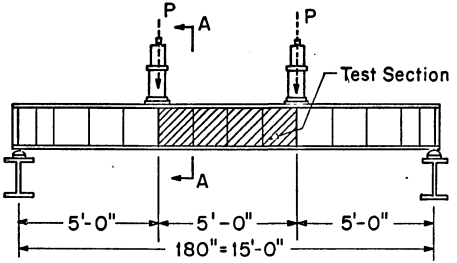

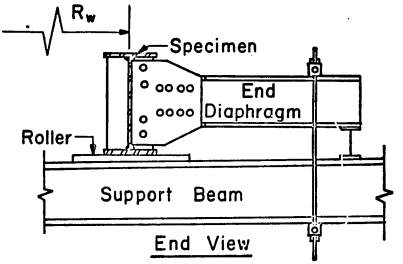

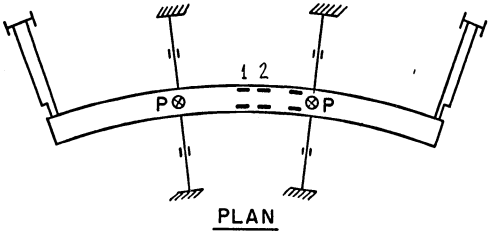

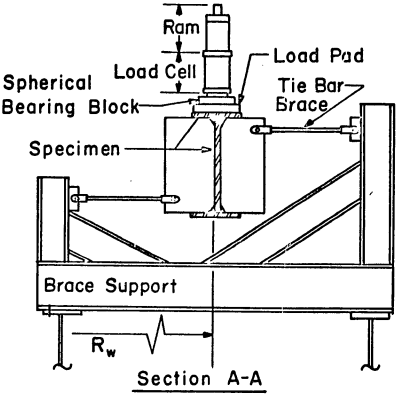

FIG. 18 - EXPERIMENTAL TEST SETUP

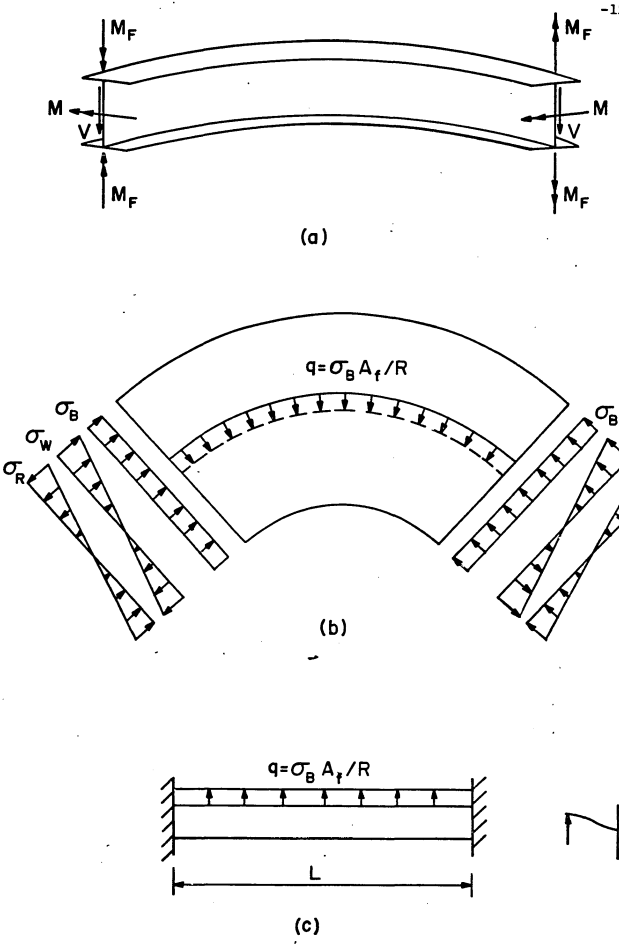

FIG. 19 - CROSS-SECTIONAL DEFORMATION LOADING

Reproduced with permission of the copyright owner. Further reproduction prohibited without permission.

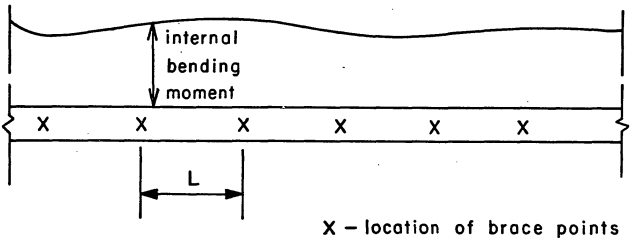

(a)

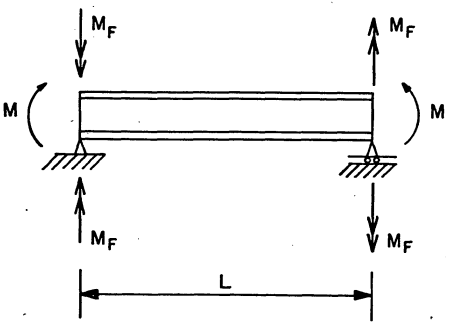

(b)

FIG. 20 - IDEALIZED SINGLE SPAN MODEL

Reproduced with permission of the copyright owner. Further reproduction prohibited without permission.

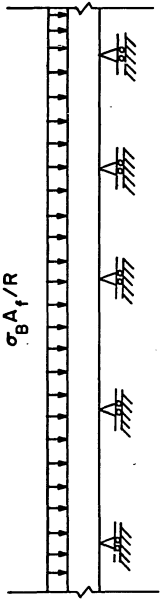

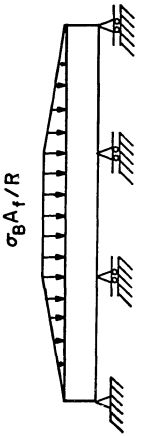

FIG. 21 - IDEALIZED FLANGE LOADING

Reproduced with permission of the copyright owner. Further reproduction prohibited without permission.

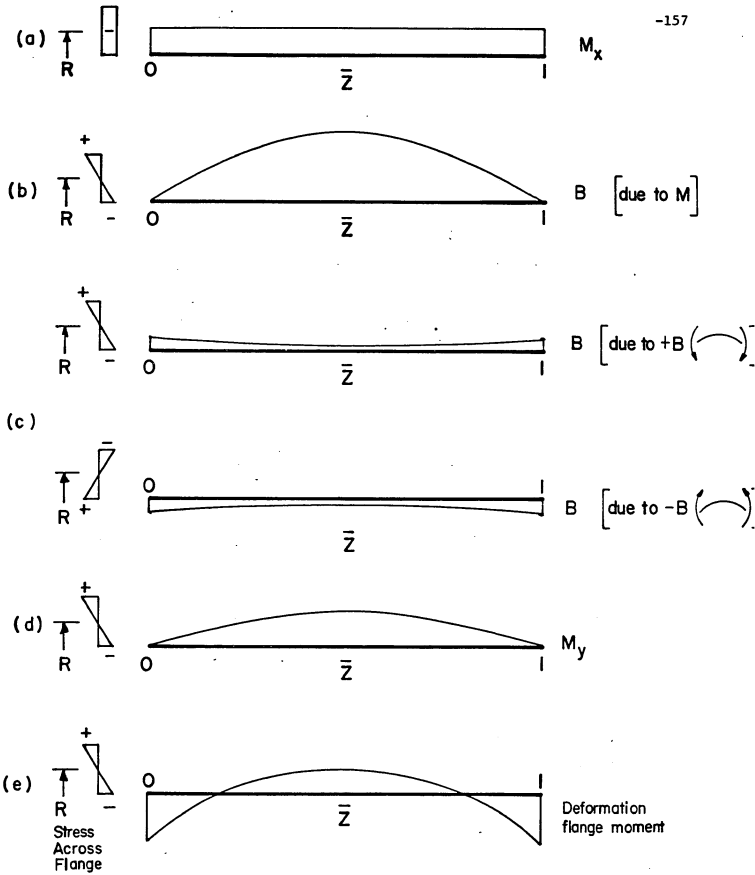

FIG. 22 - STRESS VARIATIONS IN COMPRESSION FLANGE

Reproduced with permission of the copyright owner. Further reproduction prohibited without permission.

Reproduced with permission of the copyright owner. Further reproduction prohibited without permission.

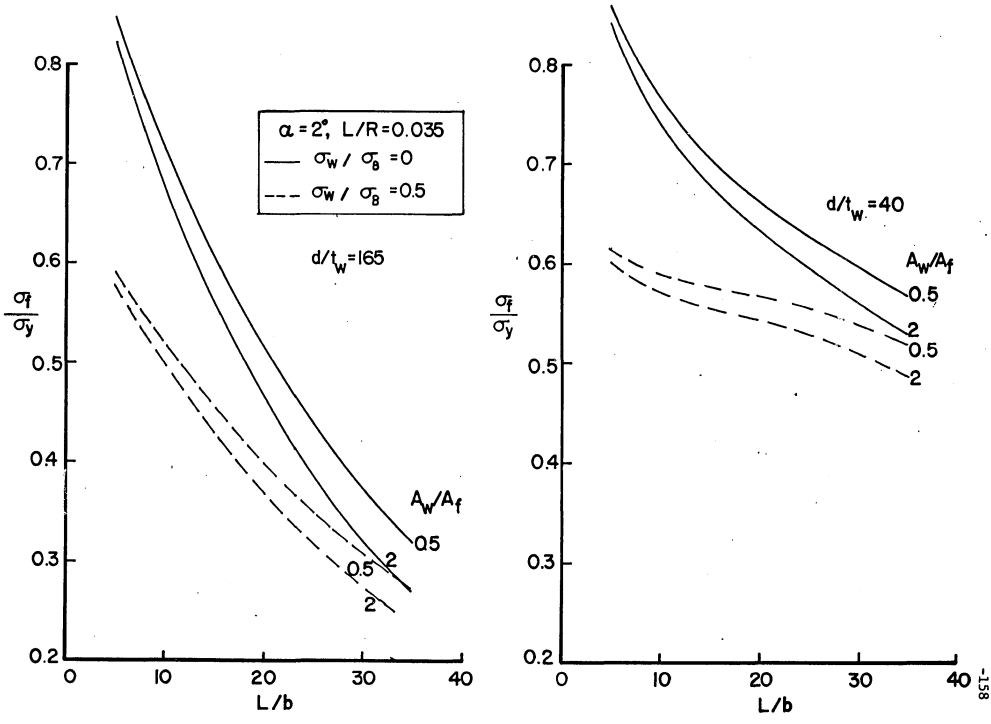

FIG. 23 - INITIAL YIELD CURVES - α = 2°

Reproduced with permission of the copyright owner. Further reproduction prohibited without permission.

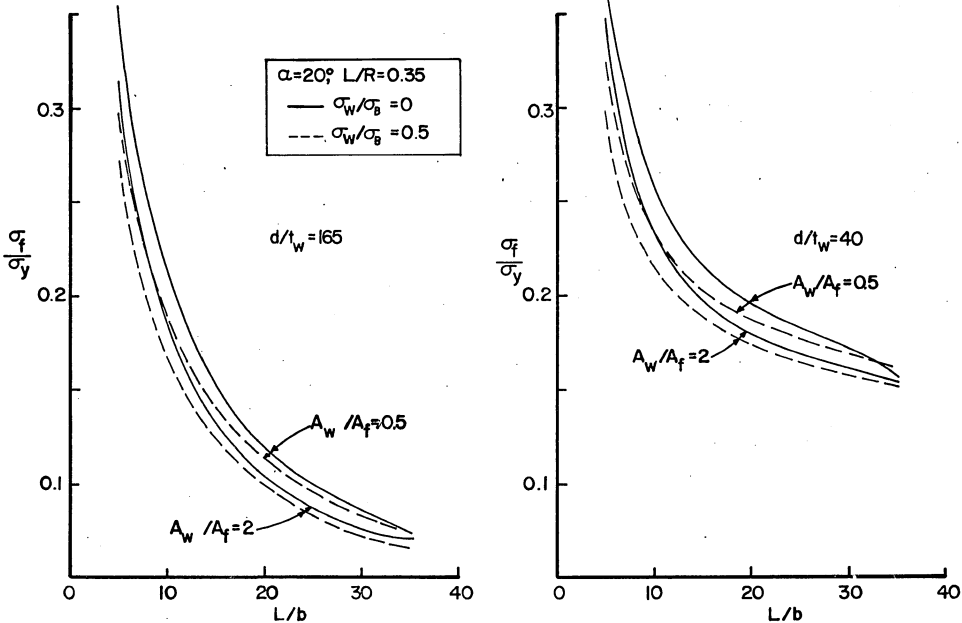

FIG. 24 – INITIAL YIELD CURVES – α = 20°

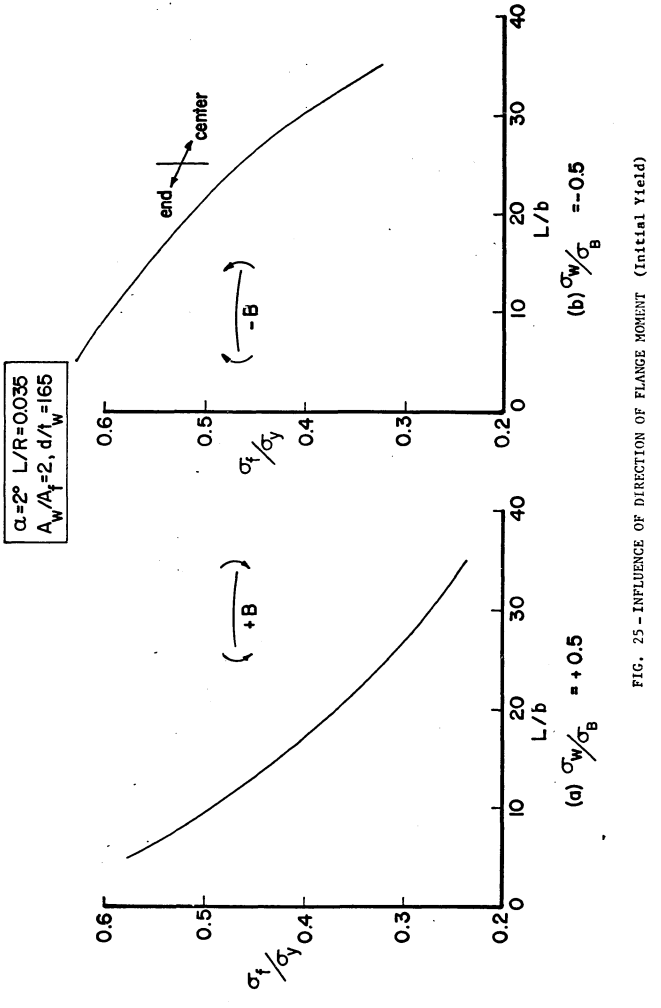

FIG. 25 - INFLUENCE OF DIRECTION OF FLANGE MOMENT (Initial Yield)

Reproduced with permission of the copyright owner. Further reproduction prohibited without permission.

Reproduced with permission of the copyright owner. Further reproduction prohibited without permission.

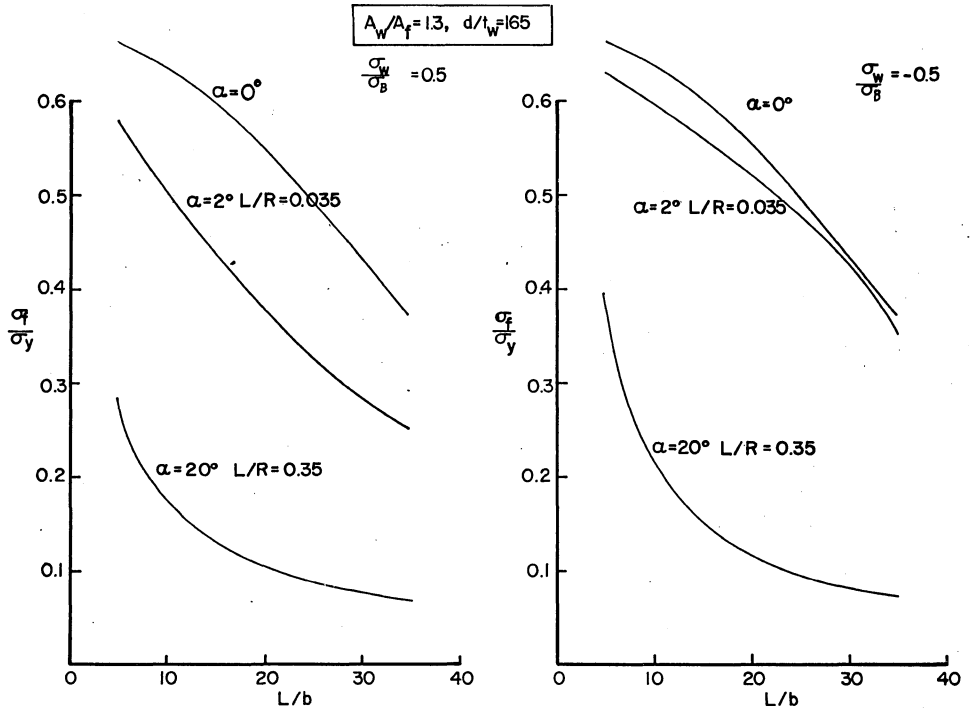

FIG. 26 - INFLUENCE OF CURVATURE ON INITIAL YIELD

Reproduced with permission of the copyright owner. Further reproduction prohibited without permission.

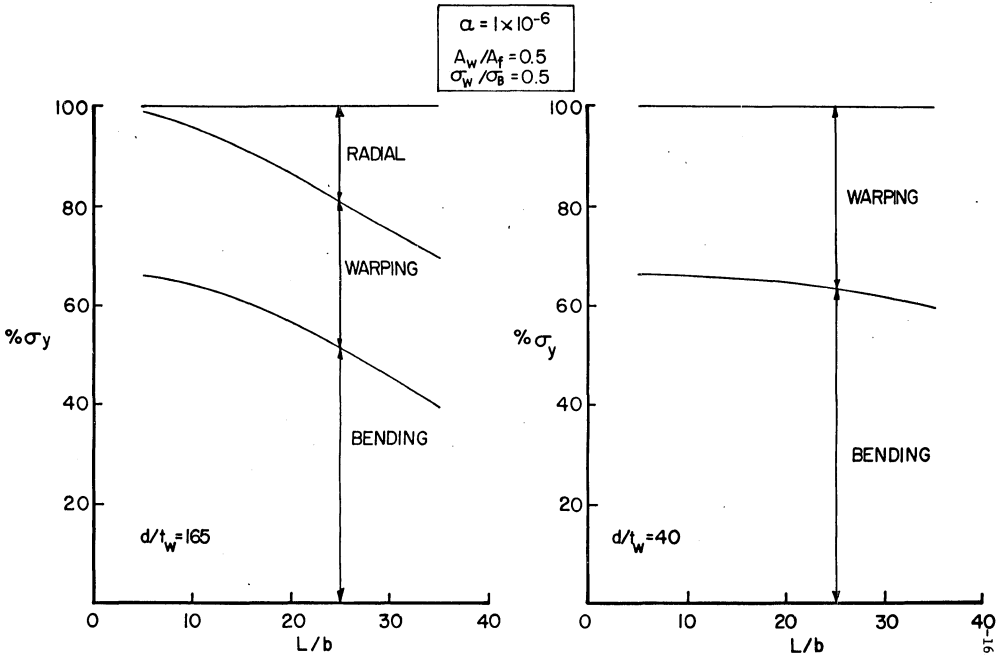

FIG. 27 - CONTRIBUTIONS OF VARIOUS EFFECTS - $\alpha \simeq 0°$ (Initial Yield)

Reproduced with permission of the copyright owner. Further reproduction prohibited without permission.

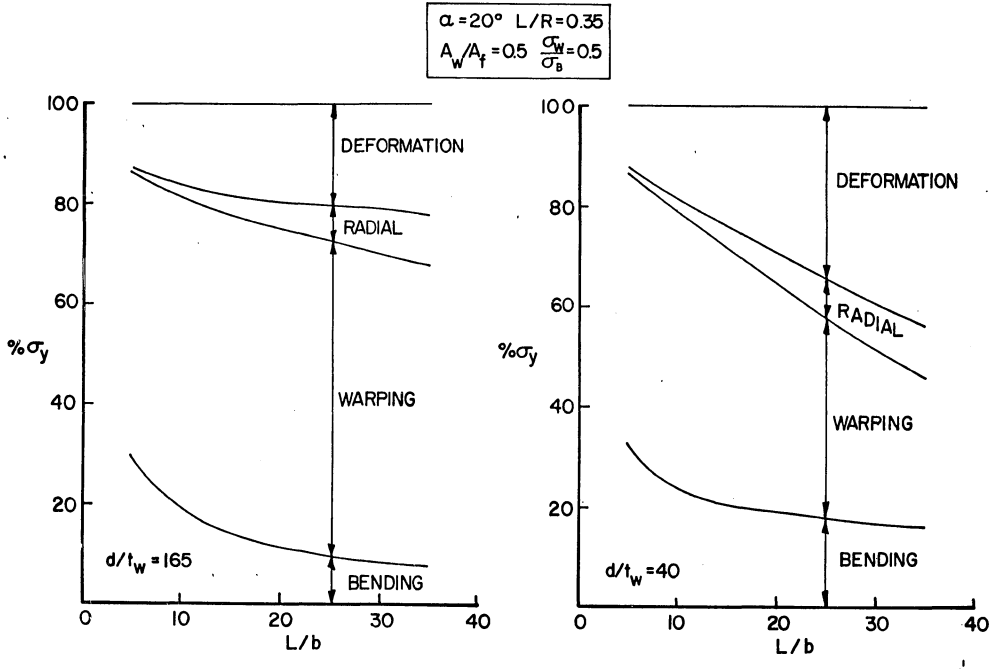

FIG. 28 - CONTRIBUTIONS OF VARIOUS EFFECTS - α = 20° (Initial Yield)

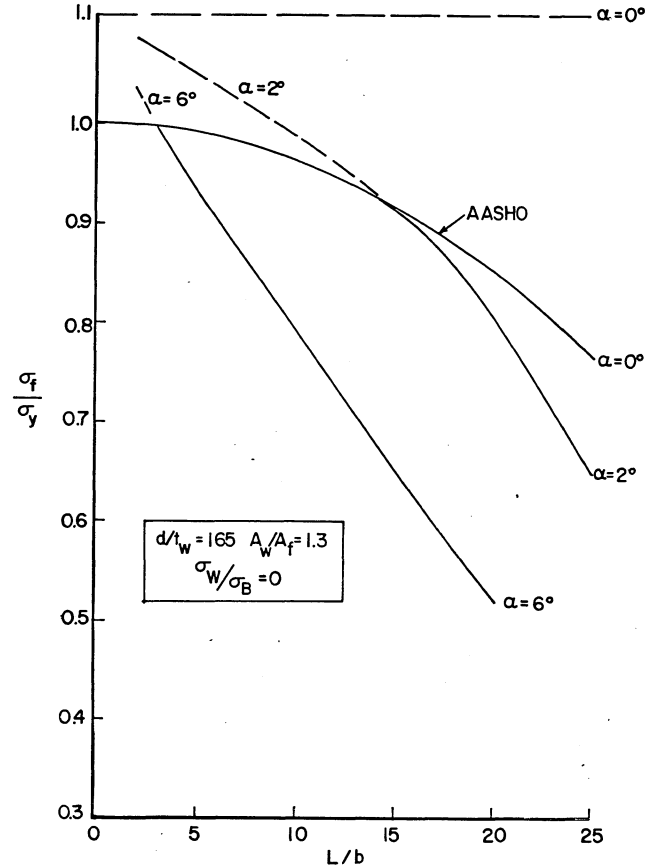

FIG. 29 - INTERACTION WITH AASHO CURVE

Reproduced with permission of the copyright owner. Further reproduction prohibited without permission.

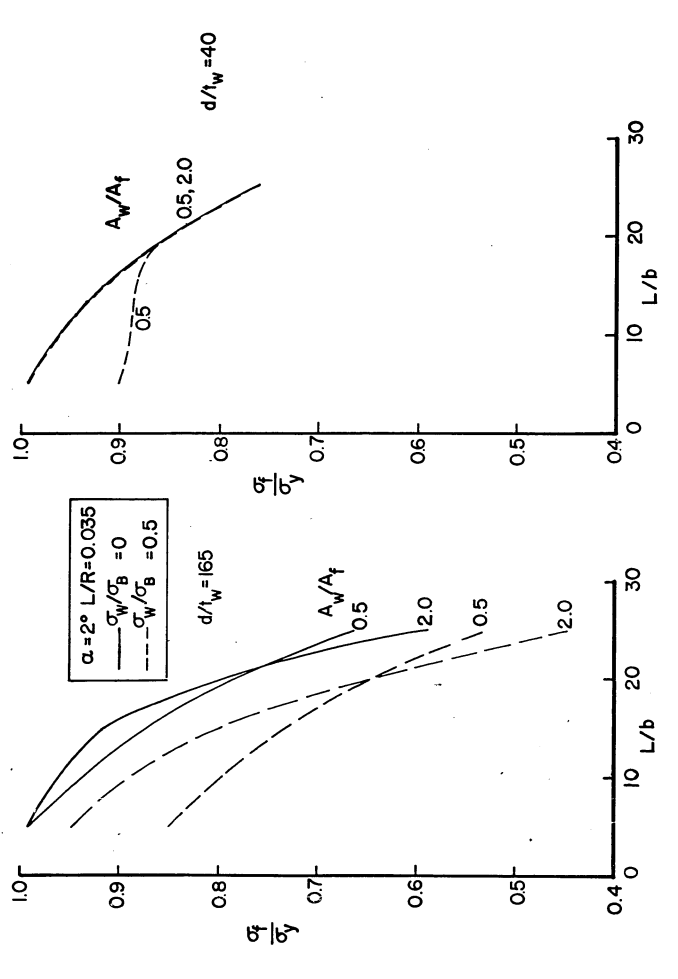

FIG. 30 - ULTIMATE STRENGTH CURVES - α=2°

Reproduced with permission of the copyright owner. Further reproduction prohibited without permission.

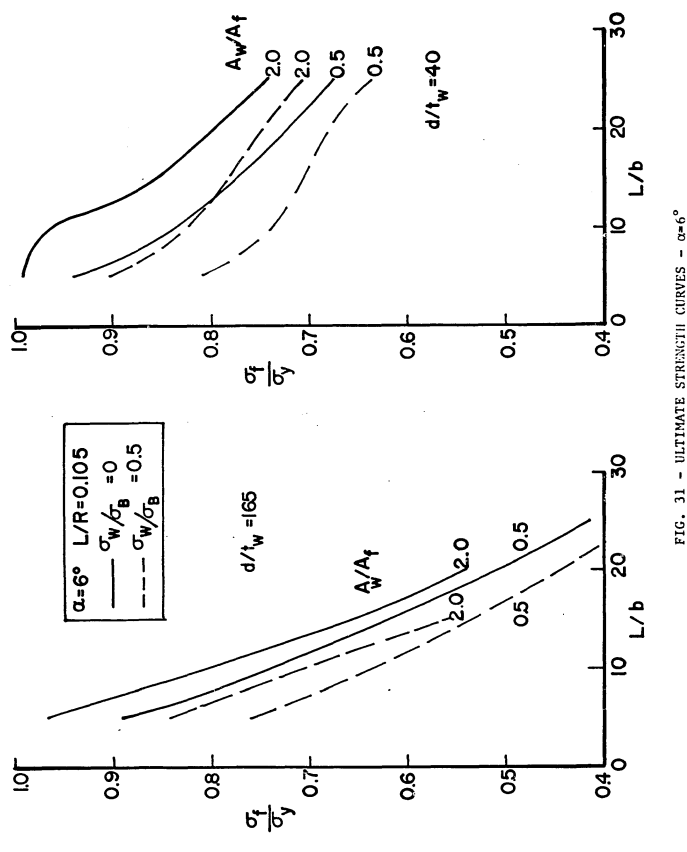

FIG. 31 - ULTIMATE STRENGTH CURVES - α=6°

Reproduced with permission of the copyright owner. Further reproduction prohibited without permission.

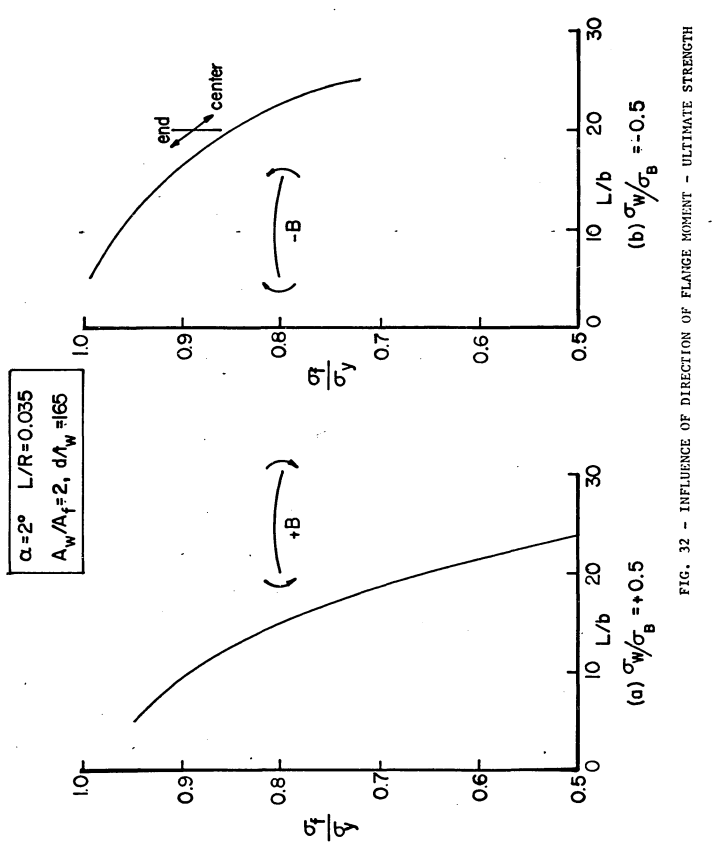

FIG. 32 - INFLUENCE OF DIRECTION OF FLANGE MOMENT - ULTIMATE STRENGTH

Reproduced with permission of the copyright owner. Further reproduction prohibited without permission.

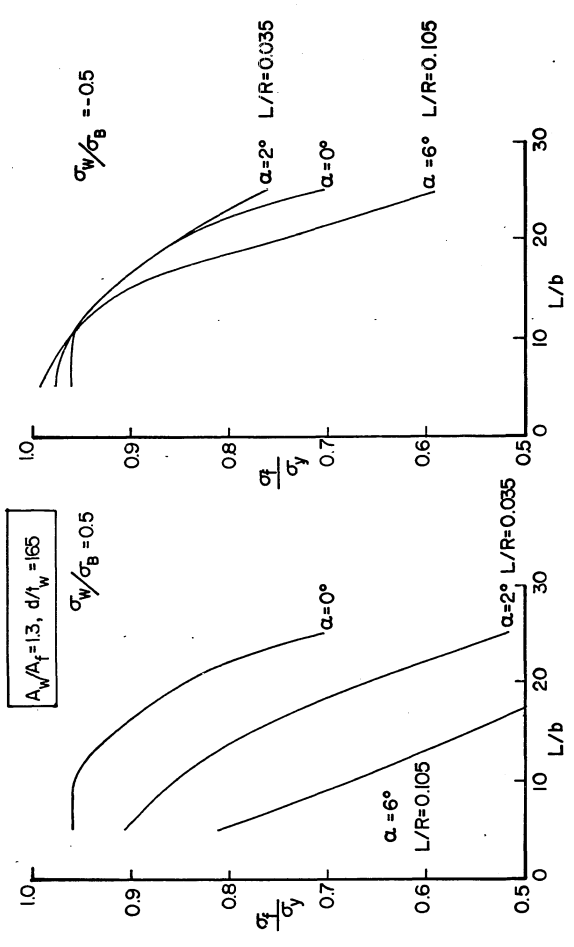

FIG. 33 - INFLUENCE OF CURVATURE ON ULTIMATE STRENGTH

Reproduced with permission of the copyright owner. Further reproduction prohibited without permission.

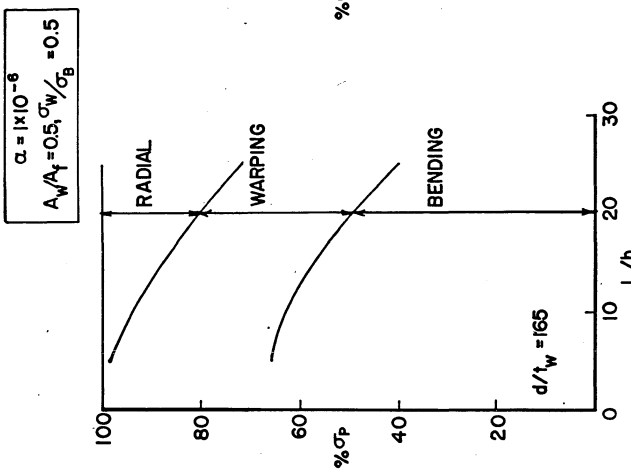

FIG. 34 - CONTRIBUTIONS OF VARIOUS EFFECTS - $\alpha^{\circ}0^{\circ}$ (ULTIMATE STRENGTH)

Reproduced with permission of the copyright owner. Further reproduction prohibited without permission.

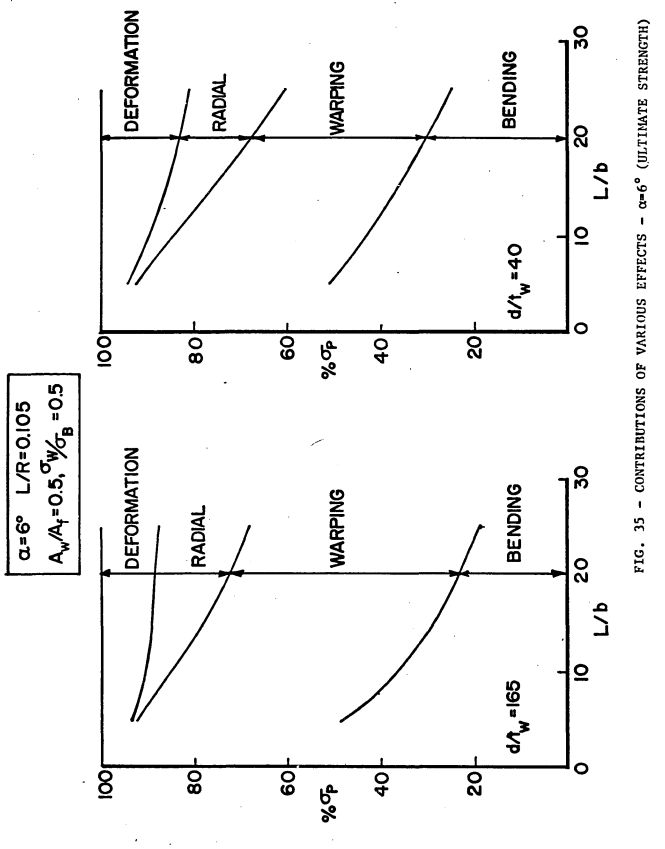

FIG. 35 - CONTRIBUTIONS OF VARIOUS EFFECTS - α=6° (ULTIMATE STRENGTH)

Reproduced with permission of the copyright owner. Further reproduction prohibited without permission.

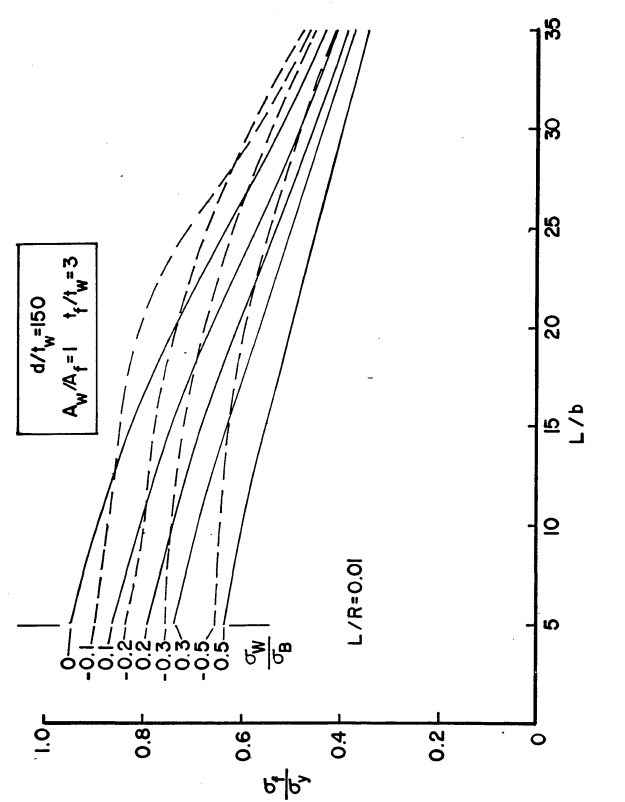

FIG. 36 - INITIAL YIELD DESIGN CURVES L/R=0.01

Reproduced with permission of the copyright owner. Further reproduction prohibited without permission.

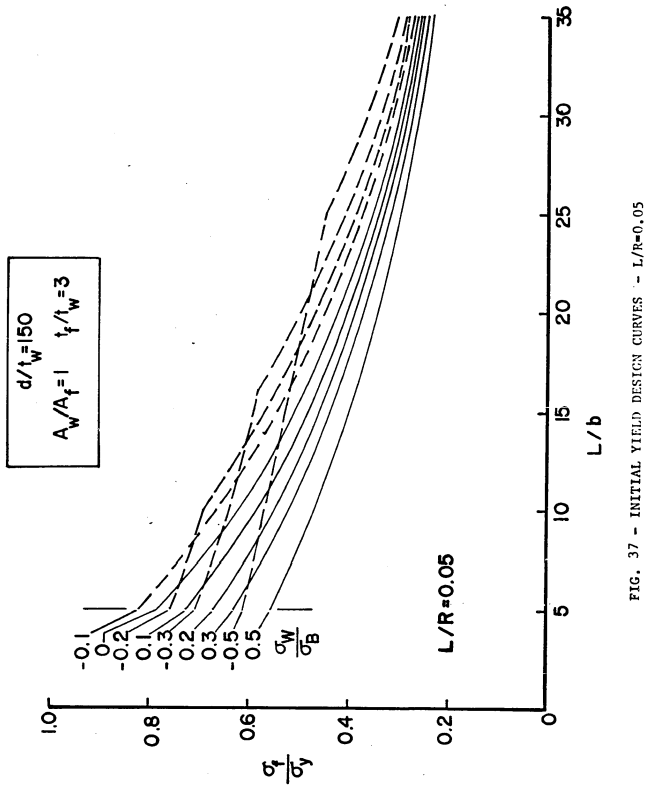

FIG. 37 - INITIAL YIELD DESIGN CURVES - L/R=0.05

Reproduced with permission of the copyright owner. Further reproduction prohibited without permission.

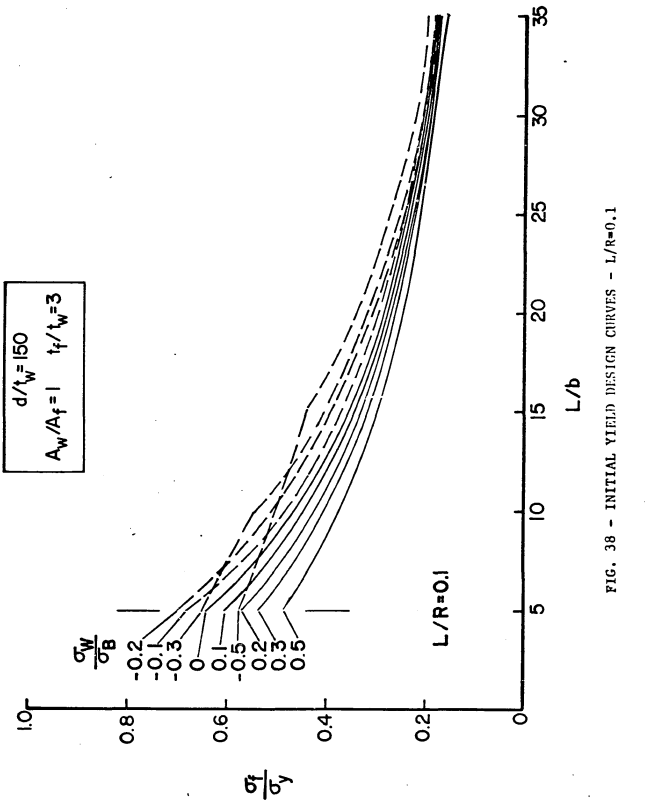

FIG. 38 - INITIAL YIELD DESIGN CURVES - L/R=0.1

Reproduced with permission of the copyright owner. Further reproduction prohibited without permission.

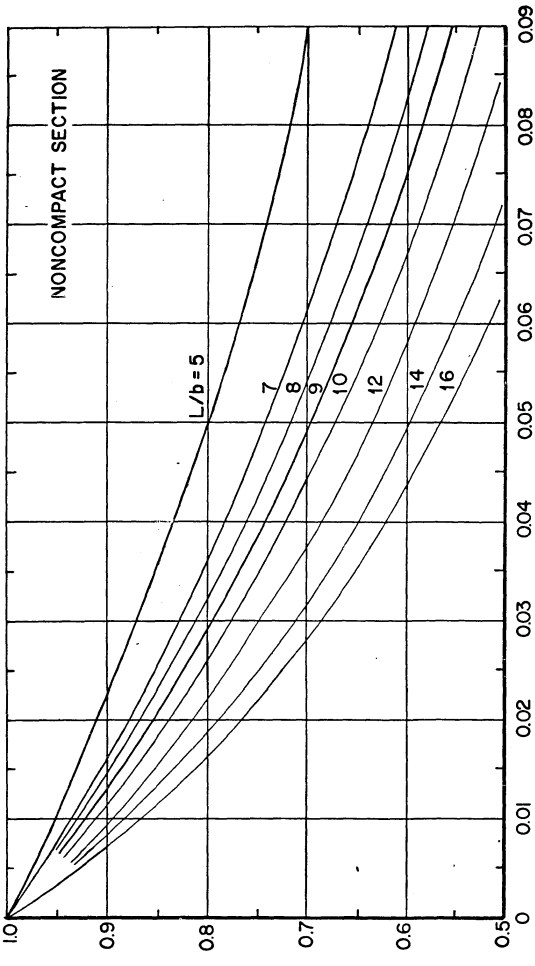

FIG 39 - CURVATURE CORRECTION FACTOR ρ_b FOR ALLOWABLE STRESS-INITIAL YIELD[9]

Reproduced with permission of the copyright owner. Further reproduction prohibited without permission.

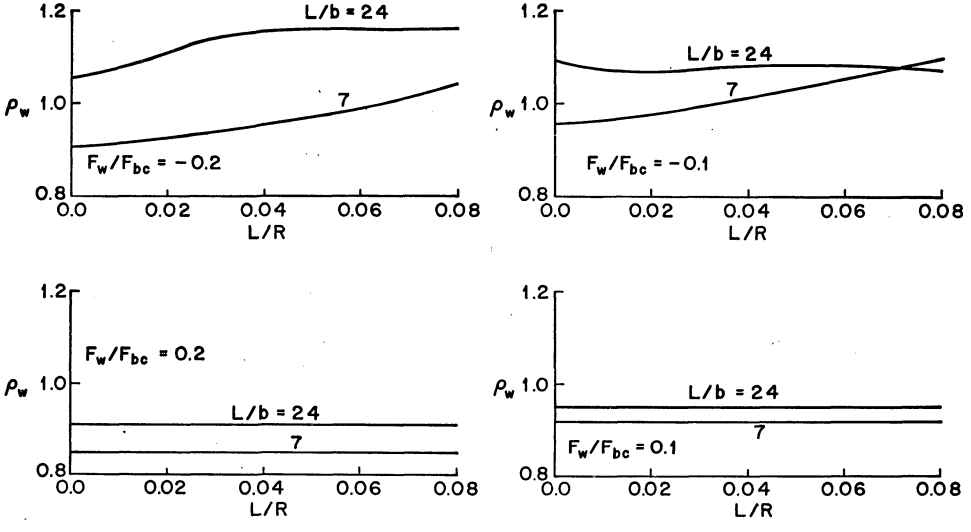

FIG. 40 - CURVATURE CORRECTION FACTOR ρ_w FOR ALLOWABLE STRESS - INITIAL YIELD

Reproduced with permission of the copyright owner. Further reproduction prohibited without permission.

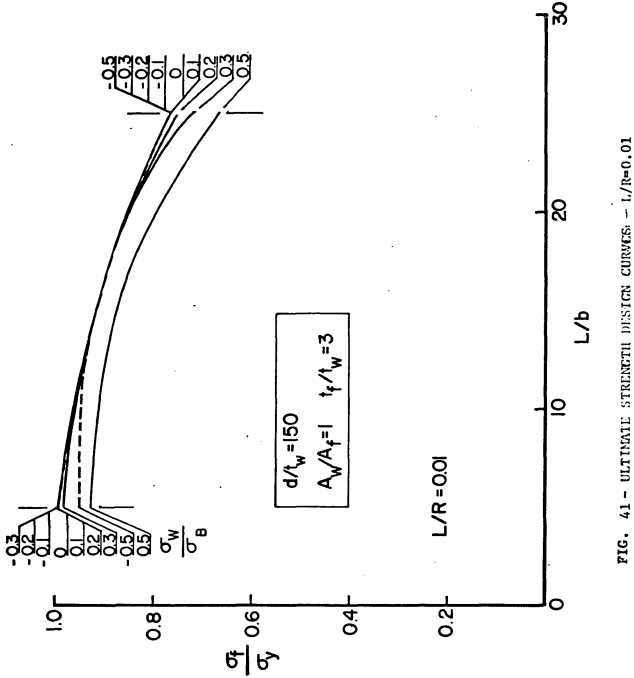

FIG. 41 - ULTIMATE STRENGTH DESIGN CURVES - L/R=0.01

Reproduced with permission of the copyright owner. Further reproduction prohibited without permission.

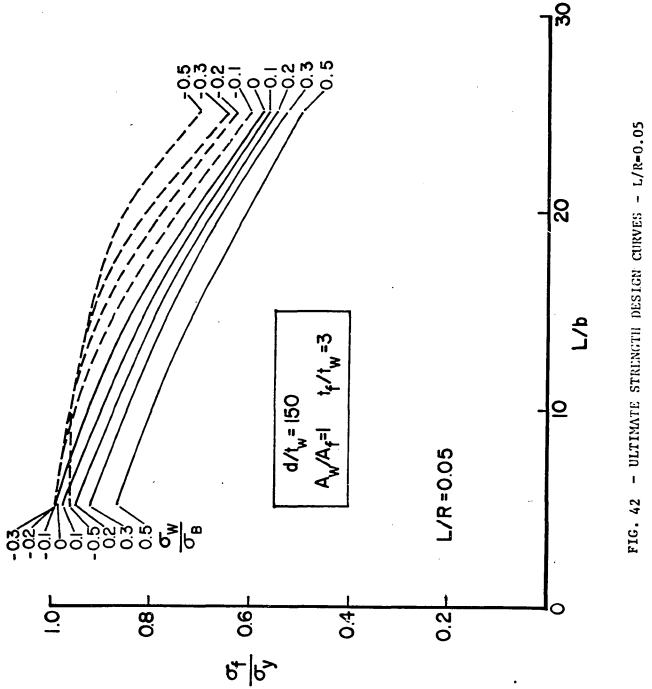

FIG. 42 - ULTIMATE STRENGTH DESIGN CURVES - L/R=0.05

Reproduced with permission of the copyright owner. Further reproduction prohibited without permission.

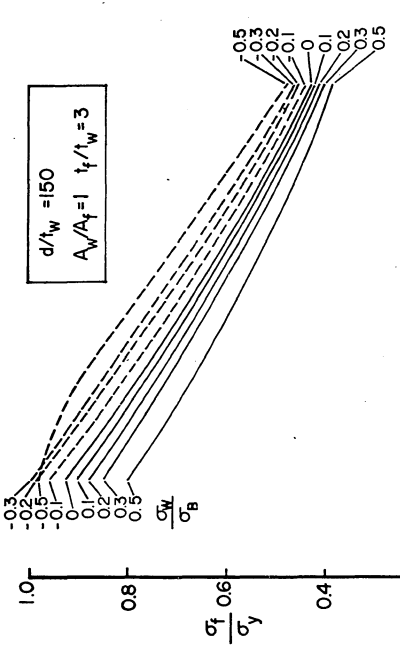

FIG. 43 - ULTIMATE STRENGTH DESIGN CURVES - L/R=0.10

Reproduced with permission of the copyright owner. Further reproduction prohibited without permission.

Reproduced with permission of the copyright owner. Further reproduction prohibited without permission.

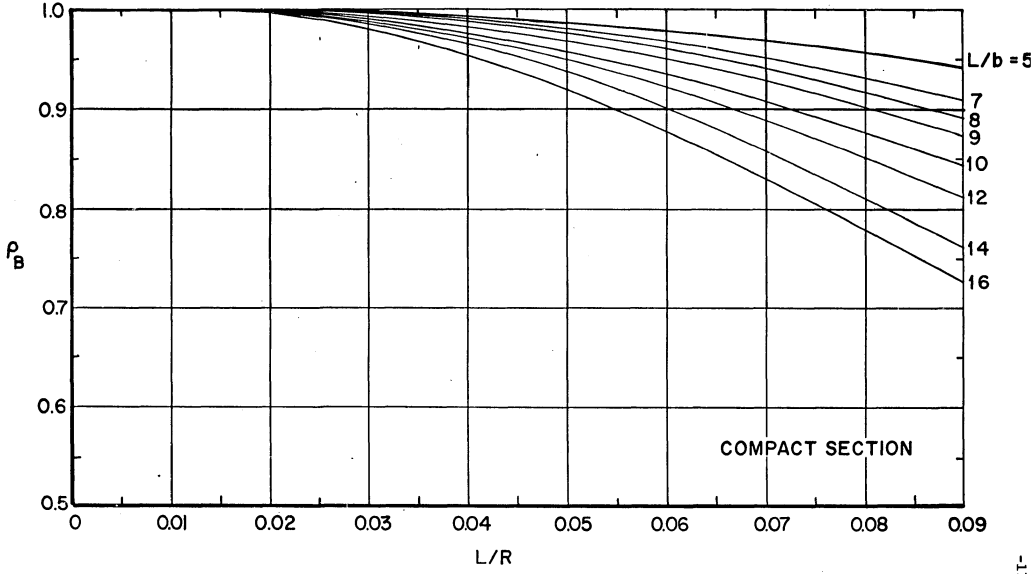

FIG. 44 - CURVATURE CORRECTION FACTOR ρ_B FOR ALLOWABLE STRESS-ULTIMATE STRENGTH

Reproduced with permission of the copyright owner. Further reproduction prohibited without permission.

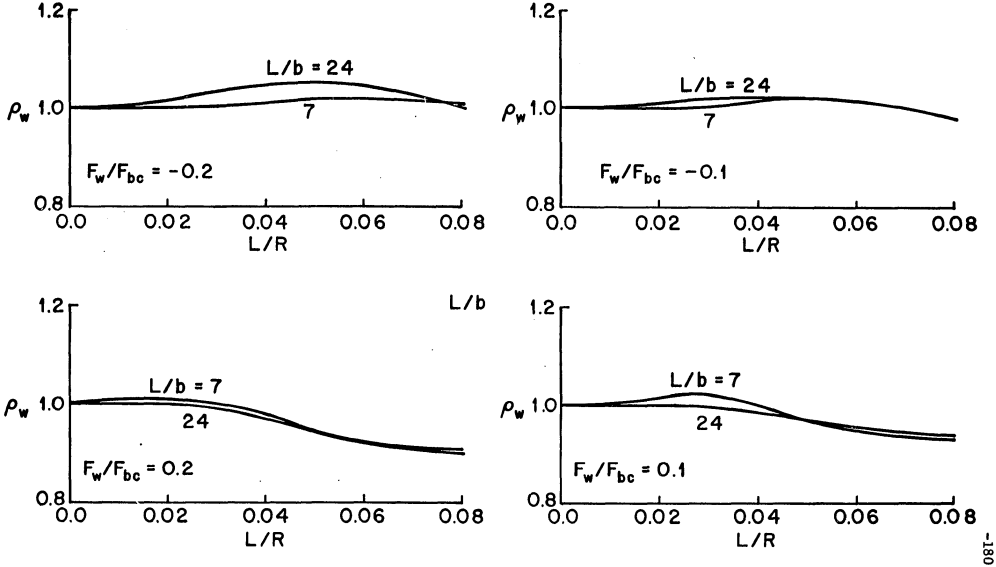

FIG. 45 - CURVATURE CORRECTION FACTOR ρ_w FOR ALLOWABLE STRESS - ULTIMATE STRENGTH

Reproduced with permission of the copyright owner. Further reproduction prohibited without permission.

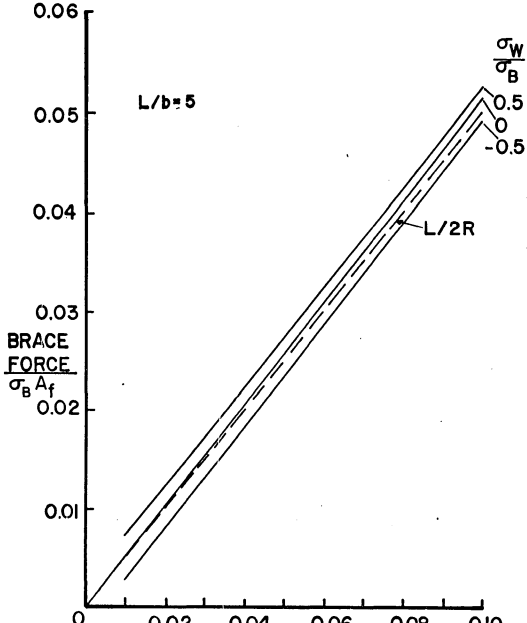

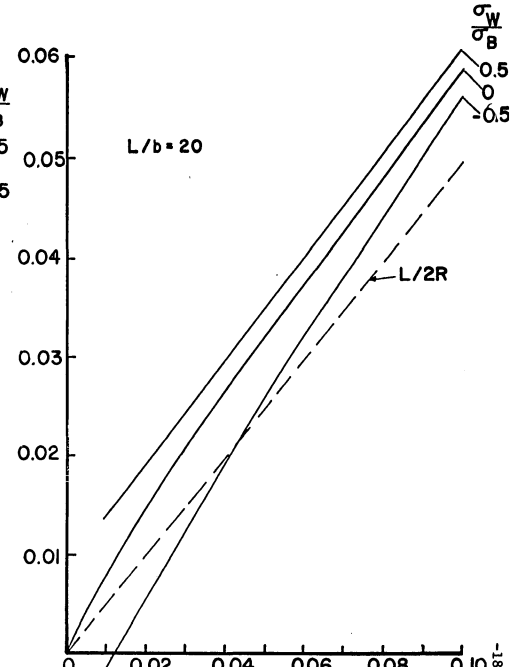

FIG. 46 - BRACE FORCES - INITIAL YIELD

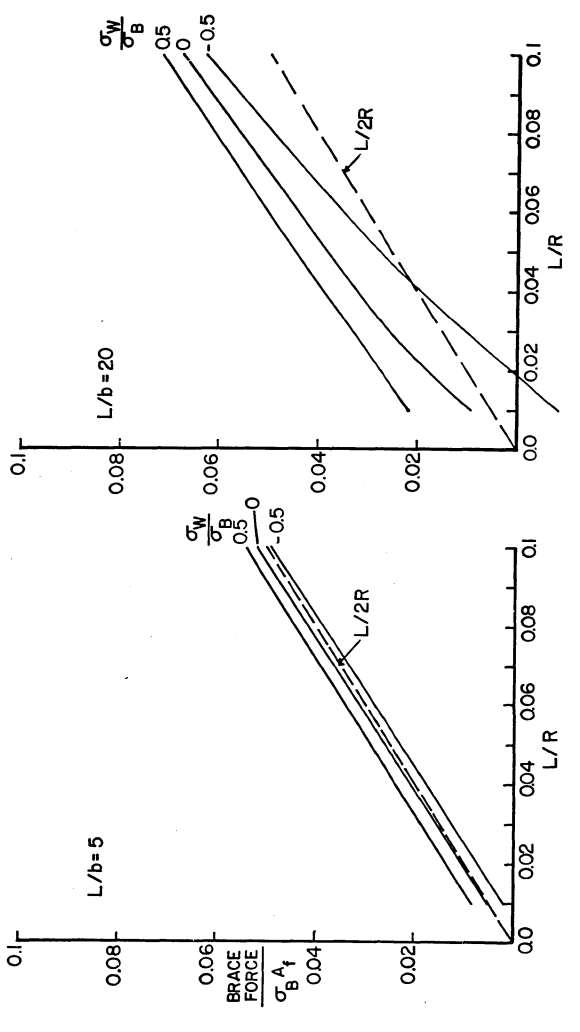

FIG. 47 - BRACE FORCES - ULTIMATE STRENGTH

Reproduced with permission of the copyright owner. Further reproduction prohibited without permission.

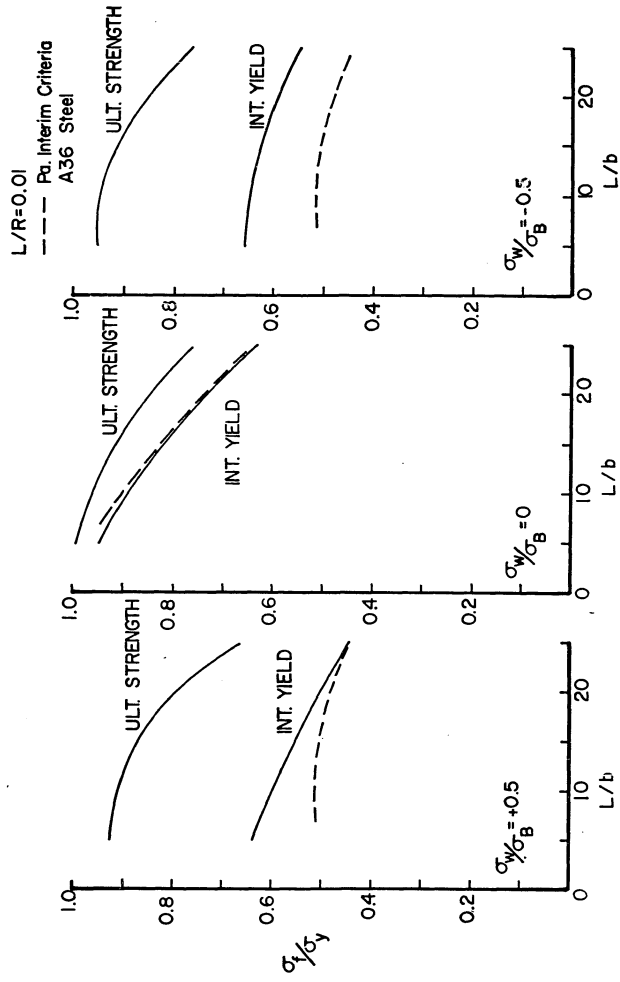

FIG. 48- COMPARISON WITH PA. INTERIM CRITERIA - L/R=0.01

Reproduced with permission of the copyright owner. Further reproduction prohibited without permission.

Reproduced with permission of the copyright owner. Further reproduction prohibited without permission.

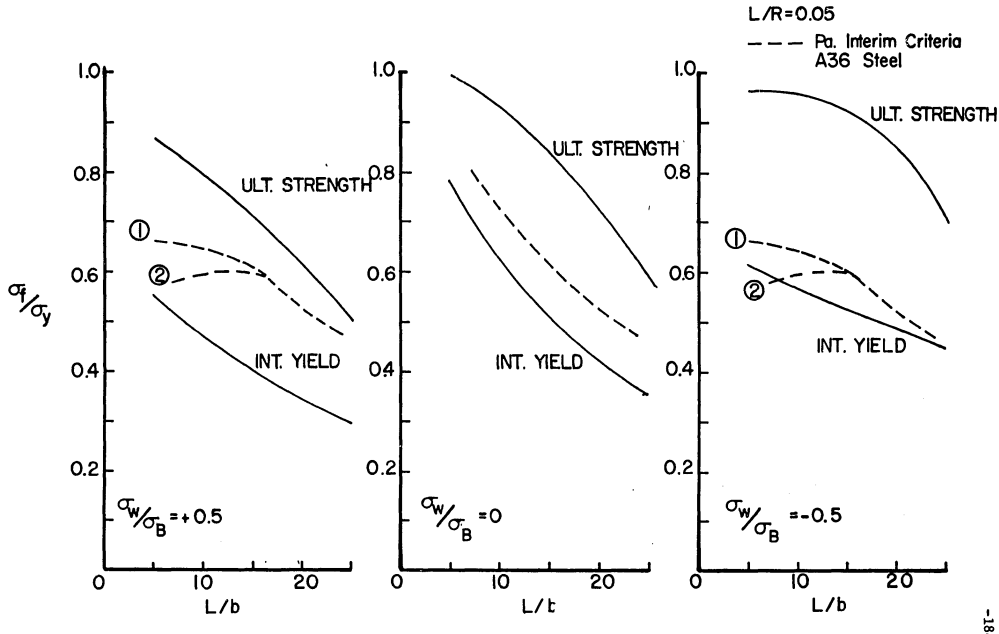

FIG. 49 - COMPARISON WITH PA. INTERIM CRITERIA - L/R=0.05

Reproduced with permission of the copyright owner. Further reproduction prohibited without permission.

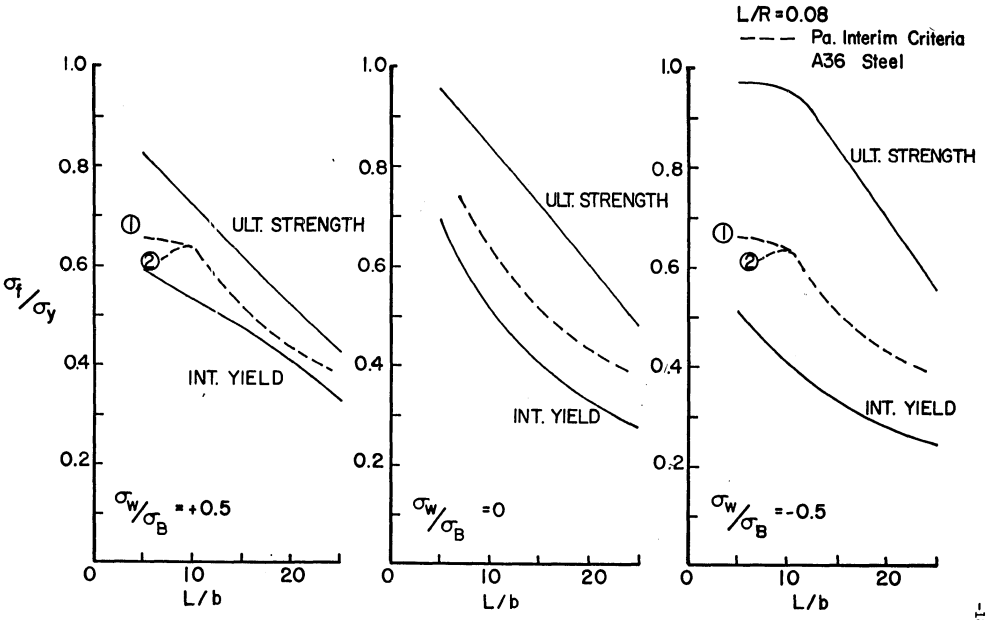

FIG. 50 - COMPARISON WITH PA. INTERIM CRITERIA - L/R = 0.08

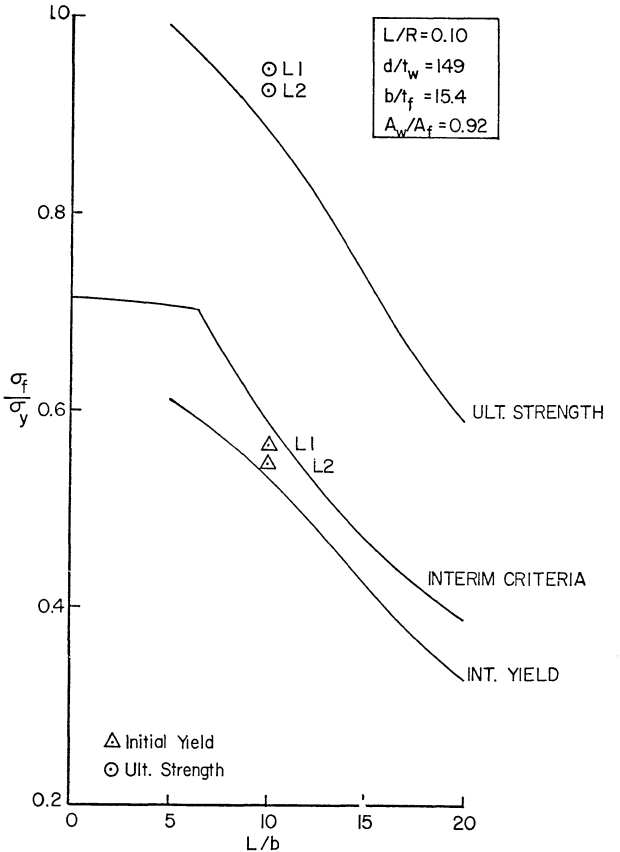

FIG. 51 - COMPARISON WITH TEST RESULTS

Reproduced with permission of the copyright owner. Further reproduction prohibited without permission.

11 REFERENCES

1. Bleich, H., Buckling Strength of Metal Structures, McGraw-Hill Book Co., Inc., New York, New York, 1952.

2. Timoshenko, S. P., Gere, J. M., Theory of Elastic Stability, 2nd Edition, McGraw-Hill Book Co., Inc., New York, New York, 1961.

3. Vlasov, V. Z., Thin Walled Elastic Beams, 2nd Edition, National Science Foundation, Washington, D.C., 1961.

4. Galambos, T. V., Fukumoto, Y., "Inelastic Lateral-Torsional Buckling of Beam-Columns," Journal of the Structural Division, ASCE, Vol. 92, No. ST 2, April, 1966.

5. Lay, M. G., Galambos, T. V., "Inelastic Steel Beams Under Uniform Moment," Journal of the Structural Division, ASCE, Vol. 91, No. ST 6, Dec., 1965.

6. Galambos, T. V., Structural Members and Frames, Prentice-Hall, Inc., Englewood Cliffs, New Jersey, 1968.

7. Johnston, B. G., Guide to Design Criteria For Metal Compression Members, 2nd Edition, John Wiley and Sons, Inc., New York, New York, 1966.

8. Lee, G. C., "A Survey of the Literature on the Lateral Instability of Beams," Welding Research Council Bulletin, No. 63, August, 1960.

9. Specification for the Design, Fabrication, and Erection of Structural Steel for Buildings, American Institute of Steel Construction, New York, New York, 1969.

10. Standard Specification for Highway Bridges, Tenth Edition, American Association of State Highway Officials, Washington, D.C., 1969.

11. Dabrowski, R., "Zur Berechnung von gekrummten dunnwandigen Trager mit offenem Profil," Der Stahlbau, Vol. 12, December, 1964, pp. 364-372.

12. Culver, C., Brogan, D., Bednar, D., "Analysis of Curved Girder Bridges," Engineering Journal, AISC, January, 1970.

13. Ojalvo, I., Newman, M., "Buckling of Naturally Curved and Twisted Beams," Journal Engineering Mechanics Division, ASCE, Vol. 94, No. EM 5, Proc. Paper 6156, Oct., 1968, pp. 1067-1087.

Reproduced with permission of the copyright owner. Further reproduction prohibited without permission.

14. Love, A. E. H., Mathematical Theory of Elasticity, 4th Edition, Dover Publications, New York, 1944.

15. Cheney, J. A., "Bending and Buckling of Thin-Walled Open-Section Rings," Journal of the Engineering Mechanics Division, ASCE, Vol. 89, No. EM 5, Proc. Paper 3665, October, 1963, pp. 17-44.

16. Bolotin, V. V., Nonconservative Problems of the Theory of Elastic Stability, The MacMillan Co., New York, 1963.

17. Ojalvo, M., Demuts, E. and Tokraz, F., "Out-of-Plane Buckling of Curved Members," Journal of the Structural Division, ASCE, Vol. 95, No. ST 10, Proc. Paper 6865, October, 1969.

18. Pettersson, O., "Combined Bending and Torsion of I Beams of Mono-symmetrical Cross Section," Bulletin No. 10, Division of Building Statics and Structural Engineering, The Royal Institute of Technology, Stockholm, Sweden, 1952.

19. McManus, P., Nasir, G., Culver, C., "Horizontally Curved Girders - State of the Art," Journal of the Structural Division, ASCE, Vol. 95, No. ST 5, Proc. Paper 6546, May, 1969, pp. 853-870.

20. McManus, Paul F., and Culver, Charles G., "Lateral Stability of Curved Girders," Proceedings of Specialty Conference on Steel Structures, ASCE, Engr. Ext. Series No. 15, University of Missouri - Columbia, June 8-12, 1970.

21. Ohlson, Roger A., Mozer, John D., and Culver, Charles G., "Horizontally Curved Highway Bridges - Stability of Curved Plate Girders (Report No. P2)," Carnegie-Mellon University Report to be submitted to CURT, July, 1971.

22. Basler, Konrad, and Thürlimann, Bruno, "Strength of Plate Girders in Bending," Journal of the Structural Division, ASCE, Vol. 87, No. ST 6, Proc. Paper 2913, Aug., 1961, pp. 153-181.

23. Design Manual Part 4 - Structures, Commonwealth of Pennsylvania, Department of Highways, Sec. 4.6.30 - 4.6.32.

24. Tall, L., et. al., Structural Steel Design, Ronald Press Co., New York, 1964, pp. 274.

25. "Survey of Curved Girder Bridges," Committee Correspondence, ASCE Task Committee on Flexural Members, Subcommittee on Curved Girders, June 17, 1971.

26. Culver, C., Nasir, G., "Instability of Horizontally Curved Members - Flange Buckling Studies," Carnegie-Mellon University Report submitted to PennDOT, November, 1969.

27. Culver, C., "Flange Proportions for Curved Plate Girders," Highway Research Board, to be published.

Reproduced with permission of the copyright owner. Further reproduction prohibited without permission.

28. Lay, M. G., Galambos, T. V., "Bracing Requirements for Inelastic Steel Beams," Journal of the Structural Division, ASCE, Vol. 92, No. St 2, Proc. Paper 4785, April, 1966, pp. 207-228.

29. Beedle, L. S., Plastic Design of Steel Frames, John Wiley and Sons, Inc., New York, 1958.

30. Standard Plans Box Highway Bridge Superstructures, U. S. Department of Commerce, Bureau of Public Roads, Washington, D. C., 1956.

31. Weissman, H. A., "Straight Element Grid Analysis of Horizontally Curved Beam Systems," Engineering Journal, AISC, Vol. 7, No. 2, April, 1970, pp. 41-49.

32. McManus, P. F., Culver, C. G., "Nonuniform Torsion of Composite Beams," Journal of the Structural Division, ASCE, Vol. 95, No. ST6, Proc. Paper 6623, pp. 1233-1256.

33. Vincent, G. S., "Tentative Criteria for Load Factor Design of Steel Highway Bridges," American Iron and Steel Institute, Bulletin No. 15, March, 1969.

34. Kuo, J. T. C., Heins, C. P., "Experimental Studies of Composite Members Subjected to Torsion," Civil Engineering Report in preparation, University of Maryland, Report No. 39.

35. Culver, C., Coston, R., "Tests of Composite Beams with Stud Shear Connectors," Journal of the Structural Division, ASCE, Vol. 87, No. ST2, Proc. Paper 2742, February 1961.

36. Slutter, R. C., Driscoll, G. C., "Flexural Strength of Steel-Concrete Composite Beams," Journal of the Structural Division, ASCE, Vol. 91, No. ST2, Proc. Paper 4294, April 1965.

Reproduced with permission of the copyright owner. Further reproduction prohibited without permission.